

UNIVERSITÀ DEGLI STUDI DI NAPOLI
FEDERICO II



SCUOLA POLITECNICA E DELLE SCIENZE DI BASE
DIPARTIMENTO DI INGEGNERIA INDUSTRIALE
SEZIONE AEROSPAZIALE
CORSO DI LAUREA MAGISTRALE IN
INGEGNERIA AEROSPAZIALE E ASTRONAUTICA
MASTER THESIS

DEVELOPMENT OF A NEW METHODOLOGY FOR THE
PREDICTION OF AIRCRAFT FUSELAGE
AERODYNAMIC CHARACTERISTICS

SUPERVISOR:
Prof. Eng.
Fabrizio Nicolosi

CANDIDATE:
Vincenzo Cusati
Matr. M53/154

CO-SUPERVISOR:
Eng. Danilo Ciliberti
Dr. Eng. Pierluigi Della Vecchia

ANNO ACCADEMICO 2012/2013

To invent an airplane is nothing. To build one is something.
But to fly is everything

-Karl Wilhelm Otto Lilienthal

ABSTRACT

The main aim of this work is to investigate, from aerodynamic point of view, a modular model of the fuselage of a regional transport turboprop aircraft with 90 seats. This approach involves the study of different fuselage components (nose, cabin and tailcone) to identify trends in aerodynamic coefficients with geometrical parameters. Usually, in the preliminary design, the aerodynamic studies are conducted with semi-empirical methods which rely on a huge database of wind-tunnel test results, such as USAF DATCOM, that are based on geometries very different from a turboprop. In the present work, the aerodynamic studies were performed by numerical analyses (Reynolds Averaged Navier Stokes equations). Therefore the results obtained with a numerical approach are presumably more suitable for a preliminary design than those achieved with semi-empirical methods. The numerical simulations have been carried out using the commercial software *Star-CCM+*. A large number of simulations have been performed on the SCoPE grid infrastructure of the University of Naples Federico II, that gave the possibility to simulate complex 3D geometries in a small amount of time. The only constraint imposed to modifications of the fuselage is the compliance to FAR 25.775 (Windshields and windows). Results of numerical analyses give useful information about trends of aerodynamic coefficients with geometric parameters. A drag and moment prediction method, accounting for the fuselage shape and wetted area, have been developed from these results and are presented with some example of application.

ACKNOWLEDGEMENTS

I am aware that this page can seem too long but I want to thank all the people (and there are many) who have contributed to the achievement of this goal.

First of all I would like to express my gratitude to Prof. Fabrizio Nicolosi for giving me the opportunity of this thesis, transforming it into a great opportunity for professional and human growth. His passion for flight and for the aircraft design making me appreciate more and more the profession that (I hope) I shall make in the future.

If I could accomplish what I hope is a good job, a lot of the credit goes to Danilo (Eng. Ciliberti) that was my "guardian angel", with whom I was lucky to deepen the knowledge outside of the workplace. In addition to being an excellent engineer, he has been a great person. Thanks for the time and attention dedicated to me. A similar considerations holds for Pierluigi (Eng. Della Vecchia), which often has shed light on obscure topics for me with simple explanations, which are not purely limited to engineering. I would also like to thank Salvatore (Eng. Corcione) for his willingness to help us to solve any kind of problem.

A special thanks goes to a special person, Amalia, my girlfriend, who has had, has and will have a fundamental role in my life. She has been always at my side, in joy and in sorrow, and was helped me to believe in my qualities even when I didn't believe anymore (in this regard I jealously guards a letter that gave me the strength to overcome any trial). I would not be here if you were not by my side. Thank you for everything my love.

I would like also to express my gratitude to my family. I don't want to bring everything to a mere economic issue, albeit an important one. They are the pillars of my life. I want to say thanks to my mum Michela, for having suffered in silence with me when I was about to suffer, for teaching me humility, and for standing and the supporting me lovingly every day. I want to say thanks to my father Raffaele: his example is for me always a guide. I'll never forget his words in a "special" moment of my college career, "one stone at a time"...and one stone at a time we built a house! If I am here today, I owe to you. I want to say thanks to my sisters Grazia and Miriam, which, in addition to their affection, have shown me that the ability and humility can reach any goal anytime, anywhere and anyhow. I would also like to thank my brother in law, Blair, for language support and his availability during the writing of the thesis.

An other special thanks goes to Piemonte family, Felice (with whom I share a passion for airplanes), Giovanna and Valeria for the love and

support they have always given me, and Mario, a true friend, with whom it is always nice to deal with. You welcomed me like a second family and I shall be forever grateful.

Last but not least, I would like to say thanks to all my friends who have accompanied me during my years spent at university: Pasquale, Angelo, Luigi, Nunzio, Vincenzo D., Vincenzo F., Mino, Aldo, Alessandro and many others. It was great to share day-by-day this adventure. I consider myself a very lucky person to have met you.

Vincenzo Cusati

CONTENTS

1	INTRODUCTION	1
1.1	The fuselage design for a transport aircraft	2
1.2	Turboprop aircraft	3
1.2.1	Turboprop Drag and Performance	4
1.3	Aim and structure of thesis work	4
2	SEMI-EMPIRICAL METHODS FOR PREDICTION OF AERODYNAMIC COEFFICIENTS	8
2.1	Fuselage drag coefficient prediction	8
2.1.1	Effect of fineness ratio	10
2.1.2	Skin friction contribution	11
2.1.3	Fuselage upsweep contribution	13
2.1.4	Fuselage base drag contribution	14
2.1.5	Windshield contribution	14
2.2	Fuselage moment coefficient prediction	16
2.3	Example of application	19
2.3.1	Drag estimation for ATR-72	19
2.3.2	Drag estimation for Dash8-Q400	23
2.3.3	Pitching moment estimation for ATR-72	24
2.3.4	Pitching moment estimation for Dash8-Q400	25
3	A NUMERICAL APPROACH	26
3.1	The software Star-CCM+	28
3.1.1	Simulation workflow	29
3.1.2	Main mesh parameter	31
3.1.3	Convergence	32
3.2	The SCoPE grid infrastructure	32
3.3	Numerical model	33
3.3.1	Test-cases	35
3.4	Processing of geometry with Matlab	37
3.4.1	Modification of the nose	40
3.4.2	Modification of the cabin	42
3.4.3	Modification of the tail	42
3.4.4	Modification of nose height	43
3.4.5	Modification of upsweep angle	45
4	CFD ANALYSIS RESULTS	48
4.1	Variation of the nose length	48
4.2	Variation of the cabin length	55
4.3	Variation of the tail length	59
4.4	Variation of the nose height	63
4.5	Variation of the upsweep angle	66
5	A NEW METHODOLOGY FOR PREDICTION OF AERODYNAMIC COEFFICIENTS	68

5.1	Methodology for drag prediction	68
5.1.1	The shape factor of the nose	69
5.1.2	The shape factor of the cabin	70
5.1.3	The shape factor of the tail	70
5.1.4	Example of application	72
5.2	Pitching moment prediction	79
5.2.1	Example of application	81
5.3	Prediction of the pitching moment derivative	84
5.3.1	Example of application	87
6	CONCLUSIONS	90
A	FAR RELATED TO WINDSHIELDS AND WINDOWS	92
B	STAR-CCM+ ON SCOPE USER GUIDE	94
B.1	Files necessary to the job	94
B.1.1	Java macro example	94
B.1.2	Executable file example	95
B.1.3	Job file example	97
B.2	Transferring files on SCoPE	98
B.3	Copying the simulation file on the LFC	98
B.4	Running, monitoring and retrieving the job	98
C	NUMERICAL SIMULATION RESULTS	100
	Bibliography	105

LIST OF FIGURES

Figure 1	The main parts of a fuselage	3
Figure 2	ATR-72 and DASH8-Q400 aircraft.	3
Figure 3	Typical regional turboprop drag breakdown.	5
Figure 4	Drag impact on aircraft performance	5
Figure 5	The reference fuselage	6
Figure 6	Semi-empirical drag estimation for smooth stream-lined bodies (ellipsoid). $Re = 10^7$. Fully turbulent flow. Flat plate analogy [23].	12
Figure 7	Definition of fuselage upsweep angle.	13
Figure 8	Flow around the rear part of the fuselage.	15
Figure 9	Afterbody drag of a fuselage tail [23].	16
Figure 10	Semi-empirical method for estimation of wind-shield drag contribution [20].	17
Figure 11	Fuselage correction for fineness ratio.	18
Figure 12	Typical layout for computing fuselage moments.	18
Figure 13	Fuselage stability coefficient. From [7].	19
Figure 14	ATR-72 dimensions.	20
Figure 15	Bombardier Dash8-Q400 dimensions.	21

List of Figures

Figure 16	Windshield drag contribution for the ATR-72.	22
Figure 17	The comparison of the nose shape.	24
Figure 18	Strips for ATR-72	25
Figure 19	Comparison of analysed geometries experimentally with that of reference.	26
Figure 20	The workflow of the proposed methodology.	28
Figure 21	Vertex, face and cell definition in Star-CCM+.	29
Figure 22	General sequence of operations in a Star-CCM+ analysis.	30
Figure 23	The SCoPE network infrastructure [22].	33
Figure 24	Some images of the SCoPE data center	34
Figure 25	Block shape that defines the fluid domain around the model.	34
Figure 26	Aerodynamic comparison between 4 and 5 abreast fuselage. $M = 0.52$, $Re = 11.5 \times 10^6$.	36
Figure 27	Mesh around the reference fuselage.	36
Figure 28	Test case on mesh convergence. $M = 0.52$, $Re = 17.4 \times 10^6$.	37
Figure 29	The $y+$ value for the reference geometry.	37
Figure 30	An example of work window.	38
Figure 31	The fuselage divided in sections.	40
Figure 32	Main geometrical parameter.	41
Figure 33	Definition of the windshield angle.	44
Figure 34	Definition of the upsweep angle.	46
Figure 35	Reference center for the calculation of moment coefficient.	49
Figure 36	Comparison of different nose.	50
Figure 37	Variation of windshield angle due to the variation of nose length.	51
Figure 38	Pressure distribution on the fuselage symmetry plane, due to nose variation, $\alpha = 0$.	51
Figure 39	Friction and pressure contributions to drag coefficient due to nose variation, $\alpha = 0^\circ$.	52
Figure 40	Drag coefficient due to nose variation (sum of pressure and friction contributions), $\alpha = 0^\circ$.	52
Figure 41	Fuselage pitching instability due to nose variation.	53
Figure 42	Moment coefficient as function of the nose geometry variation, $\alpha = 0^\circ$ e $\alpha = 2^\circ$	53
Figure 43	Comparison of the pressure distribution for two nose configurations, $\alpha = 0^\circ$.	54
Figure 44	Change of the fuselage slenderness by stretching the cabin.	55
Figure 45	Pressure distribution on the fuselage symmetry plane, due to cabin variation, $\alpha = 0^\circ$.	56

List of Figures

Figure 46	Friction and pressure contributions to drag coefficient due to cabin variation, $\alpha = 0^\circ$. 56
Figure 47	Drag coefficient due to cabin variation (sum of pressure and friction contributions), $\alpha = 0^\circ$. 57
Figure 48	Fuselage pitching instability due to cabin variation. 57
Figure 49	Moment coefficient as function of the cabin geometry, $\alpha = 0^\circ$ e $\alpha = 2^\circ$ 58
Figure 50	Comparison of different tail. 60
Figure 51	Variation in fuselage tail length and upsweep angle. 60
Figure 52	Pressure distribution on the fuselage symmetry plane, due to tail variation, $\alpha = 0^\circ$. 60
Figure 53	Friction and pressure contributions to drag coefficient due to tail variation, $\alpha = 0^\circ$. 61
Figure 54	Drag coefficient due to tail variation (sum of pressure and friction contributions), $\alpha = 0^\circ$. 61
Figure 55	Effect of the upsweep angle on fuselage longitudinal stability. 62
Figure 56	Moment coefficient as function of the tail geometry variation, $\alpha = 0^\circ$ e $\alpha = 2^\circ$ 62
Figure 57	Comparison of the pressure distribution for two nose configurations, $\alpha = 0^\circ$. 63
Figure 58	Variation of the windshield angle. 63
Figure 59	Effect of the nose height (and hence windshield angle) on drag coefficient, $\alpha = 0^\circ$. 64
Figure 60	Effect of the nose height (and hence windshield angle) on fuselage longitudinal stability. 65
Figure 61	Effect of the nose height (and hence windshield angle) on the moment coefficient, $\alpha = 0^\circ$ 65
Figure 62	Variation of the upsweep angle. 66
Figure 63	Effect of the upsweep angle on fuselage longitudinal stability. 66
Figure 64	Effect of the upsweep angle on drag coefficient, $\alpha = 0^\circ$. 67
Figure 65	Effect of the upsweep angle on moment coefficient, $\alpha = 0^\circ$. 67
Figure 66	Nose shape factor as a function of FR_n , $\alpha = 0^\circ$. 71
Figure 67	Nose shape factor as a function of windshield angle ψ , $\alpha = 0^\circ$. 72
Figure 68	Cabin shape factor as a function of FR , $\alpha = 0^\circ$. 73
Figure 69	Tail shape factor as a function of FR_t , $\alpha = 0^\circ$. 74
Figure 70	Scheme of the geometric relationship between maximum value of upsweep angle (θ) and the fineness ratio of the tailcone (FR_t). 74

List of Figures

Figure 71	Tail shape factor as a function of upsweep angle θ , $\alpha = 0^\circ$. 75	
Figure 72	The value of the nose shape factor for the "103201" fuselage, $\alpha = 0^\circ$. 77	
Figure 73	The value of the cabin shape factor for the "103201" fuselage, $\alpha = 0^\circ$. 77	
Figure 74	The value of the tailcone shape factor for the "103201" fuselage, $\alpha = 0^\circ$. 78	
Figure 75	Definition of the position of reference center and of the angle of attack α . 79	
Figure 76	Moment coefficient (referred to S_{front} and L_f) as a function of fineness ratio FR, $\alpha = 0^\circ$. 80	
Figure 77	The nose correction term for the moment coefficient as a function of windshield angle ψ , $\alpha = 0^\circ$. 80	
Figure 78	The tail correction term for the moment coefficient as a function of upsweep angle θ , $\alpha = 0^\circ$. 81	81
Figure 79	Moment coefficient as a function of fineness ratio FR, $\alpha = 0^\circ$. 82	
Figure 80	The nose correction term for the moment coefficient as a function of windshield angle ψ , $\alpha = 0^\circ$. 82	
Figure 81	The tail correction term for the moment coefficient as a function of upsweep angle θ , $\alpha = 0^\circ$. 83	83
Figure 82	The curve slope of moment coefficient (referred to S_{front}) as a function of fineness ratio FR. 85	
Figure 83	The nose correction term for the curve slope of the moment coefficient as a function of windshield angle ψ . 85	
Figure 84	The tail correction term for the moment coefficient as a function of upsweep angle θ . 86	
Figure 85	The curve slope of moment coefficient (referred to S_{front}) as a function of fineness ratio FR. 87	
Figure 86	The nose correction term for the moment curve slope coefficient as a function of windshield angle ψ . 88	
Figure 87	The tail correction term for the derivative of moment coefficient as a function of upsweep angle θ . 88	

LIST OF TABLES

Table 1	Features of the reference fuselage.	6
Table 2	The parameters of ATR-72 to compute the skin friction contribution to drag coefficient.	20
Table 3	The parameters of Dash8-Q400 to compute the skin friction contribution to drag coefficient.	23
Table 4	Reasons to not compare CFD and wind-tunnel results [11].	27
Table 5	Principal mesh parameters [21].	31
Table 6	Mesh and physics data for numerical model.	35
Table 7	Fineness ratios of the fuselage components for the parametric investigation.	40
Table 8	Windshield analysis parameter.	44
Table 9	Upsweep analysis parameter.	46
Table 10	Parameters of the nose investigation.	49
Table 11	Parameters of the cabin investigation.	55
Table 12	Parameters of the tail investigation.	59
Table 13	Main parameter of the proposed method.	69
Table 14	Notations about the fuselage configurations used to validate the methodology.	76
Table 15	The necessary values to apply the methodology for the "103201" fuselage.	76
Table 16	The necessary values to apply the method for drag coefficient.	78
Table 17	Comparison between the simulation results and that obtained using the proposed methodology for the drag coefficient.	78
Table 18	The necessary values to apply the method for the moment coefficient.	84
Table 19	Comparison between the simulation results and that obtained using the proposed methodology for moment coefficient.	84
Table 20	The necessary values to apply the method for the curve slope moment coefficient	89
Table 21	Comparison between the simulation results and that obtained using the proposed methodology for curve slope moment coefficient.	89
Table 22	Results of numerical simulation for the configuration with nose geometry modifications, $M = 0.52$, $Re_{L_f} = 2.02 \times 10^8$.	100

Table 23	Results of numerical simulation for the configuration with cabin geometry modifications, $M = 0.52$, $Re_{L_f} = 2.02 \times 10^8$. 101
Table 24	Results of numerical simulation for the configuration with tailcone geometry modifications, $M = 0.52$, $Re_{L_f} = 2.02 \times 10^8$. 102
Table 25	Results of numerical simulation for the configuration with windshield geometry modifications, $M = 0.52$, $Re_{L_f} = 2.02 \times 10^8$. 103
Table 26	Results of numerical simulation for the configuration with upsweep geometry modifications, $M = 0.52$, $Re_{L_f} = 2.02 \times 10^8$. 104

LISTINGS

Listing 1	Part of MATLAB code that rebuild the fuselage geometry. 38
Listing 2	Part of MATLAB code that modifies the fuselage nose. 40
Listing 3	Part of MATLAB code that modifies the fuselage cabin. 42
Listing 4	Part of MATLAB code that modifies the fuselage tail. 42
Listing 5	Part of MATLAB code that modifies the windshield angle. 44
Listing 6	Part of MATLAB code that modifies the upsweep angle. 46

ACRONYMS

AIAA	American Institute of Aeronautics and Astronautics
ATR	Avions de Transport Regional
CAD	Computer Aided Design
CFD	Computational Fluid Dynamics
CFR	Code of Federal Regulations

CLI	Command Line Interface
CPU	Central Processing Unit
DIAS	Dipartimento di Ingegneria AeroSpaziale
DII	Dipartimento di Ingegneria Industriale
FAR	Federal Aviation Regulations
LFC	Local File Catalogue
m.a.c.	mean aerodynamic chord
MATLAB	Matrix Laboratory
NACA	National Advisory Committee for Aeronautics
NASA	National Aeronautics and Space Administration
SCoPE	Sistema Cooperativo Per Elaborazioni Scientifiche Multidisciplinari
SFTP	Secure File Transfer Protocol
SSH	Secure Shell
USAF DATCOM	United States Air Force Data Compendium

LIST OF SYMBOL

α	Angle of attack
ϵ	Downwash angle
ϕ	Shape factor
ψ	Windshield angle
θ	Upsweep angle
$^{\circ}$	Degree
AR	Aspect Ratio
C_D	Drag Coefficient
$C_{D_{base}}$	Base drag coefficient
$C_{D_{fp}}$	Drag coefficient of equivalent flat plate

C_{D_f}	Friction drag coefficient
$C_{D_{int}}$	Interference drag coefficient
C_{D_p}	Pressure drag coefficient
$C_{D_{sf}}$	Drag coefficient due to skin friction
$C_{D_{trim}}$	Trim drag coefficient
$C_{D_{wave}}$	Wave drag coefficient
$C_{D_{WS}}$	Windshield drag coefficient
C_{D_f}	Friction drag coefficient
C_f	Friction coefficient
C_f^{turb}	Turbulent skin friction coefficient
\bar{C}_f	Skin friction coefficient for the equivalent flat plate
C_L	Lift Coefficient
C_{L_α}	Lift curve slope
C_{M_α}	Pitching Moment Coefficient derivative
C_M	Pitching Moment Coefficient
C_p	Pressure Coefficient
CG	Center of gravity
D	Drag
D_f	Friction drag
d_b	Base diameter
d_f	Fuselage diameter
e	Oswald factor
F_f	Form factor
f	Areas of equivalent flat plat
FR	Fineness ratio of the fuselage L_f/d_f
FR _n	Fineness ratio of the nose L_n/d_f
FR _t	Fineness ratio of the tailcone L_t/d_f
K_c	Cabin shape factor
k_f	Untreated metal surface roughness

LIST OF SYMBOLS

K_n	Nose shape factor
K_t	Tail shape factor
L_c	Cabin length
L_f	Fuselage length
L_n	Nose length
L_t	Tailcone length
M	Pitching moment
M	Mach number
q	Dynamic pressure
Re	Reynolds number
Re_{L_f}	Reynolds number referred to fuselage length.
S_{front}	Maximum frontal surface
S_{ref}	Reference surface
S_{wet}	Wet surface
$S_{wet_{cabin}}$	Wet surface of the cabin
$S_{wet_{nose}}$	Wet surface of the nose
$S_{wet_{tail}}$	Wet surface of the tailcone
S_{wing}	Wing surface
V	Velocity

1

INTRODUCTION

Contents

1.1	The fuselage design for a transport aircraft	2
1.2	Turboprop aircraft	3
1.2.1	Turboprop Drag and Performance	4
1.3	Aim and structure of thesis work	4

The preliminary general arrangement of an aircraft is closely tied up with the fuselage, the main dimensions of which should be laid down in some detail. In fact, the fuselage represents such an important item in the total concept that its design might well be started before the overall configuration is settled.

The main characteristics of the fuselage are as follows.

- It constitutes the shell containing the payload which must be carried a certain distance at a specified speed. It must permit rapid loading before the flight and rapid unloading after it. The fuselage structure also offers protection against climatic factors (cold, low pressure, a very high wind velocity) and against external noise, provided suitable measures have been taken.
- The fuselage is the most suitable part for housing the cockpit, the most functional location generally being in the nose.
- The fuselage may be regarded as the central structure member to which the other main parts are joined (wings, tail unit and in some cases the engines) on the one hand, and as the link between the payload and the aircraft on the other.
- Most of the aircraft system are generally housed in the fuselage, which sometimes also carries the engines, fuel and/or the retractable undercarriage.

Selection of the best layout requires a detailed study of these trade-offs. This is generally done by selecting a value not too different from existing aircraft with similar requirements, for which such a detailed study has presumably been done. In the absence of such guidance, one selects an initial layout that satisfies the payload requirements.

1.1 THE FUSELAGE DESIGN FOR A TRANSPORT AIRCRAFT

The fuselage of transport aircraft are seldom streamlined in shape. It should be designed "from the inside outwards", and the skin should envelop the load in such a way that the wetted area is minimum, thus avoiding breakaway of the airflow as far as possible.

In effect the design of the fuselage is based on payload requirements, aerodynamics, and structures. It is possible to consider the fuselage like a body of revolution and it can be designed starting from the characteristics of the cross-section and longitudinal geometry of the same, to then derive from these data all the necessary parameters for a proper sizing.

The arrangement of passengers affects the sizing of the cross-section, being the binding parameter for the characterization of fuselage diameter. Most cross-sections are relatively circular in shape. This is done for the following reasons.

- By eliminating corners, the flow will not separate at moderate angles of attack or sideslip.
- When the fuselage is pressurized, a circular fuselage can resist the loads with tension stresses, rather than the more severe bending loads that arise on non-circular shapes.
- Structural design and manufacture are considerable simplified.
- It is possible to obtain an efficient internal layout with little loss of space.
- The flexibility of the seating arrangement is improved.
- Further development by increasing the length of the fuselages (stretching) is facilitated.

As for the longitudinal dimension the fuselage length is usually divided into three part.

NOSE is the front part of fuselage, tapered to get the best possible penetration for the aircraft

CABIN is the central part of the fuselage (with a constant diameter), where the passengers are accommodated

TAILCONE is the final part of the fuselage, tapered so appropriate.

In the following figure (fig. 1) is depicted an example of fuselage with the parts just introduced and with the main parameters: the fuselage length, L_f , and maximum diameter, d_f .

An extensive analysis is presented in [23] and [10].

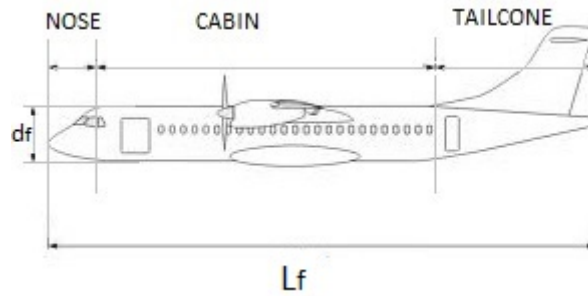


Figure 1: The main parts of a fuselage

1.2 TURBOPROP AIRCRAFT

A recent work [5] has shown that the need to develop regional turboprop transport aircraft is tied to particular needs of both passengers and airlines. First of all, a generic regional turboprop aircraft has to be faster than conventional transport means as trains, cars or ships and it has to be relatively cheap.

Looking at aircraft performance, a turboprop aircraft has a short take-off and landing distance (sometimes on semi prepared runways) and a cruise airspeed not higher than 350 knots. From a deeper airlines point of view, this aircraft has to meet the requirements of low operative and maintenance costs, it is cheaper than an equivalent regional jet and above all it has a lower fuel consumption saving money and pollution.

Passengers want to have a reliable aircraft, competitive in terms of costs, with low noise emission and, also on this aircraft category a good comfort. Aircraft industries were deeply involved in the design of new regional turboprop aircraft during the seventies and eighties in conjunction with the oil crisis. During these years several turboprop aircraft were designed and produced worldwide, increasing the competition stimulation. Nowadays the leaders of the market are ATR and Bombardier with, respectively, ATR-72 and Dash8-Q400 (figure. 2).



(a) ATR 72-600



(b) DASH8-Q400

Figure 2: ATR-72 and DASH8-Q400 aircraft.

It is possible to identify the main features of large turboprop aircraft:

- High-wing
- T-tail
- Slender fuselage
- Engine wing mounted
- Easy cabin accessibility both for passengers and baggage
- Reliable, low maintenance and construction costs structure
- Advanced system instrumentations, glass-cockpit and Fly-by-wire
- Cabin comfort.

It is quite evident that an aircraft of this category in order to satisfy all these requirements must have a very accurate design. In particular, the aerodynamic design of these aircraft involves many aspects that must be assessed and addressed very thoroughly in the design phase. A very important feature of the aerodynamic design is the aerodynamic drag. For these reasons in the following Sec.1.2.1 the aerodynamic drag breakdown of typical large turboprop aircraft is addressed to better understand which are the main drag sources and which the influence of drag reduction on the aircraft performance.

1.2.1 Turboprop Drag and Performance

From [5], it is known that the fuselage of a regional turboprop constitutes the main contribution to the aerodynamic drag.

A typical drag breakdown is shown in figure 3. The term *fuselage* in the pie chart also includes windshield, upsweep, base drag, and some of the excrescences. For the same aircraft, the impact of drag in cruise performance is shown in figure 4. A reduction of 2.5 drag counts increases the maximum true airspeed (TAS) by 1 knot. An overall drag decrease of 15 counts saves 3% fuel on a typical 200 nm mission.

1.3 AIM AND STRUCTURE OF THESIS WORK

The main aim of this work is to investigate, from an aerodynamic point of view, a modular model of the fuselage of a regional transport turboprop aircraft with 90 seats. This approach involves the study of different fuselage components (nose, cabin and tailcone) to

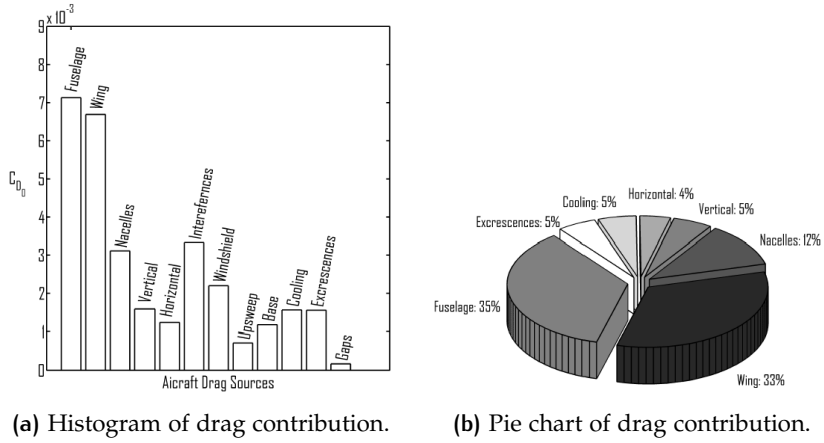


Figure 3: Typical regional turboprop drag breakdown.

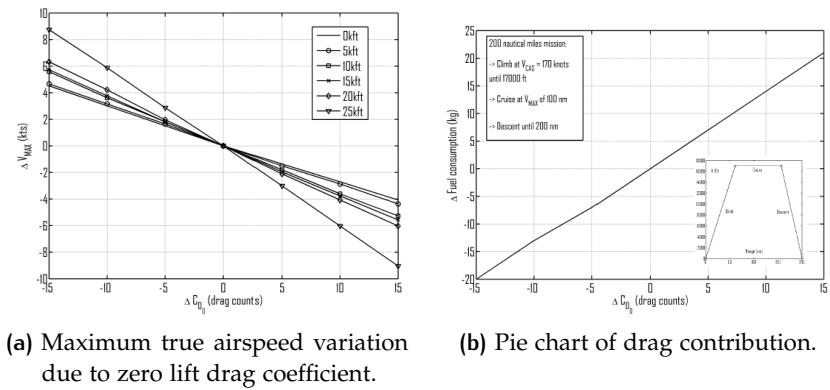


Figure 4: Drag impact on aircraft performance

identify trends in aerodynamic coefficients with geometrical parameters. The only constraint imposed to modifications of the fuselage is the compliance to FAR 25.775 (Windshields and windows). Appendix A shows some details of regulation. The starting point of the work is the reference fuselage. It is shown in figure 5 and the parameters are reported in table 1. In order to point out the aerodynamic trends, hereinafter the results of aerodynamic studies are presented by graphics and mathematical relationships which can be useful also for other aircraft in the preliminary design phase as previously argued.

The work has been structured as follows.

Chapter 2 In this chapter the semi-empirical methods to calculate the aerodynamic coefficients are introduced. In the first part are described the semi-empirical methods which calculate the drag coefficient as the sum of different contributions and then the most famous method for the calculation of moment coefficient, the strip method, is introduced.

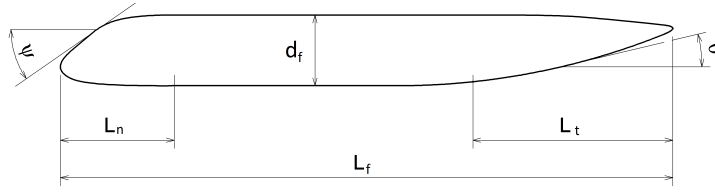


Figure 5: The reference fuselage

The reference fuselage		
L_n	$0.19 \cdot L_f$	Nose length
L_c	$0.43 \cdot L_f$	Cabin length
L_t	$0.38 \cdot L_f$	Tailcone length
FR	8.69	Slenderness ratio
FR_n	1.60	Nose slenderness ratio
FR_t	2.83	Tail slenderness ratio
ψ	39.7°	Windshield angle
θ	13.6°	Upsweep angle

Table 1: Features of the reference fuselage.

Chapter 3 Once the semi-empirical methods have been described, a procedure that make use of CFD to compute the same aerodynamic coefficients is explained. This procedure is the core of the present work. The fuselage geometry of a turboprop is given as a CAD model which is modified with MATLAB in order to derive some different fuselage configurations. The latter have been analysed with the commercial software *Star-CCM+* to evaluate the aerodynamic coefficients. At the same time it is presented the MATLAB code that modifies the geometry of the fuselage. The results of some test cases are also shown to validate the CFD model.

Chapter 4 This chapter is fully dedicated to show the results of numerical simulations. The different cases are obtained changing one at time the fineness ratio of the nose (FR_n), the fineness ratio of the cabin (FR) and the fineness ratio of the tailcone (FR_t) and keeping the other equal to those of the reference fuselage. Other cases are obtained by changing the upsweep angle maintaining constant FR_t and changing the windshield angle maintaining constant FR_n . Moreover the effect of the combined changes are evaluated.

Chapter 5 A new methodology to predict the drag and moment coefficient have been carried out and are described in this chapter. The method supplies the parametric relationships between the aerodynamic coefficients and the geometry of the fuselage. This CFD-born methodology is based on a general turboprop geometry and this is its strength compared to the semi-empirical methods. It can be very useful in preliminary design phase.

Chapter 6 Finally in this chapter the main achievements of this thesis work are summarized and some conclusions are drawn.

2

SEMI-EMPIRICAL METHODS FOR PREDICTION OF AERODYNAMIC COEFFICIENTS

Contents

2.1	Fuselage drag coefficient prediction	8
2.1.1	Effect of fineness ratio	10
2.1.2	Skin friction contribution	11
2.1.3	Fuselage upsweep contribution	13
2.1.4	Fuselage base drag contribution	14
2.1.5	Windshield contribution	14
2.2	Fuselage moment coefficient prediction	16
2.3	Example of application	19
2.3.1	Drag estimation for ATR-72	19
2.3.2	Drag estimation for Dash8-Q400	23
2.3.3	Pitching moment estimation for ATR-72	24
2.3.4	Pitching moment estimation for Dash8-Q400	25

In this chapter the methods to calculate the aerodynamic coefficients, that are normally used in the preliminary phase to guide the design choices, are introduced. In the first section the semi-empirical methods are described and it shows how they predict the drag coefficient. These methods consider the drag coefficient as the sum of different contributions that can be evaluated by relations obtained from wind tunnel test. The content of this chapter is mostly excerpt from works of Prof. Roskam [19] and [20], Kroo et al. [10] and Raymer [18].

Afterwards the *strip method* is reported for the prediction of moment coefficient. It is so called because the fuselage is divided into *strips* each of which gives a contribution to pitching moment in a function of distance from the polo. This method was developed by Munk [15] and Multhopp [14]. Perkins and Hage explained how the fuselage affects the longitudinal stability [17].

2.1 FUSELAGE DRAG COEFFICIENT PREDICTION

Usually, in preliminary design phases, the estimation of drag coefficient (C_D) is obtained through semi-empirical methods. They are based on the results of wind-tunnel tests of the past, mainly collected

in the USAF DATCOM database. The total drag coefficient of an aircraft is given by the sum of the zero lift drag coefficient and the induced drag coefficient. This assumption is made when the approximation of a parabolic drag polar is assumed in order to estimate the drag coefficient for low incidence such as cruise and climb, that is until the lift coefficient becomes greater than 1. The approximation leads to the following formulation:

$$C_D = C_{D0} + \frac{C_L^2}{\pi AR e} \quad (2.1)$$

where AR is the aspect ratio of the wing and e is the Oswald factor of the complete aircraft. While the induced drag coefficient can be easily computed, the zero lift drag coefficient has to be estimated by semi-empirical approaches in the preliminary design phase.

The zero lift drag coefficient is also known as parasite drag coefficient and it includes skin friction, base, interference, wave, and trim drag coefficients, thus resulting in the following

$$C_{D0} = C_{D_{sf}} + C_{D_{base}} + C_{D_{int}} + C_{D_{wave}} + C_{D_{trim}} \quad (2.2)$$

In the present work it accounts for the contributions to C_{D0} of the fuselage and therefore are taken into account only the $C_{D_{sf}}$, the $C_{D_{base}}$ and the $C_{D_{int}}$ (due to the windshield and upsweep angle). In effect the fuselage is responsible for a large percentage of the overall drag (in particular the parasite drag) of the airplanes (about 25% - 50% of total drag) and since it is desirable to have as little drag as possible, the fuselage should be sized and shaped accordingly. The parasite drag coefficient (see eq. (2.2)) of an aircraft can be computed by adding each contribute of the different components and assuming an interference effect. If C_{Di} and S_i are respectively the drag coefficient and the surface of the component i , q the dynamic pressure, the total drag given by n components is:

$$D = q \sum_{i=1}^n C_{Di} S_i$$

Since each component is characterized by a different reference surface, it is not possible to sum directly the drag coefficients but it is possible to sum the products $C_{Di} S_i$. These products are known as the areas of the equivalent flat plate, that is f_i ; since a flat plate normal to the free stream has a drag coefficient equal to 1, f_i represents the area of a flat plate that, when it is normal to the free stream, has the same drag coefficient of the component i . Thus, the previous formulation becomes

$$D = q \sum_{i=1}^n C_{Di} S_i = q \sum_{i=1}^n f_i = q f_{TOT}$$

Moreover, the skin friction coefficient for a generic component is:

$$C_f = \frac{D_f}{qS_{wet}}$$

where S_{wet} represents the wetted area that is the surface of that component wetted by the fluid. The skin friction drag coefficient is

$$C_{Df} = \frac{D_f}{qS_{ref}}$$

thus, it is easy to find that

$$C_{Df} = \frac{D_f S_{wet}}{S_{ref}}$$

The link between a generic component and the flat plate is necessary since the skin friction coefficient is exactly computed for a flat plate so that, once known C_f for the equivalent flat plate, the skin friction drag coefficient becomes a function of the geometry of the component. In fact, the skin friction coefficient for a generic component can be obtained by

$$C_f = \bar{C}_f F_f$$

where \bar{C}_f is the skin friction coefficient for the equivalent flat plate and F_f is the form factor that takes into account that the component is not a flat plate and the boundary layer develops in presence of pressure gradients. Finally, the skin friction drag coefficient of a generic component can be computed as follows

$$\boxed{C_{Df} = \bar{C}_f F_f \frac{S_{wet}}{S_{ref}}} \quad (2.3)$$

In order to point out the contributes of the fuselage to parasite drag, it is possible to split up this contribution in 4 parts:

1. Skin friction contribution
2. Fuselage upsweep contribution
3. Fuselage base drag contribution
4. Windshield contribution

2.1.1 Effect of fineness ratio

Before to study how the semi-empirical methods to calculate a various contributions to C_D , it's important introduce an older approach (reported in [23]) that highlights the effect of one of most important parameter, the fineness ratio L_f/d_f (or slenderness ratio).

The fuselage is considered a body of revolution (ellipsoid). It's possible to calculate the drag coefficient of the axisymmetric fuselage by evaluating the skin friction coefficient of a flat plate, whose surface is equal to the wet surface of the fuselage and the Reynolds number is evaluated on the fuselage length, and a shape factor to account for pressure drag. The formula is:

$$C_D S_{\text{ref}} = C_f S_{\text{wet}} (1 + \phi) \quad (2.4)$$

where C_D is the drag coefficient, S_{ref} is the reference surface, C_f is the flat plate skin friction coefficient, S_{wet} is the wet surface of the fuselage, and ϕ is the shape factor that is a function of the slenderness ratio. The drag coefficient for bodies of different slender ratio and reference area is represented in figure 6. The slender ratio of 1 represents a sphere, whereas very streamlined bodies are indicated by high values of the slender ratio. Three reference areas are considered: the body wetted surface, the body frontal area, and the area representative of the body volume. The drag coefficient strongly depends from the reference area. The curve that refers to the frontal area (which is constant with slender ratio) presents a minimum between values of L_f/d_f between 2 and 3. On the contrary, the curve that refers to the wetted area (which increases with the slender ratio) presents an asymptote equal to the drag coefficient of the flat plate for high values of the slender ratio. Finally, the curve that refers to the volume presents a minimum for $L_f/d_f = 5$.

By looking at these last two curves it is apparent the convenience of high values of the slender ratio, because of the low value of the drag coefficient and the availability of space for payload (bigger volume for a given frontal area).

2.1.2 Skin friction contribution

The fuselage form factor is computed according to the following equation

$$F_{f,\text{fus}} = \left[1 + \frac{60}{\left(\frac{ZLF}{SWF}\right)^2} + 0.0025 \cdot \left(\frac{ZLF}{SWF}\right) \right] \quad (2.5)$$

where ZLF is the fuselage length and SWF is fuselage equivalent diameter. The skin friction coefficient depends on the Reynolds and on the Mach number and it is known for the flat plate since this problem has been analytically resolved. A formulation for the turbulent skin friction coefficient is the following, which has been used in the fuselage estimation

$$C_f^{\text{turb}} = \frac{0.455}{(\log Re)^{2.58} \cdot (1 + 0.144 \cdot M^2)^{0.58}} \quad (2.6)$$

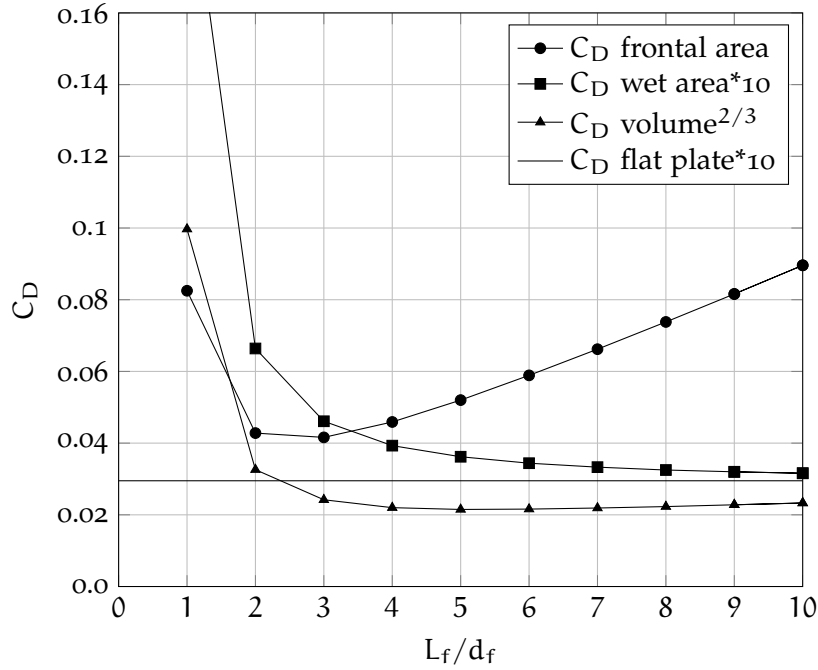


Figure 6: Semi-empirical drag estimation for smooth streamlined bodies (ellipsoid). $Re = 10^7$. Fully turbulent flow. Flat plate analogy [23].

The skin friction coefficient depends on the Reynolds number, which is different for each aircraft components. A "cut-off" Reynolds number Re_{co} has been computed for each component. This Re_{co} depends on the characteristic dimensions of the component, l , (i.e. the length for the fuselage) and on a coefficient k that takes into account the effect of the surface roughness, through the following formulation

$$Re_{co} = 38.21 \cdot \left(\frac{l}{k}\right)^{1.053} \quad (2.7)$$

If the component Reynolds number is greater than Re_{co} , the skin friction coefficient is computed considering Re_{co} in the formulation, otherwise the reference Reynolds number should be used.

Wetted surface

In the semi-empirical methods the wet surface assumes a considerable importance. Therefore it's important estimate the correct value of it for each part of aircraft. As regard the fuselage the wetted area can be computed by adding the contribution of the nose section, cabin section and tapered tailcone. This requires knowledge of the actual fuselage shape, but for typical transport aircraft, the wetted area of the nose and tail cone may be approximated by:

$$S_{wetnose} = 0.75 \cdot \pi \cdot d_f \cdot L_n \quad S_{wettail} = 0.72 \cdot \pi \cdot d_f \cdot L_t \quad (2.8)$$

where d_f is the diameter of the constant section and L_n and L_t are the length of the nose and tailcone respectively.

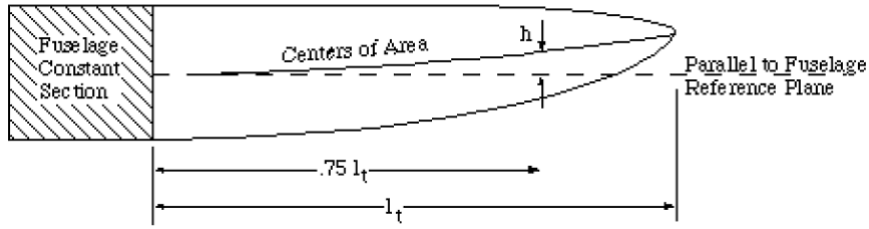


Figure 7: Definition of fuselage upsweep angle.

Considering the effect of the fairing¹ and of the karman², the total wetted area should be increased of about 20% thus leading to :

$$S_{\text{wetFAIR+KARM+FUS}} = 1.20 \cdot S_{\text{wetFUS}}$$

2.1.3 Fuselage upsweep contribution

The drag due to the upward curvature of the aft fuselage is the sum of a fuselage pressure drag increment due to the upsweep and a drag increment due to a loss of lift. Because of the loss of lift, the airplane must fly at a higher wing lift coefficient in order to maintain the required net airplane C_L . This causes an increase in lift-dependent drag [10]. The geometric parameter used to correlate upsweep drag with fuselage shape is the vertical displacement of the fuselage centerline in the tail cone above the fuselage reference plane. The vertical position of the center of cross-sectional area is measured, not at the end of the fuselage, but at a point that is located 75% of the total upsweep length (see figure 7). The parameter is thus $(\frac{h}{l})_{.75l_t}$. This is to minimize the effect of modifications at the very aft end of the fuselage that do not produce much change in the effective upsweep. The total upsweep drag increment (including each of the two terms discussed previously) increases with the parameter, $(h/l)_{.75l_t}$, according to the following expression, derived from wind tunnel data:

$$C_{D\pi_{\text{upsweep}}} = 0.075 \cdot \left(\frac{h}{l}\right)_{.75l_t} \quad (2.9)$$

The subscript π denotes the fact that this C_D is nondimensionalized by fuselage maximum cross-sectional area, rather than reference wing area. To obtain the increment in C_D based on wing area, remember to multiply by the ratio of fuselage cross section area to wing area. Typical values of $C_{D\text{upsweep}}$ are around 0.006. Two points are of interest with regard to aft-fuselage upsweep [10]:

1. Tests of fuselage shapes in the absence of the wing yield results that greatly overestimate the magnitude of the upsweep drag.

¹ fairing is a structure in the areas of landing gear whose primary function is to produce a smooth outline of the fuselage in order to reduce the drag

² karman is the fuselage-wing joint surface

2. Wind tunnel test results have indicated that the loss of lift due to upsweep is significantly greater than just the download on the aft fuselage, which suggests that there is a flow change over the wing and forward fuselage due to the aft-fuselage upsweep. Also, the net change in pitching moment due to upsweep is an increased nose-down moment instead of a nose-up moment that might be expected. As a result, the loss in lift does not complement the download on the tail that is required to trim the airplane. In fact, the effect of upsweep is to slightly increase the airplane trim drag.

2.1.4 Fuselage base drag contribution

The base drag coefficient is not negligible for bodies of revolution such as the fuselage and nacelles, since the flow is not completely attached to the body, but it separates in its rear part generating an increase of the total drag coefficient. In order to clarify the origin of this drag source, the flow around the reference fuselage has been compared with that around an other geometry which has a different tailcone (more sharp than that of reference). The comparison has been carried out with the CFD software *Star-CCM+*. Figure 8 shows the flow in the rear part is attached for the reference fuselage while for the other there's a separation due to a squat shape of rear part, which causes a higher base drag.

The base drag coefficient can be computed using the following formulation for a body of revolution [20]:

$$C_{D_{\text{base}}} = \left\{ 0.029 \cdot \left(\frac{d_b}{d} \right)^3 / \left[C_D \cdot \left(\frac{S_{\text{ref}}}{S} \right) \right]^{1/2} \right\} \left(\frac{S}{S_{\text{ref}}} \right) \quad (2.10)$$

where d_b is the base diameter, d is the diameter of the body of revolution, C_D is the skin friction drag coefficient of the body of revolution, S_{ref} is the reference surface, and S is the surface of the body of revolution (i.e. the maximum frontal area). In the figure 9, the plot of drag due to the form of rear part as a function of the tailcone fineness ratio is reported.

2.1.5 Windshield contribution

Profile drag is a strong function of front body shape. Blunt forebodies promote flow separations which lead to high profile drag. Fore-body bluntness can be caused by:

- Poor cockpit window or canopy shaping
- Requirement for front and loading

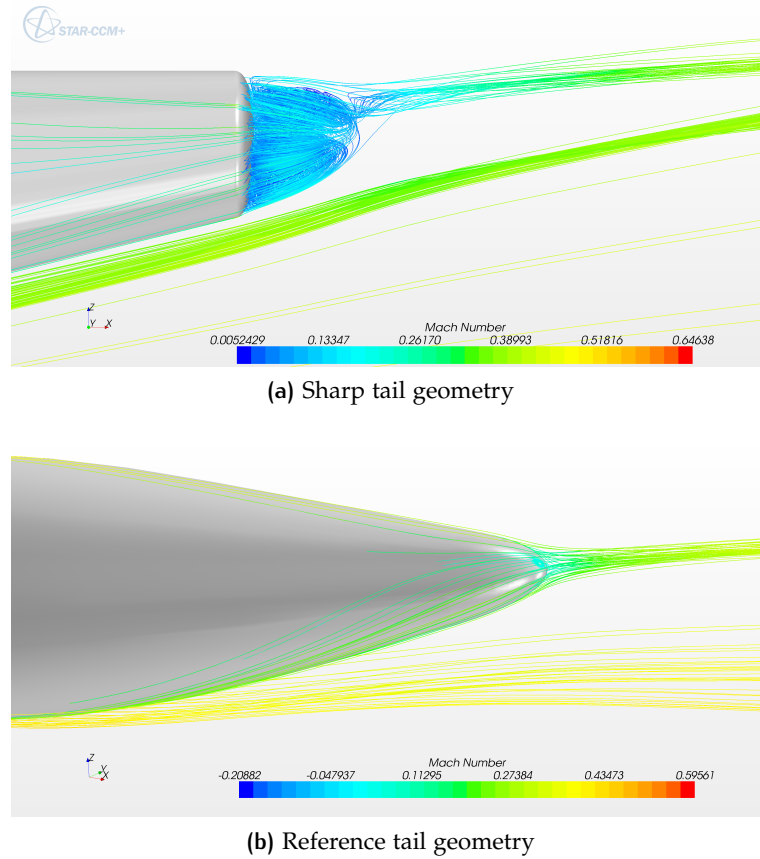


Figure 8: Flow around the rear part of the fuselage.

The ideal "streamline" nose shape can be achieved only if the windshields are integrated into the surface fuselage. Although drag can be considerably reduced by these types of windshield fairing, image distortions may be introduced if the "fairing angle" becomes too acute. In the case of transport aircraft the requirement for good visibility from the cockpit becomes a dominant design criterion. This calls for a large canopy. Therefore the canopy drag becomes an important factor in the design of the fuselage. The contribution of the windshield can be estimated as a percentage of the fuselage drag coefficient referred to the streamlined configuration [20].

If the skin friction drag coefficient ($C_{D_{sf}}$) of the fuselage is known, the effect of the windshield can be estimated as follows (for $\Delta C_{D_{ws}}$ and $C_{D_{FUS}}$ see figure 10):

$$C_{D_{ws}} = \frac{\Delta C_{D_{ws}}}{C_{D_{FUS}}} \cdot C_{D_{sf}} \quad (2.11)$$

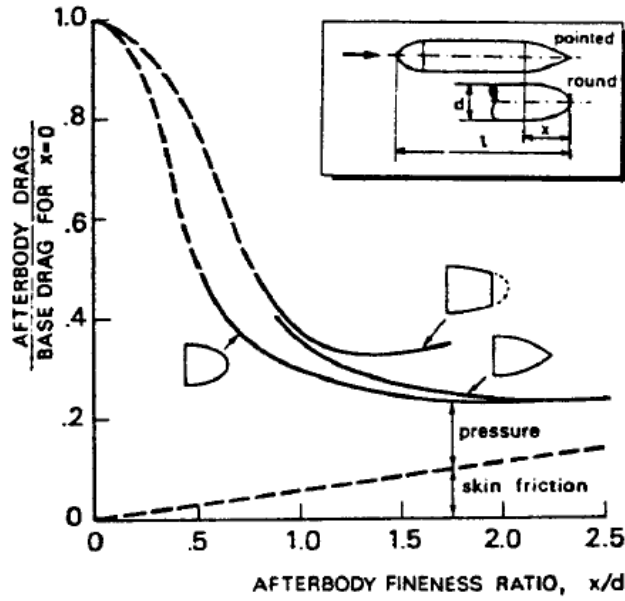


Figure 9: Afterbody drag of a fuselage tail [23].

2.2 FUSELAGE MOMENT COEFFICIENT PREDICTION

It is known that the contribution of the fuselage to the static longitudinal stability of the airplane are nearly always destabilizing, and in many cases the destabilizing effects are quite large in magnitude [17]. If the fuselage is considered operating at some angle of attack to the free stream in an ideal fluid, the resulting pressure distribution over the fuselage yields only a pure couple, with no resultant force, the center of pressure being at infinity.

M. Munk [15] demonstrated that, for a very slender body of revolution, the variation of the pitching moment with angle of attack in degrees is a function of the volume and the dynamic pressure.

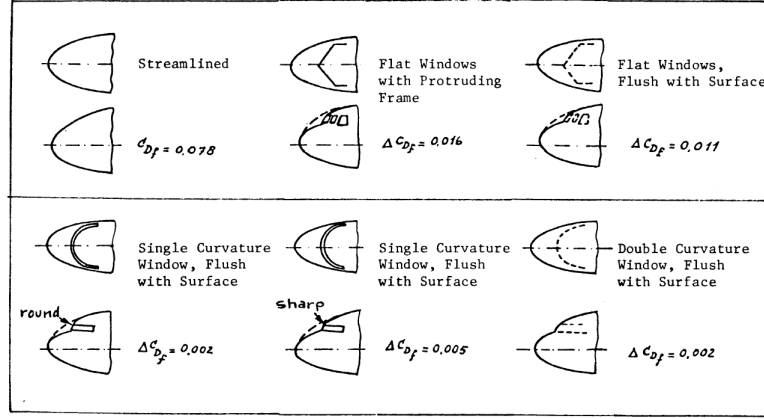
$$\left(\frac{\partial M}{\partial \alpha}\right) = \frac{\text{Volume}}{28.7} \cdot q \quad (2.12)$$

This equation is corrected by a factor $(K_2 - K_1)$, depending on the fuselage fineness ratio (L/D) as given in figure 11.

$$\left(\frac{\partial M}{\partial \alpha}\right) = \frac{\text{Volume}}{28.7} \cdot q \cdot (K_2 - K_1) \quad (2.13)$$

For axially unsymmetric bodies equation (2.13) can be written as approximately

$$\left(\frac{\partial M}{\partial \alpha}\right) = \frac{q \cdot (K_2 - K_1)}{36.5} \cdot \int_0^{l_f} w_f^2 dx \quad (2.14)$$



C_{D_f} = Fuselage Drag Coefficient Referenced to the Frontal Area of the Fuselage

ΔC_{D_f} = Drag Coefficient of the Windshield Referenced to the Frontal Area of the Fuselage

Figure 10: Semi-empirical method for estimation of windshield drag contribution [20].

where w_f^2 is the local width of the fuselage, and dx an increment of fuselage length l_f .

The wing's induced flow, consisting of heavy upwash in front of the wing due to the bound vortex, has a heavy destabilizing influence on the fuselage sections ahead the wing, whereas the downwash behind the wing reduces the unstable contribution of the fuselage segments behind the wing.

Multhopp proposed the formula (2.15) to account for this phenomenon:

$$\left(\frac{\partial M}{\partial \alpha}\right) = \frac{q}{36.5} \cdot \int_0^{l_f} w_f^2 \left(\frac{\partial \beta}{\partial \alpha}\right) dx \quad (2.15)$$

where β is the angle of the local flow and is equal to the free stream angle of attack plus the induced flow due to wing. Ahead of the wing the induced upwash adds to the angle of free stream, making $(\partial \beta / \partial \alpha)$ greater than unity, while behind the wing the induced downwash subtracts from the free stream angle and $(\partial \beta / \partial \alpha)$ is less than unity and becomes $(1 - \partial \epsilon / \partial \alpha)$ at the tail. In the region between the wing leading and trailing edge, $(\partial \beta / \partial \alpha)$ is considered zero.

The integral equation (2.15) is evaluated by dividing the fuselage into segments (see 12), computing the value of $w_f^2 (\partial \beta / \partial \alpha) \cdot \Delta x$ for each segment and adding them up. For the evaluation of contributions please refer to [14]. A simpler, but less accurate, method for estimating the fuselage contribution to equilibrium and stability is to use the following formula [17]:

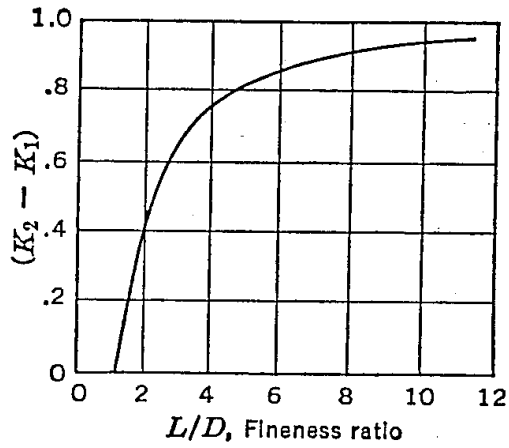


Figure 11: Fuselage correction for fineness ratio.

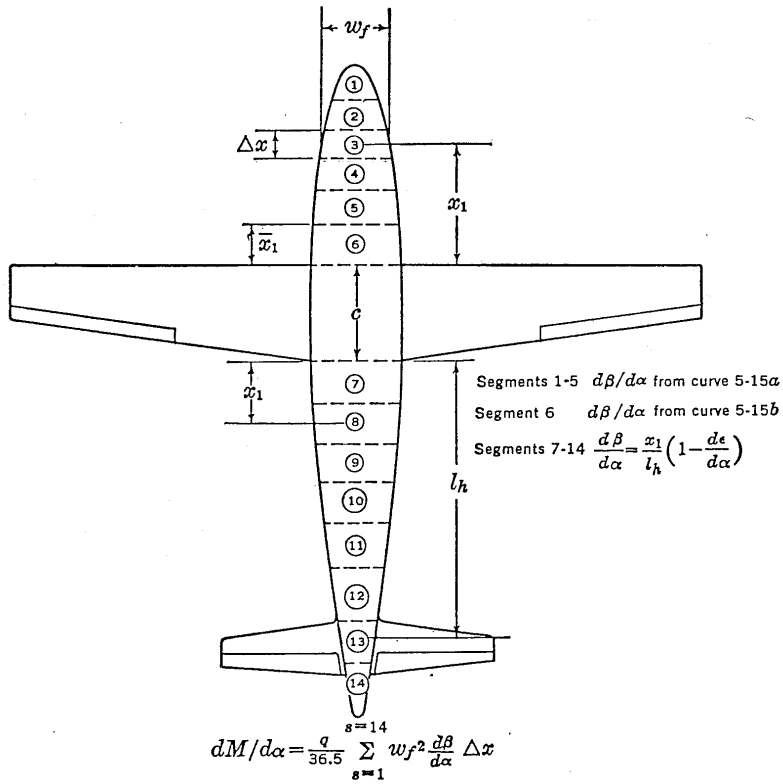


Figure 12: Typical layout for computing fuselage moments.

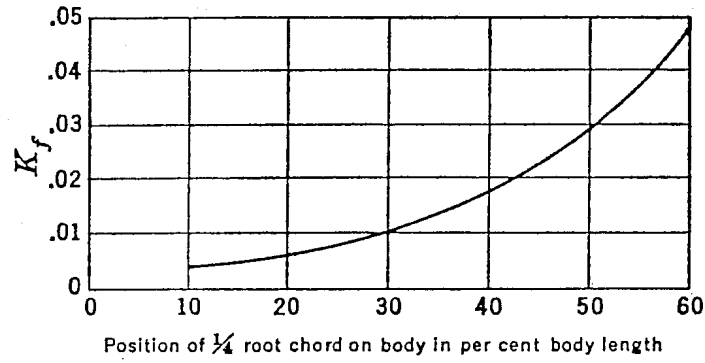


Figure 13: Fuselage stability coefficient. From [7].

$$\left(\frac{\partial C_M}{\partial C_L} \right) = \frac{K_f \cdot w_f^2 \cdot L_f}{S_w \cdot c \cdot C_{L\alpha}} \quad (2.16)$$

where L_f is the overall fuselage length, w_f is the maximum width of the fuselage, c is the m.a.c. and the K_f is an empirical factor developed from experimental evidence [7]. The variation of this factor with the wing position is given in figure 13.

2.3 EXAMPLE OF APPLICATION

In this section the semi-empirical methods are used to obtain the drag and moment coefficients for the most famous regional turboprops, that's to say the ATR-72 (figure 14) and Bombardier Dash8-Q400 (figure 15). The aircraft data have been taken from [2], [9] and [5].

2.3.1 Drag estimation for ATR-72

As it has been seen in the previous sections, in the fuselage parasite drag contributions can be accounted:

1. Skin friction contribution
2. Fuselage upsweep contribution
3. Fuselage base drag contribution
4. Windshield contribution

Skin friction contribution

The skin friction contribution can be evaluated from equation 2.3 and therefore it is necessary to estimate the form factor and the skin friction coefficient. The latter is obtained from equation 2.6, with the

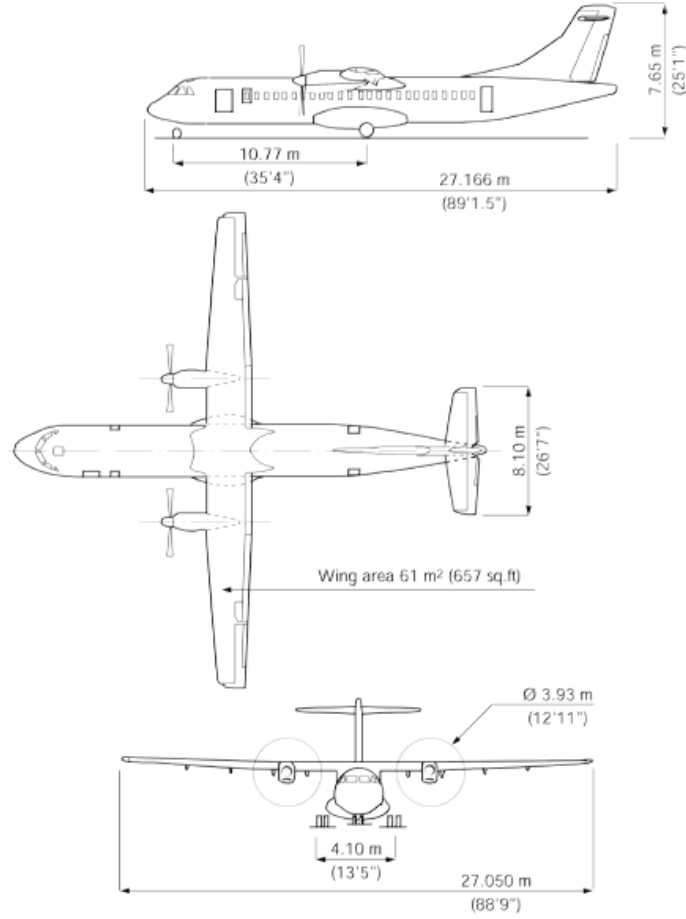


Figure 14: ATR-72 dimensions.

Mach and the Reynolds number (the last one referred to fuselage length) respectively equal to 0.43 and to 138×10^6 . In table 2 the necessary parameters are shown. From equations 2.8 it has been possible to estimate the wet surfaces of the nose and of the tailcone, while for cabin, the wet surface is simply equal to that of a cylinder.

$$S_{\text{wet}_{\text{nose}}} = 0.75 \cdot \pi \cdot d_f \cdot L_n = 32.84 \text{ m}^2$$

$$S_{\text{wet}_{\text{cabin}}} = \pi \cdot d_f \cdot L_c = 99.10 \text{ m}^2$$

$$S_{\text{wet}_{\text{tail}}} = 0.72 \cdot \pi \cdot d_f \cdot L_t = 63.05 \text{ m}^2$$

$$S_{\text{wet}} = S_{\text{wet}_{\text{nose}}} + S_{\text{wet}_{\text{cabin}}} + S_{\text{wet}_{\text{tail}}} = 195.00 \text{ m}^2$$

	ZLF (m)	SWF (m)	S_{wet} (m ²)	S_{ref} (m ²)	k_f (m)	\bar{C}_f
Value	27.17	2.70	195.00	61.00	0.405×10^{-5}	0.0019

Table 2: The parameters of ATR-72 to compute the skin friction contribution to drag coefficient.

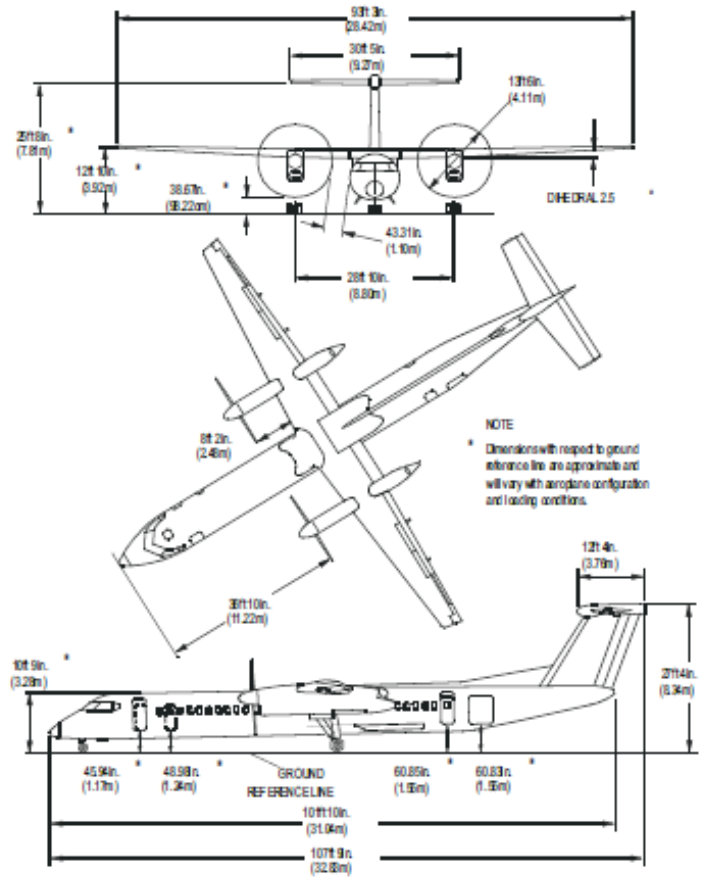


Figure 15: Bombardier Dash8-Q400 dimensions.

The fuselage Reynolds number is lower than Re_{co} (to compute the Re_{co} , see equation 2.7), therefore the skin friction coefficient is computed considering the reference Reynolds number.

$$F_{f,fus} = \left[1 + \frac{60}{\left(\frac{ZLF}{SWF}\right)^2} + 0.0025 \cdot \left(\frac{ZLF}{SWF}\right) \right] = 1.0840$$

The value of the skin friction coefficient is the following.

$$C_{D_{sf}} = \bar{C}_f F_f \frac{S_{wet}}{S_{ref}} = 0.0069;$$

Fuselage upsweep contribution

The contribution of the upsweep angle to drag can be evaluated from equation 2.9, where h is equal to 0.61 m and l equal to 13.4 m (these values can be pull out graphically from figure 14).

$$C_{D_{\text{upsweep}}} = 0.075 \cdot \left(\frac{h}{l}\right) \cdot 0.75lt = 0.0003$$

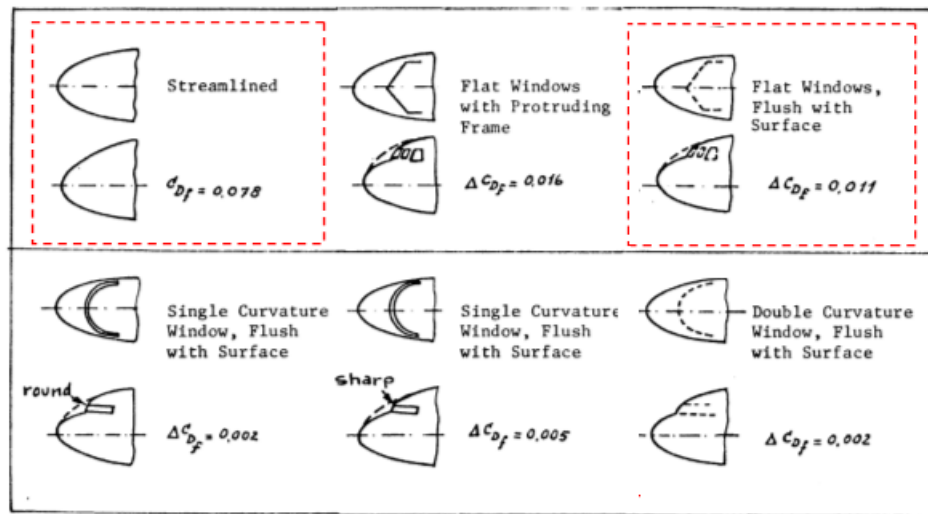
Fuselage base drag contribution

The contribution of the base drag can be evaluated from equation 2.10, where d_b is equal to 0.35 m (estimated from the figure 14), d is the fuselage diameter (SWF in the table 2), S and S_{ref} are respectively the wet and reference surface, and these are reported in table 2.

$$C_{D_{\text{base}}} = \left\{ 0.029 \cdot \left(\frac{d_b}{d}\right)^3 / \left[C_D \cdot \left(\frac{S_{\text{ref}}}{S}\right) \right]^{1/2} \right\} \left(\frac{S}{S_{\text{ref}}}\right) = 0.0002$$

Windshield contribution

The windshield contribution can be evaluated from equation 2.11 and with the help of the figure 16.



C_{D_f} = Fuselage Drag Coefficient Referenced to the Frontal Area of the Fuselage

ΔC_{D_f} = Drag Coefficient of the Windshield Referenced to the Frontal Area of the Fuselage

Figure 16: Windshield drag contribution for the ATR-72.

$$C_{D_{WS}} = \frac{\Delta C_{D_{WS}}}{C_{D_{FUS}}} \cdot C_{D_{sf}} = 0.0010$$

Once estimated the different contributions, the total drag coefficient is simply the sum of these contributions.

$$C_D = C_{D_{sf}} + C_{D_{upsweep}} + C_{D_{base}} + C_{D_{ws}} = 0.0085$$

2.3.2 Drag estimation for Dash8-Q400

In a similar manner to what was done for the ATR-72, in this section the semi-empirical methods are used to estimate the different contributions to drag coefficient for Dash8-Q400. The flight conditions are the similar those of ATR-72: Mach number equal to 0.50 and Reynolds number (referred to fuselage length) equal to 149×10^6 . The wet surfaces are estimated with equations 2.8 and in the table 3, the necessary parameters are reported.

$$\begin{aligned} S_{\text{wet}_{\text{nose}}} &= 0.75 \cdot \pi \cdot d_f \cdot L_n = 22.04 \text{ m}^2 \\ S_{\text{wet}_{\text{cabin}}} &= \pi \cdot d_f \cdot L_c = 149.14 \text{ m}^2 \\ S_{\text{wet}_{\text{tail}}} &= 0.72 \cdot \pi \cdot d_f \cdot L_t = 60.32 \text{ m}^2 \\ S_{\text{wet}} &= S_{\text{wet}_{\text{nose}}} + S_{\text{wet}_{\text{cabin}}} + S_{\text{wet}_{\text{tail}}} = 231.51 \text{ m}^2 \end{aligned}$$

	ZLF _(m)	SWF _(m)	S _{wet} (m ²)	S _{ref} (m ²)	k _f (m)	\bar{C}_f
Value	31.04	2.69	231.51	63.08	0.405×10^{-5}	0.0020

Table 3: The parameters of Dash8-Q400 to compute the skin friction contribution to drag coefficient.

As before, the fuselage Reynolds number is lower than Re_{c_o} therefore the skin friction coefficient is computed considering the reference Reynolds number.

$$F_{f, fus} = \left[1 + \frac{60}{\left(\frac{ZLF}{SWF}\right)^2} + 0.0025 \cdot \left(\frac{ZLF}{SWF}\right) \right] = 1.0679$$

The value of the skin friction coefficient is the following.

$$C_{D_{sf}} = \bar{C}_f F_f \frac{S_{\text{wet}}}{S_{\text{ref}}} = 0.0078$$

The contribution of the upsweep angle to drag can be evaluated from equation 2.9, where h is equal to 0.97 m and l equal to 7.43 m (these values can be pull out graphically from figure 15).

$$C_{D_{upsweep}} = 0.075 \cdot \left(\frac{h}{l}\right)_{.75lt} = 0.0009$$

The contribution of the base drag can be evaluated from equation 2.10, where d_b is equal to 0.35 m (estimated from the figure 14), d is the fuselage diameter (SWF in the table 2), S and S_{ref} are respectively the wet and reference surface, and these are reported in table 2.

$$C_{D_{base}} = \left\{ 0.029 \cdot \left(\frac{d_b}{d} \right)^3 / \left[C_D \cdot \left(\frac{S_{ref}}{S} \right) \right]^{1/2} \right\} \left(\frac{S}{S_{ref}} \right) = 0.0001$$

The windshield contribution can be neglected because, unlike the ATR-72, the shape of the nose is very smooth as it can be seen from figure 17.



(a) ATR-72

(b) Dash8-Q400

Figure 17: The comparison of the nose shape.

$$C_{D_{ws}} = 0$$

The total drag coefficient is simply the sum of the contributions.

$$C_D = C_{D_{sf}} + C_{D_{upsweep}} + C_{D_{base}} + C_{D_{ws}} = 0.0088$$

2.3.3 Pitching moment estimation for ATR-72

The strip method has been used to evaluate the moment coefficient at α equal to 0° and the moment curve slope for ATR-72. The fuselage is divided into 46 strips (20 forward the wing, 6 on the wing, and 20 behind the wing) as it's possible to see in the figure 18. The flight conditions are the same of that used to estimate the drag coefficient (for ATR-72).

- $M = 0.43$
- $Re_{L_f} = 138 \times 10^6$
- $\alpha = 0^\circ - 2^\circ$

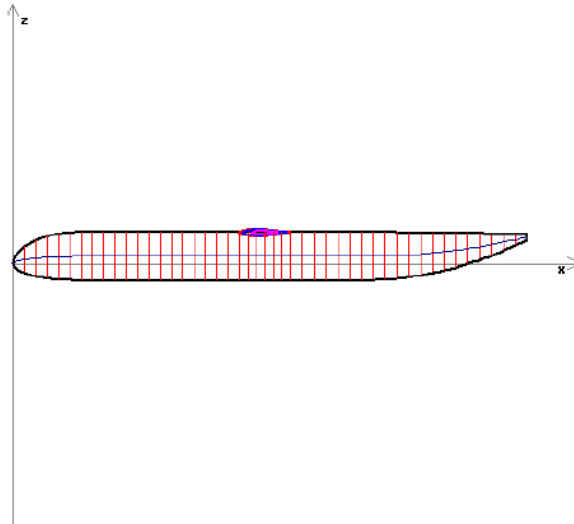


Figure 18: Strips for ATR-72

The results are the following.

$$C_{M_{\alpha=0}} = -0.0832$$

$$C_{M_{\alpha}} = 0.0222$$

2.3.4 Pitching moment estimation for Dash8-Q400

The strip method has been used also to evaluate the moment coefficient at α equal to 0° and the moment curve slope for Dash8-Q400. As before the fuselage are divided into 46 strips (20 forward the wing, 6 on the wing, and 20 behind the wing). The flight conditions are the same of that used to estimate the drag coefficient (for Dash8-Q400).

- $M = 0.50$
- $Re_{L_f} = 149 \times 10^6$
- $\alpha = 0^\circ - 2^\circ$

The results are the following.

$$C_{M_{\alpha=0}} = -0.0859$$

$$C_{M_{\alpha}} = 0.0247$$

3 | A NUMERICAL APPROACH

The method developed in this thesis permits to evaluate the aerodynamic coefficients for fuselages of an entire aircraft category (regional turboprops) and it can be very helpful in preliminary design phase because it permits to make trade-offs choices quickly. The need to develop a numerical approach to predict the aerodynamic coefficients is due to lack of experimental data. In fact, to extract the fuselage contributions to aerodynamic forces from flight tests, when possible, is quite difficult. Moreover the wind-tunnel tests data, those of public domain, are referred to geometries of fuselage too different from that of a turboprop. For instance, Abbott evaluated, in a density variable wind-tunnel, the drag coefficient for few forms of fuselage but all these have a fineness ratio equal to 5 [1]. Draley studied the drag coefficient but taking into account the "wing-body" configuration [6]. However, even in this case, the geometries were very different from that of a turboprop. In the figure 19 is reported a comparison of the geometries cited before. An other limit for the wind-tunnel tests is one for which is possible to investigate only few fuselage geometries because it would be necessary to build a different model for each analysis whereas with the CFD method is possible to investigate lots of geometries varying the numerical model in a small amount of time. Perhaps this aspect is the most important strength point for the CFD approach.

The lack of experimental data is a problem also to validate the numerical results. However it has emerged from five NASA workshops about the aerodynamics drag prediction [11], that maybe it is not necessary to make a comparison between the experimental and numerical results to validate the latter, because the boundary condi-

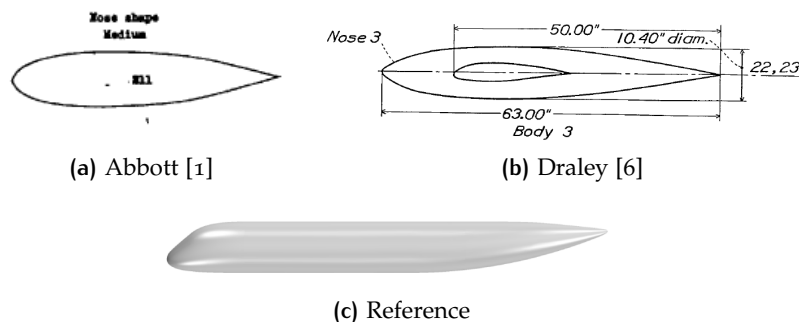


Figure 19: Comparison of analysed geometries experimentally with that of reference.

WIND TUNNEL TEST		CFD
Walls		Free Air
Support System (Sting)		Free Air
Laminar/Turbulent (Tripped)	"Fully" Turbulent (usually)	
Aeroelastic Deformation		Rigid
Measurement Uncertainty	Numerical Uncertainty & Error	
Corrections for known effects		No Corrections

Table 4: Reasons to not compare CFD and wind-tunnel results [11].

tions are quite different. The table 4 summarizes the reasons of the above. From the last workshop it was come light that:

- Drag comparisons to wind tunnel generally favorable (although it is not clear if they actually would have to agree).
- Force/Moment predictions are better at low α

In this thesis, the numerical results have been validated comparing it with that presented in [5] and with other previous works done by DIAS (now DII).

To investigate numerous fuselage shapes, a MATLAB script has been developed to modify a given reference geometry. The modifications concern the fineness ratio of nose, cabin and tailcone, the upsweep angle or the windshield angle. It's possible to do multiple changes at the same time. The modifications are done altering the disposition of the sections along x or z axis or along both directions. Afterwards the geometry is passed to *Star-CCM+* where the new CAD model is obtained through the loft¹ operation. The latter is possible to build the numerical domain in automatically using JAVA macros. To cut down the CPU time, the software *Star-CCM+* has been used on the University's grid computing infrastructure SCoPE to simulate lots configurations. The files and the procedure necessary to run the simulation on SCoPE are reported in appendix B. The post-processing has been done in automatic way using *Star-CCM+* in batch mode in MATLAB environment and two JAVA macros which extract the aerodynamic coefficients. Data results have been gathered and plotted in charts to highlight trendlines of aerodynamic coefficients with geometric parameters. In the figure 20 is reported the work flow.

In the following sections the software *Star-CCM+* and SCoPE are described in depth. These sections are excerpt from [4]. Afterwards it is analysed the numerical model used for the simulations and the test cases done to raise the mesh quality. Finally the MATLAB code that modifies the reference geometry is introduced.

¹ Please see [21]

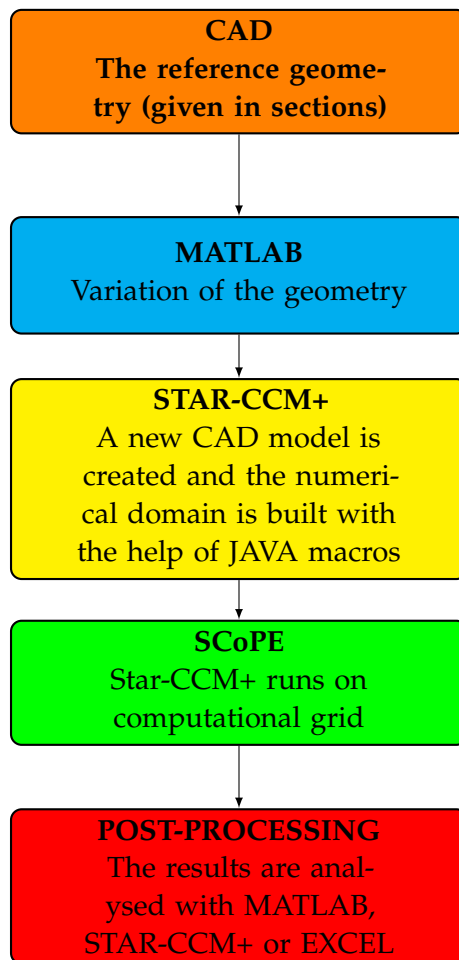


Figure 20: The workflow of the proposed methodology.

3.1 THE SOFTWARE STAR-CCM+

Solving the Navier-Stokes equations, even in their simplest form, for a three-dimensional complex geometry, it's not a trivial task. It is necessary a (bundle) software that provides CAD geometry import, mesh generation, solver and post-process analysis. It has to be reliable and possibly easy to use, the latter to better concentrate on the physics of the problem. Star-CCM+ is more than a Computational Fluid Dynamics (CFD) solver. It is an entire engineering process for solving problems involving flow (of fluids or solids), heat transfer and stress, based on object-oriented programming technology. It can handle large models with parallel solver both in local (desktop computer) and on hundreds of CPU on a cluster grid by CLI. In the local client everything run in a single environment, from the geometry creation to the results visualization.

Another interesting feature is the possibility to automate tasks with Java macros. They can be recorded and played inside the software environment, though they can be edited manually and called from

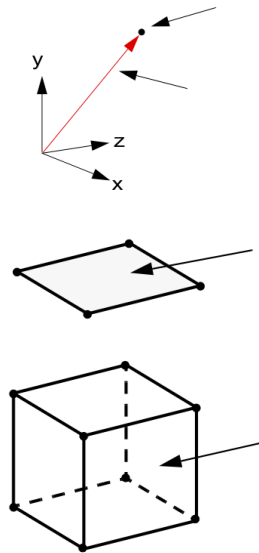


Figure 21: Vertex, face and cell definition in Star-CCM+.

CLI. This resulted convenient in the present work, since lot's of runs were similar, changing only a parameter per run. Java macros are mandatory when executing Star-CCM+ on a cluster grid like SCoPE.

Star-CCM+ solver is based on the finite volume method. The solution domain is subdivided into a finite number of small control volumes, called *cells*, formed by a collection of *faces*, that in turn are a collection of *vertices* (points in space defined by a position vector, see figure 21). The faces of a cell should not intersect each other, except where they touch along the common edges, that is the control volumes must not overlap. The *volume mesh* obtained is the mathematical representation of the space where the problem is being solved, i.e. the computational domain. To preserve sharp edges, *feature curves* can be defined. Last, but not least, the software generates a single simulation (.sim) file, containing everything necessary to run locally.

3.1.1 Simulation workflow

The most general workflow is represented in Figure 22 and briefly described here.

GEOMETRY can be imported from other CAD software or created directly in Star-CCM+ , though in version 8.04 (used in this work) the CAD environment can handle only very simple shapes. Whatever the method, geometry is a collection of surfaces and curves.

SIMULATION TOPOLOGY is the computational model defined as *regions* and *boundaries* to which physics can be applied. For external aerodynamics, a volume (e. g.a block shape) representing

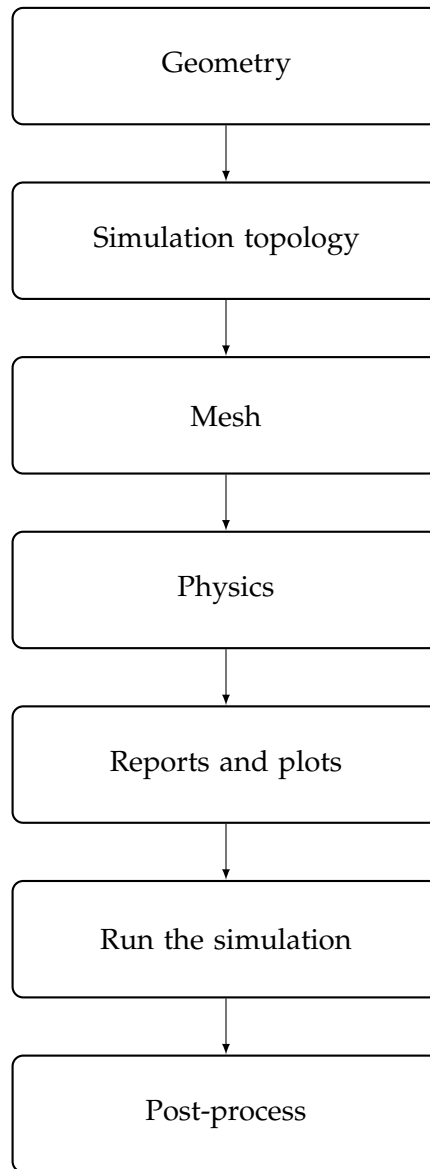


Figure 22: General sequence of operations in a Star-CCM+ analysis.

the fluid domain to be simulated must contain the entire geometry inside.

MESH is the numerical domain. Star-CCM+ can easily and automatically generate surface and volume mesh, once defined several parameters, including size and refinement quality.

PHYSICS MODELS can be easily enabled. Star-CCM+ can handle single and multi-phase fluid flow, heat transfer, turbulence, solid stress, dynamic fluid-body interaction, aeroacoustics and related phenomena.

REPORTS, MONITORS AND PLOTS should be defined and activated to check for convergence, since Star-CCM+ uses an iterative

procedure to reach the solution to the transport equations that satisfies the boundary conditions for a chosen scenario.

RUN THE SIMULATION will automatically initialize the solution and launch the solver. For an interactive session, residuals will be plotted in the client workspace and reported in the output window. For batch sessions, residuals will be echoed to the command console. The simulation can be stopped and resumed anytime.

RESULTS can be visualized with *scenes* as contours, vectors and streamlines. It is possible to create animated scenes. Scatter plots are also possible. In an interactive session, graphical results can be visualized as the simulation run, step by step.

3.1.2 Main mesh parameter

For a greater clarity, the definitions of principal mesh parameters are reported in the table 5. It is recommended to read [21].

Base Size	Characteristic dimension of the model.
Number of Prism Layers	Number of cell layers that are generated within the prism layer on a boundary surface.
Stretch Factor	Ratio of the thickness of one cell layer to the thickness of the cell layer beneath it.
Prism Layer Thickness	Total overall thickness of all the prism layers.

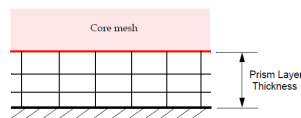
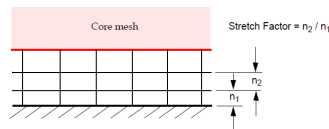
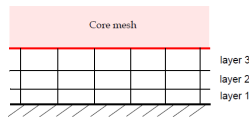


Table 5: Principal mesh parameters [21].

3.1.3 Convergence

The stopping criterium chosen is a prescribed number of iterative steps order of magnitude as thousand. Convergence is judged by looking at the oscillations of the aerodynamic coefficients and the wall y^+ . The oscillations must be reduced beneath of a certain threshold that, in this work, has been fixed equal to $\pm 10^{-6}$. Having chosen Spalart-Allmaras as turbulence model, it is important to check the value of the dimensionless wall distance

$$y^+ = \frac{u^*y}{\nu} \quad (3.1)$$

where y is the normal distance from the wall to the wall-cell centroid, u^* is a reference velocity and ν is the kinematic viscosity. According to the model's formulation, the entire turbulent boundary layer, including the viscous sublayer, ought to be accurately resolved and the model can be applied on fine meshes, that is small values, order of magnitude as unity, are required [21].

3.2 THE SCOPE GRID INFRASTRUCTURE

At time of writing, no desktop computer could handle CFD 3D simulations of millions of cells in a reasonable amount of time. This work saw the light also thanks to the availability of the University's cluster grid, since lots of configurations, from wing alone to the whole airplane, at several angles of incidence and Reynolds numbers had to be analyzed. Runs with 16, 32 or 64 CPUs per simulation were commons to get results within a day.

SCoPE is a scientific data center, based on a grid computing infrastructure, and it is a collaborative system for scientific applications in many areas of research. It is a project started in 2006 by the University of Naples 'Federico II'.

The data center hosts about 300 eight-core blade servers, 220 terabyte of storage, and is already able to accommodate 500 more servers. Actually it has over 2400 CPUs. The scientific applications are of the areas of Astrophysics, Chemistry, Mathematics, Medicine, Engineering and Physics. The data center is located in the Monte S. Angelo Campus, which already hosts the Faculty of Sciences and it is close to the Faculty of Engineering, with kilometers of preexisting optical fibers. The network infrastructure is shown in Figure 23.

Here follows some interesting data:

- localization in a building of about 150 m²;
- power plant capable of delivering 1 MW of electric power in a continuous mode;

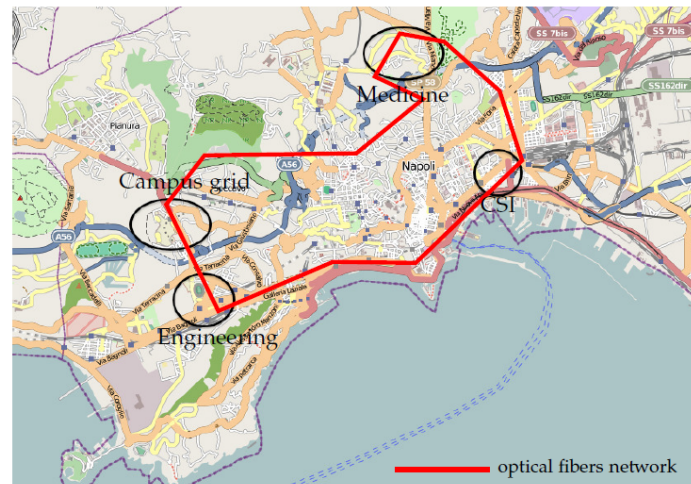


Figure 23: The SCoPE network infrastructure [22].

- efficient cooling system, capable of dissipating 2000 W/m^3 and $30\,000 \text{ W}$ per rack;
- standard (Gigabit Ethernet) networking infrastructure, with a high capacity switching fabric;
- low latency (Infiniband) networking infrastructure, with a single switching fabric for each group of 256 servers;
- large storage capacity, both *NAS* (Network Attached Storage) working with the *iscsi* protocol, and *SAN* (Storage Area Network), working with a Fibre Channel Infrastructure;
- open source (Scientific Linux) for the operating system;
- integrated monitoring system for all the devices of the data center, able to monitor the most relevant parameters of server, storage, networking, as well as all the environmental parameters (as temperature, humidity and power consumption) [13].

Figure 24 is a glance of the data center. Running a Star-CCM+ simulation on SCoPE requires three external files, described in Appendix B.

3.3 NUMERICAL MODEL

The model investigated in this work, as argued in the previous sections, is the fuselage of a regional transport turboprop aircraft with 90 seats. The latter has the dimensions similar to those of ATR-72 fuselage. In order to define the numerical model, in particular way for the mesh, the recommendations of the last NASA workshop [11] have been followed. The numerical domain consists in a parallelepiped which represents the *farfield* with the model of the fuselage located on

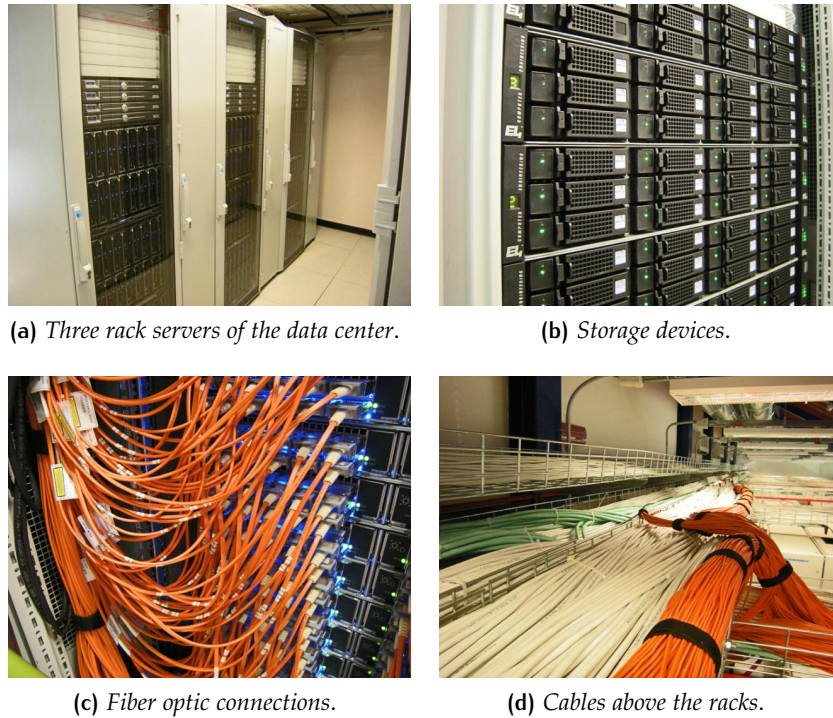


Figure 24: Some images of the SCoPE data center [22].

the longitudinal plane of symmetry, at one third of the block length from the inlet face (figure 25).

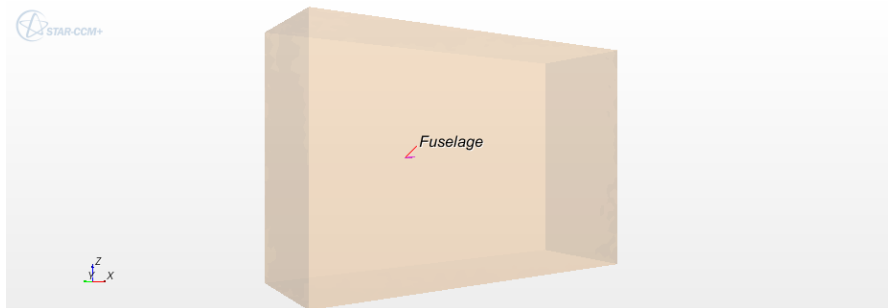


Figure 25: Block shape that defines the fluid domain around the model.

The block defines the *farfield* numerical region which was shaped with the *free stream* boundary condition. As regarding the fuselage the *no-slip* boundary condition was fixed [21]. To modelling flow and energy, it was chosen the *coupled flow* model which solves the conservation equations for mass and momentum simultaneously using a time- (or pseudo-time-) marching approach. One advantage of this formulation is that CPU time scales linearly with cell count; in other words, the convergence rate does not deteriorate as the mesh is refined [21]. The turbulent model chosen is Spalart-Allmaras which solves a single transport equation that determines the turbulent viscosity. This is in contrast to many of the early one-equation models

that solve an equation for the transport of turbulent kinetic energy and required an algebraic prescription of a length scale. Therefore it is faster than other turbulence model and reliable for external aerodynamics [21]. With this model, it must be verified if the value of the dimensionless wall distance y^+ is of order of magnitude as unity. The whole analysis in this work refers to cruise conditions. The main physics and mesh data are resumed in the table 6.

Mesh data	
Mesh type	Polyhedral cells
Base size	12.0 m
Farfield dimensions	$30 \cdot L_f$ $10 \cdot L_f$ $20 \cdot L_f$
Number of prism layers	20
Prism layer stretching	1.3
Number of cells	2380515
Min. cell size	0.1% base size
Target cell size	1% base size
Prism layer size	0.03% base size
Physics data	
Angle of attack	0° - 2°
Reynolds number	2.02×10^8 (based on L_f)
Mach number	0.52
Flow regime	Fully turbulent (Spalart-Allmaras model)

Table 6: Mesh and physics data for numerical model.

3.3.1 Test-cases

The test-cases have been performed to compare two kinds of passengers accommodation and to improve the mesh quality. In the first case it was chosen the 5 abreast accommodation for the passengers to achieve a comfort comparable to that of transport jet. The advantages of 5 abreast comparing with 4 abreast can be resume as following [8].

- Cargo area sub-floor shorter and more usable; ample luggage in the cabin.
- Easier installation of landing gear.
- Less two emergency doors.
- Less one component of cabin crew.

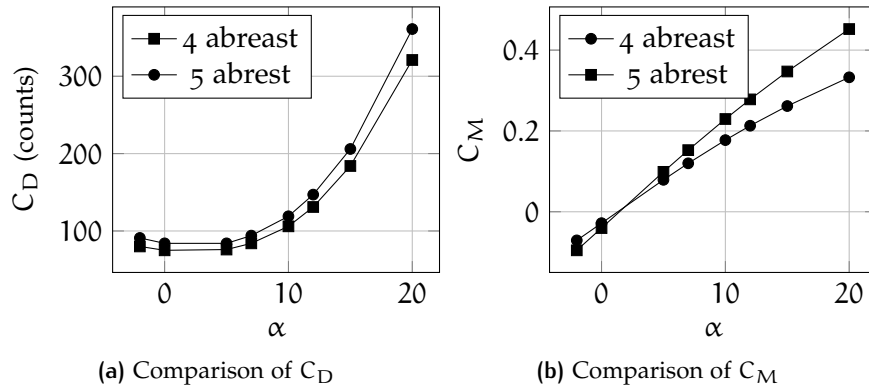


Figure 26: Aerodynamic comparison between 4 and 5 abreast fuselage. $M = 0.52$, $Re = 11.5 \times 10^6$.

From aerodynamic point of view, the choice of 5 abreast is little disadvantageous [16]. As evidence, a comparison between 4 and 5 abreast fuselage configuration has been done. In the figure 26 are reported the results of comparison. For the 5 abreast configuration a certain amount of drag counts plus and a lower longitudinal stability. This is the price to pay for a more comfortable fuselage.

Other test-cases have been performed, both to assess how fine must be the mesh to provide an accurate and computationally affordable result. A typical mesh scene is reported in figure 27.

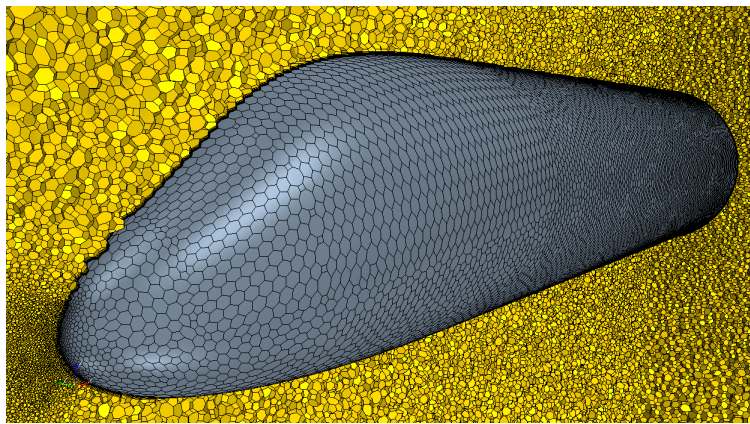


Figure 27: Mesh around the reference fuselage.

The optimal value for the mesh size has been calculated by scaling a mesh with a good representation of the underlying geometry and running a simulation in the same cruise conditions ($M = 0.52$, $Re = 17.4 \times 10^6$). The aerodynamic drag coefficient C_D has been plotted versus the number of cells of each mesh (figure 28). Once the C_D curve does not vary with the number of cells, the "mesh convergence" has been achieved. It means that it is not useful to increase the number of cells because the aerodynamic coefficients do not vary, whereas the

computational time increases. Finally the figure 29 shows how the value of y^+ is less than unity as desired.

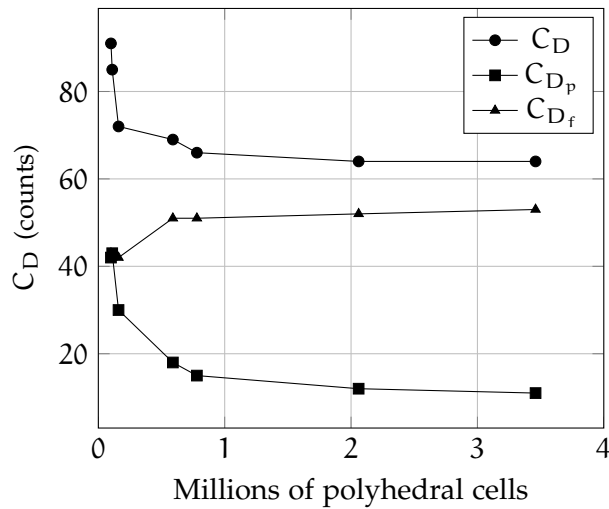


Figure 28: Test case on mesh convergence. $M = 0.52$, $Re = 17.4 \times 10^6$.

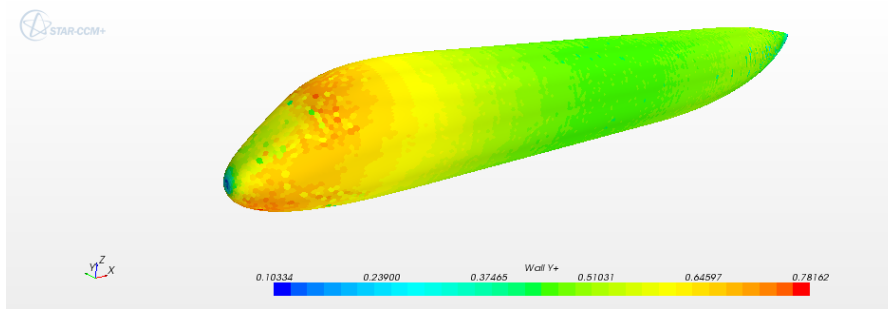


Figure 29: The y^+ value for the reference geometry.

3.4 PROCESSING OF GEOMETRY WITH MATLAB

The geometry of fuselage was modified through a MATLAB script which, as mentioned before, allows to modify the fineness ratio of each part of the fuselage (nose, cabin and tailcone), the windshield and/or the upsweep angle. The code is implemented in a "interactive" way, that's to say it prompts to user what changes to make avoiding to look for the part of interest within the code. This feature is very helpful because it makes the code *user friendly*. In the figure 30 there's an example of a work window.

The reference fuselage has been divided into 43 sections which are imported in MATLAB. For each of them the points are stored in a cell array². Therefore each cell of the array incorporates the points of one

² For a definition of cell array see [12]

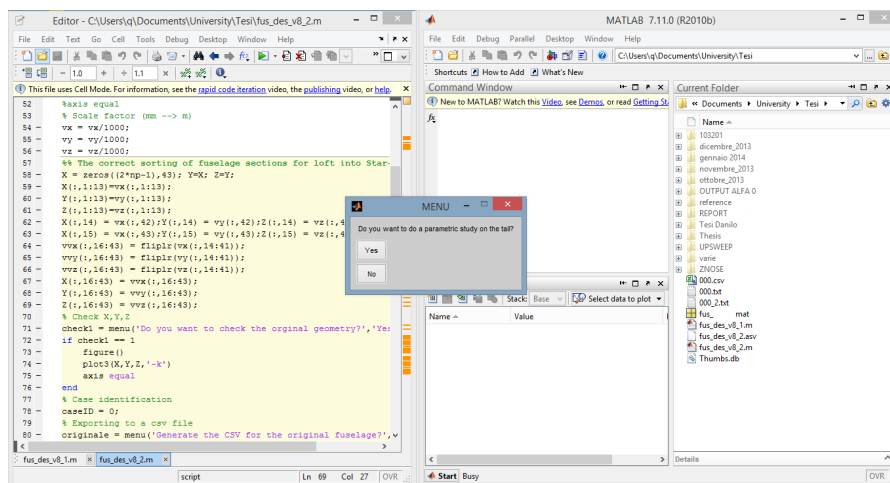


Figure 30: An example of work window.

section. It is necessary to sort the sections along the x axis. At this point, the geometry of fuselage is ready to be modified. The part of the code described until now is reported in the listing 1. In particular, the next part is excerpt from the ninth version of the code. This initial part is equal for all versions.

```

1 clear all; close all; clc;
2 %
3 % V.Cusati, D.Ciliberti,
4 %
5 % Naples, 2014.
6 %
7 % The code creates the profile of fuselage starting from points of the CAD
8 % model. The points are stored in a cell array (thanks to Danilo).
9 % Then the code allows to change slenderness ratio of the
10 % fuselage, those of the nose and tail. The geometry is exported in a
11 % ".csv" file in order to create a CAD through Star-CCM+.
12 %
13 % This version of the code implements the "COMBINATED" changes of geometry
14 % along x-axis and z-axis. Particularly the code modifies the windshield
15 % angle shifting the nose sections along z-axis for fixed SR. At the same
16 % way, it modifies the upsweep angle shifting the tail sections along
17 % z-axis for fixed SR.
18 %
19 %
20 load 'fus_alenia.mat'
21 %
22 % Section: NOSE=1:13. CABIN=14:22. TAIL=23:43.
23 np = 18; % Number of points useful to describe the contour
24 % of a section
25 %%
26 %figure()
27 for j = 1:numel(sezioni)
28 dummy = [sezioni{j}];
29 dummy = unique(dummy, 'rows');
30 yM(j) = max(dummy(:,2));
31 ym(j) = min(dummy(:,2));
32 zM(j) = max(dummy(:,3));
33 zm(j) = min(dummy(:,3));
34 % rr is the ratio between the (max(y)-min(y)) and (max(z)-min(z))/2
35 % for each section. If rr=1 --> section=circumference.
36 rr(j) = (zM(j)-zm(j))/(2*(yM(j)-ym(j)));
37 % Right part of the fuselage.

```

```

38     vxr(:,j) = ones(np,1).*dummy(1,1);
39     vzr(:,j) = linspace(zm(j),zM(j),np);
40     vyr(:,j) = interp1(dummy(:,3),dummy(:,2),vzr(:,j));
41     vyr(1,j) = 0;
42     vyr(end,j) = 0;
43 end
44 rr = rr'; % Column vector.
45 % Left part of the fuselage.
46 vyl = flipud(-1*vyr);
47 vyl = vyl(2:end,:);
48 vxl = vxr(2:end,:);
49 vzl = flipud(vzr);
50 vzl = vzl(2:end,:);
51 % v complete
52 vy=[vyr;vyl];
53 vx=[vxr;vxl];
54 vz=[vzr;vzl];
55 %plot3(vx,vy,vz,'-r')
56 %axis equal
57 % Scale factor (mm --> m)
58 vx = vx/1000;
59 vy = vy/1000;
60 vz = vz/1000;
61 %% The correct sorting of fuselage sections for loft into Star-CCM+
62 X = zeros((2*np-1),43); Y=X; Z=Y;
63 X(:,1:13)=vx(:,1:13);
64 Y(:,1:13)=vy(:,1:13);
65 Z(:,1:13)=vz(:,1:13);
66 X(:,14) = vx(:,42);Y(:,14) = vy(:,42);Z(:,14) = vz(:,42);
67 X(:,15) = vx(:,43);Y(:,15) = vy(:,43);Z(:,15) = vz(:,43);
68 vvx(:,16:43) = fliplr(vx(:,14:41));
69 vvy(:,16:43) = fliplr(vy(:,14:41));
70 vvz(:,16:43) = fliplr(vz(:,14:41));
71 X(:,16:43) = vvx(:,16:43);
72 Y(:,16:43) = vvy(:,16:43);
73 Z(:,16:43) = vvz(:,16:43);
74
75 % Case identification
76 caseID = 0;
77 % Exporting to a csv file
78 originale = menu('Generate the CSV for the original fuselage?', 'Yes', 'No');
79     if originale == 1
80         m = 1;
81         for k = 1:length(sezioni) % length([sezioni])=43
82             S((m+size(X,1)-1),:) = [X(:,k), Y(:,k), Z(:,k)]; % X(:,k)=(35,k)
83             m = m + size(X,1); % size(X,1)= 35
84         end
85         csvwrite(['oo',mat2str(caseID),'.csv'],S)
86     end

```

Listing 1: Part of MATLAB code that rebuild the fuselage geometry.

For all modifications, the fuselage diameter, d_f , is always constant. Therefore, to change the fineness ratio of the fuselage components, these are simply stretched (or shortened). This has been done translating rigidly the sections along x axis. Instead, in the case of windshield and upsweep angle modifications, the sections are translated along z axis in opportune way. Each parameter is changed keeping the other constant. For instance, a change in fuselage slenderness ratio requires a stretch of the cabin, without changing the shape of nose and tail. Conversely, a change in nose or tail shape does not alter the

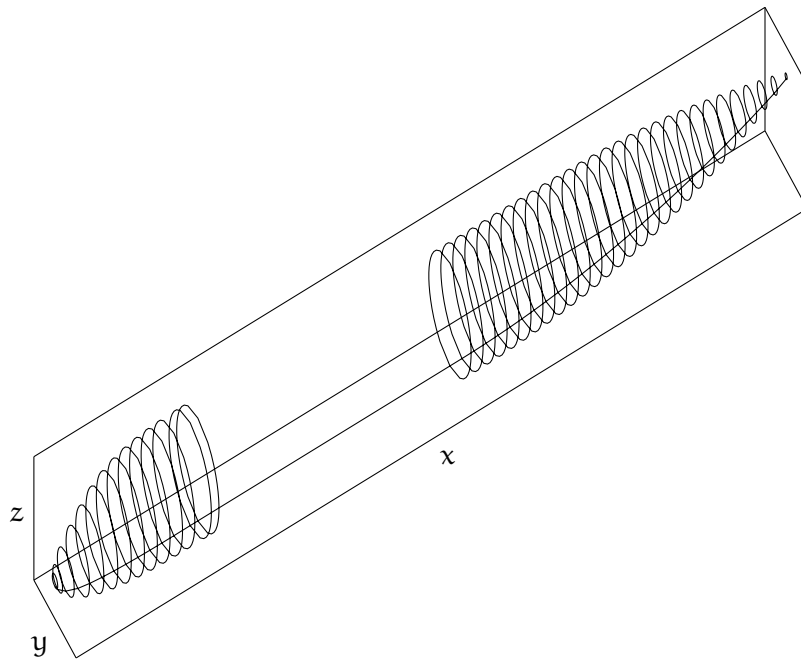


Figure 31: The fuselage divided in sections.

geometry of the other components. Table 7 lists the parameters investigated and their values. For the definition of the parameters refer to figure 5.

FR	-	-	-	7	8	8.69	9.5	11	12
FR _n	1.1	1.2	1.3	1.4	1.5	1.6	1.7	-	-
FR _t	2.3	2.4	2.5	2.6	2.7	2.83	2.9	3	-

Table 7: Fineness ratios of the fuselage components for the parametric investigation.

3.4.1 Modification of the nose

In the listing 2 is reported the part of the script which modifies only the nose along x axis. This part (as the next two parts which modify cabin and tailcone) is excerpted from the sixth version of the code which implements all different changes along x axis. As previously stated, the nose is modified while the cabin and tail are the same of those of reference. The fineness ratios investigated are reported in the second row of table 7. For any doubts about MATLAB functions used it is suggested to consult the manual [12].

```

1 %% NOSE
2 %
3 % Design slenderness ratio of nose: srn = 1.61
4 %
5 var_nose = menu('Do you want to do a parametric study on the nose?',...
```

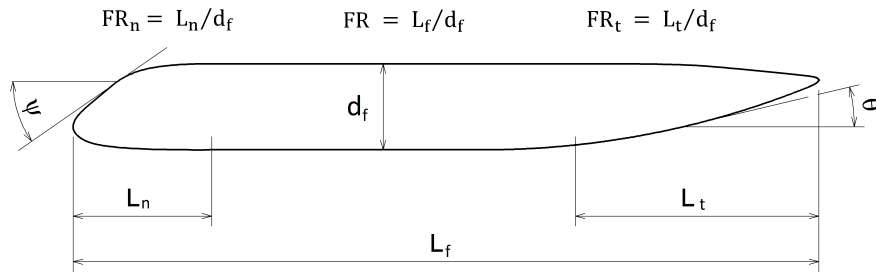


Figure 32: Main geometrical parameter.

```

6         'Yes', 'No');
7
8     if var_nose == 1
9         Ln = unique(X(:,13)-X(:,1)); % Design Lnose.
10        dn = Dfus; % Design dnose.
11        srn = Ln/dn; % Design slenderness ratio of nose.
12
13        prompt = {'Enter nose slenderness ratios to study:'};
14        dlg_title = 'Waiting for user input';
15        num_lines = 1;
16        def = {'1.1, 1.2, 1.3, 1.4, 1.5, 1.6, 1.7'}; % Default values
17        answer = inputdlg(prompt,dlg_title,num_lines,def);
18        stringa = cell2mat(answer);
19        new_srn = str2num(stringa); % New slenderness ratio of nose.
20        % Pre-allocation
21        Xsrn = zeros(length(X(:,1)),43);
22        for srni=1:length(new_srn)
23            % Case IDentification
24            caseID = srni;
25            Dsrn(srni) = new_srn(srni)/srn; % Delta slenderness ratio of nose
26            % (design - new).
27
28            for i=1:12
29                % It doesn't move the last section. For this reason i goes from 1 to
30                % 13 (and not to 14). Besides, the ratio between new and old slen.
31                % ratio nose is equal to that between the new and old length of nose.
32                % Therefore the shift of section is equal to (1-newLength/oldLength)=
33                % (1-new_srnose/old_srnose)=(1-Dsrn).
34                if new_srn(srni) > srn % Dsrn > 1
35                    Xsrn(:,i) = X(:,i) - (Dsrn(srni)-1)*(X(:,13)-X(:,i));
36                else % Dsrn < 1
37                    Xsrn(:,i) = X(:,i) + (1-Dsrn(srni))*(X(:,13)-X(:,i));
38                end
39            end
40            % Cabin and Tail are the same
41            Xsrn(:,13:43) = X(:,13:43);
42            % ===== Exporting to a csv file =====
43            m = 1;
44            for k = 1:length(sezioni) % length(sezioni)=43
45                Ssrn((m:size(X,1)-1),:) = [Xsrn(:,k), Y(:,k), Z(:,k)];
46                m = m + size(Xsrn,1);
47            end
48            csvwrite(['io',mat2str(caseID),'.csv'],Ssrn)
49        end

```

Listing 2: Part of MATLAB code that modifies the fuselage nose.

3.4.2 Modification of the cabin

As done for the nose, in this section is reported the part of the script which modifies only the cabin along x axis (listing 3). The fineness ratios investigated are reported in the first row of table 7.

```

1 %% CABIN
2 % Design slenderness ratio: srd = 8.69
3 %
4 var_cabin = menu('Do you want to do a parametric study on the cabin?',...
5                 'Yes', 'No');
6 if var_cabin == 1
7     srd = Lfus/Dfus; % Design slenderness ratio.
8
9     prompt = {'Enter cabin (passengers) slenderness ratios to study:'};
10    dlg_title = 'Waiting for user input';
11    num_lines = 1;
12    def = {'7 8 8.69 9.50 11 12'}; % Default values
13    answer = inputdlg(prompt,dlg_title,num_lines,def);
14    stringa = cell2mat(answer);
15    sr = str2num(stringa); % New slenderness ratio.
16    % Pre-allocation
17    Xsr = zeros(length(X(:,1)),43);
18    for sri = 1:length(sr)
19        caseID = sri; % Case IDentification.
20        Lf_new(sri) = Dfus*sr(sri); % New fuselage lenght.
21        delta(sri) = Lf_new(sri) - Lfus;
22        for j=15:43
23            Xsr(:,j) = X(:,j)+ delta(sri);
24        end
25
26    Xsr(:,1:14) = (X(:,1:14));
27
28    end
29
30    % Exporting to a csv file
31    m = 1;
32    for k = 1:length(sezioni) length([sezioni])=43
33        Ssr((m:m+size(Xsr,1)-1),:) = [Xsr(:,k), Y(:,k), Z(:,k)];
34        m = m + size(Xsr,1); % size(X,1)= 35
35    end
36    csvwrite(['oo',mat2str(caseID),'.csv'],Ssr)
37    end

```

Listing 3: Part of MATLAB code that modifies the fuselage cabin.

3.4.3 Modification of the tail

In this section is reported the part of the script which modifies only the tail along x axis (listing 4). The fineness ratios investigated are reported in the third row of table 7.

```

1 %% TAIL
2 % Design slenderness ratio of tail: srt = 2.83
3 var_tail = menu('Do you want to do a parametric study on the tail?',...
4               'Yes', 'No');
5
6 if var_tail == 1
7     Lt = unique(X(:,43)-X(:,23)); % Design Ltail.

```

```

8      dt = Dfus;                                % Design dtail.
9      srt = Lt/dt;                              % Design slenderness ratio of nose.
10
11     prompt = {'Enter tail slenderness ratios to study:'};
12     dlg_title = 'Waiting for user input';
13     num_lines = 1;
14     def = {'2.3, 2.4, 2.5, 2.6, 2.7, 2.83, 2.9, 3.0'}; % Default values
15     answer = inputdlg(prompt,dlg_title,num_lines,def);
16     stringa = cell2mat(answer);
17     new_srt = str2num(stringa); % New slenderness ratio of nose.
18
19     for srti=1:length(new_srt)
20         % Case IDentification
21         caseID = srti;
22         Dsrt(srti)= new_srt(srti)/srt;      % Delta slenderness ratio of tail
23                                             % (design - new).
24     % Pre-allocation
25     Xsrt = zeros(length(X(:,1)),43);
26     Xsrt(:,1:23)=X(:,1:23);
27     for i=24:43
28         % It doesn't move the first section. For this reason i goes from 24
29         % to 43 ( and not from 23).
30         if new_srt(srti)> srt % Dsrt>1
31             Xsrt(:,i) = X(:,i)+ (Dsrt(srti)-1)*(X(:,i)-X(:,23));
32         else % Dsrt<1
33             Xsrt(:,i) = X(:,i)- (1-Dsrt(srti))*(X(:,i)-X(:,23));
34         end
35     end
36     % ===== Exporting to a csv file =====
37     m = 1;
38     for k = 1:length(sezioni) % length(sezioni)=43
39         Ssrt((m:m+size(X,1)-1),:) = [Xsrt(:,k), Y(:,k), Z(:,k)];
40         m = m + size(Xsrt,1);
41     end
42     csvwrite(['20',mat2str(caseID),'.csv'],Ssrt)
43 end

```

Listing 4: Part of MATLAB code that modifies the fuselage tail.

3.4.4 Modification of nose height

In order to investigate the effect of nose windshield angle, the nose sections was translated along z axis for some FR_n . The windshield angle is considered as the slope of the upper surface on the fuselage symmetry plane, as shown in figure 33. Two modifications for each FR_n were performed: one upward and one downward. The following part (listing 5) is excerpted from the ninth version of the code which modifies the geometry of the nose both along x and z axis simultaneously. The angles and fineness ratios studied for windshield modification are reported in the table 8 and table 9 respectively. The values of reference geometry are highlighted in bold.

FR_n	1.2	1.4	1.6	1.7
	51.7	48.4	44.6	43.9
ψ (deg)	47.7	43.3	39.7	38.0
	45.4	40.5	37.0	35.8

Table 8: Windshield analysis parameter.

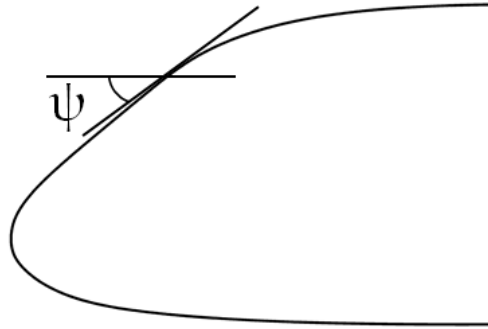


Figure 33: Definition of the windshield angle.

```

1 % 2) NOSE
2 % Design slenderness ratio of nose: srn = 1.61
3 %
4 var_nose = menu('Do you want to do a parametric study on the nose?',...
5                 'Yes', 'No');
6 if var_nose == 1
7     Ln = unique(X(:,13)-X(:,1)); % Design Lnose.
8     dn = Dfus; % Design dnose.
9     srn = Ln/dn; % Design slenderness ratio of nose.
10
11 prompt = {'Enter nose slenderness ratios to study (must be 4 input):'};
12 dlg_title = 'Waiting for user input';
13 num_lines = 1;
14 def = {'1.2, 1.4, 1.6, 1.7'}; % Default values
15 answer = inputdlg(prompt,dlg_title,num_lines,def);
16 stringa = cell2mat(answer);
17 new_srn = str2num(stringa); % New slenderness ratio of nose.
18 % Pre-allocation
19 Xsrn = zeros(length(X(:,1)),43);
20 for srni=1:length(new_srn)
21     % Case IDentification
22     caseID = srni;
23     Dsrn(srni) = new_srn(srni)/srn; % Delta slendrness ratio of nose
24                                     % (design - new).
25
26 for i=1:12
27     % It doesn't move the last section. For this reason i goes from 1 to
28     % 13 (and not to 14). Besides, the ratio between new and old slen.
29     % ratio nose is equal to that between the new and old length of nose.
30     % Therefore the shift of section is equal to (1-newLength/oldLength)=
31     % (1-new_srnose/old_srnose)=(1-Dsrn).
32     if new_srn(srni) > srn % Dsrn>1
33         Xsrn(:,i) = X(:,i) - (Dsrn(srni)-1)*(X(:,13)-X(:,i));
34     else % Dsrn<1
35         Xsrn(:,i) = X(:,i) + (1-Dsrn(srni))*(X(:,13)-X(:,i));
36     end

```

```

36     end
37     % Cabin and Tail are the same
38     Xsrn(:,13:43)=X(:,13:43);
39     %%%%%%%%%%%%%%%%%%%%%%%%%%%%%%%%%%%%%%%%%%%%%%%%%%%%%%%%%%%%%%%%%%%%%%%%%
40     % ----- Modification of Z nose -----
41     % This part of code modifies the windshield angle with constant SR nose.
42     %
43     % Design slenderness ratio of nose: srn = 1.6 (constant).
44     %
45     % For each fineness ratio of the nose, there are 2 modifications along z axis:
46     % one upward and the other downward.
47     %
48     %% Upward modification of the nose
49     caseIDznup = 2;
50     DZ = 0.3;           % Up Displacement [m].
51     ls = 9;            % Last section.
52     w = linspace(1,0,ls);
53     DZun = w.*DZ;
54     Zun = Z;
55     Zun(:,(ls+1):43) = Z(:,(ls+1):43);
56     jj = 1;
57     for ii=1:length(DZun)
58         Zun(:,jj)= Z(:,jj) + DZun(ii);
59         if max(Zun(:,jj)) > max(Z(:,ls))
60             Zun(:,jj) = Z(:,jj) + (max(Z(:,ls))- max(Z(:,jj)));
61         end
62         jj = jj+1;
63     end
64     % Exporting to a csv file
65     m = 1;
66     for k = 1:length(sezioni)      % length([sezioni])=43
67         Sznu((m:m+size(X,1)-1),:) = [Xsrn(:,k), Y(:,k), Zun(:,k)]; % X(:,k)=(35,k)
68     m = m + size(X,1); % size(X,1)= 35
69     end
70     csvwrite(['30',mat2str(caseID),mat2str(caseIDznup)','.csv'],Sznu)
71
72     %% "Train form" for the nose
73     caseIDzn = 1;
74     for ii = 1:13
75         Dzz(ii) = Z(1,ii)-(Z(1,13));
76         ZnewT(:,ii)= Z(:,ii)-Dzz(:,ii);
77     end
78     ZnewT(:,14:43)=Z(:,14:43);
79     % ===== Exporting to a csv file =====
80     m = 1;
81     for k = 1:length(sezioni)      % length([sezioni])=43
82         SznT((m:m+size(X,1)-1),:) = [Xsrn(:,k), Y(:,k), ZnewT(:,k)]; % X(:,k)=(35,k)
83     m = m + size(X,1); % size(X,1)= 35
84     end
85     csvwrite(['30',mat2str(caseID),mat2str(caseIDzn)','.csv'],SznT)
86     end
87     end

```

Listing 5: Part of MATLAB code that modifies the windshield angle.

3.4.5 Modification of upsweep angle

The tail sections have been translated along z axis for some FR_t in order to investigate the effect of the upsweep angle. Even in this case, two modification for each FR_t were performed: one upward and one

downward. The upsweep angle is evaluated at the tail station which crosses the longitudinal nose axis, as shown in figure 34.

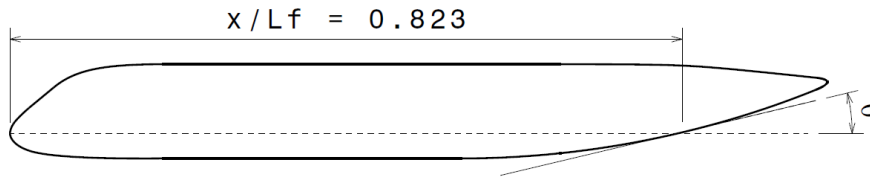


Figure 34: Definition of the upsweep angle.

It has been assumed this reference because the gear height is unknown and the tail low surface is not straight. The listing 6 is excerpted from the ninth version of the code which modifies the geometry of the tail both along x and z axis simultaneously. The angles and fineness ratios studied are reported in the table 9. The baseline values are highlighted in bold.

FR _t	2.5	2.83	3.0
	12.2	15.3	18.2
θ (deg)	10.8	13.6	16.2
	10.2	12.9	15.3

Table 9: Upsweep analysis parameter.

```

1 % 3)TAIL
2 % Design slenderness ratio of tail: srt = 2.83
3 var_tail = menu('Do you want to do a parametric study on the tail?',...
4               'Yes', 'No');
5 if var_tail == 1
6     Lt = unique(X(:,43)-X(:,23));           % Design Ltail.
7     dt = Dfus;                             % Design dtail.
8     srt = Lt/dt;                            % Design slenderness ratio of tail.
9     prompt = {'Enter tail slenderness ratios to study:'};
10    dlg_title = 'Waiting for user input';
11    num_lines = 1;
12    def = {'2.5', '2.83', '3.0'}; % Default values
13    answer = inputdlg(prompt,dlg_title,num_lines,def);
14    stringa = cell2mat(answer);
15    new_srt = str2num(stringa); % New slenderness ratio of nose.
16    for srti=1:length(new_srt)
17        % Case IDentification
18        caseID = srti;
19        Dsrt(srti)= new_srt(srti)/srt;      % Delta slendrness ratio of tail
20                                             % (design - new).
21    % Pre-allocation
22    Xsrt = zeros(length(X(:,1)),43);
23    Xsrt(:,1:23)=X(:,1:23);
24    for i=24:43
25        % It doesn't move the first section. For this reason i goes from 24
26        % to 43 ( and not from 23).
27        if new_srt(srti)> srt % Dsrt>1
28            Xsrt(:,i) = X(:,i)+ (Dsrt(srti)-1)*(X(:,i)-X(:,23));
29        else % Dsrt<1
30            Xsrt(:,i) = X(:,i)- (1-Dsrt(srti))*(X(:,i)-X(:,23));
31    end

```

```

32 end
33 %%%%%%%%%%%%%%%%%%%%%%%%%%%%%%%%%%%%%%%%% Modifications along Z-axis for tail %%%%%%%%%%%%%%%%%%%%%%%%%%%%%%%%%%%%%%%%%
34 %
35 % For each fineness ratio of the tail, there are 2 modifications along :
36 % one upward and the other downward.
37 %
38 % Design Upsweep angle
39 Z32 = min(Z(:,32)); Z33 = min(Z(:,33));
40 aud = rad2deg(atan((Z33-Z32)/(X(1,33)-X(1,32))));
41
42 %% Upward modification
43 caseIDup = 2; % CaseId in increasing order
44 Zup = Z;
45 for i=16:43
46     DZup(:,i)= max(Z(:,15))-max(Z(:,i));
47     Zup(:,i) = Z(:,i)+ DZup(:,i);
48 end
49 Zup32= min(Zup(:,32)); Zup33 = min(Zup(:,33));
50 aup = rad2deg(atan((Zup33-Zup32)/(Xsrt(1,33)-Xsrt(1,32))))
51 % ===== Exporting to a csv file =====
52 m = 1;
53 for k = 1:length(sezioni) % length(sezioni)=43
54     Sup((m:size(X,1)-1,:)) = [Xsrt(:,k), Y(:,k), Zup(:,k)];
55     m = m + size(X,1);
56 end
57 csvwrite(['40',mat2str(caseID),mat2str(caseIDup),'.csv'],Sup)
58 %% Downward modification.
59 caseIDupd = 1;
60 fs =22; % first section
61 DZupdend = .5;
62 w = linspace(0,1,43-fs);
63 DZupd = w.*DZupdend;
64 Zupd = Z;
65     Zupd(:,1:22) = Z(:,1:22);
66     jj = 23;
67     for ii=1:length(DZupd)
68         Zupd(:,jj)= Z(:,jj) - DZupd(ii);
69         jj = jj+1;
70     end
71 Zupd32= min(Zupd(:,32)); Zupd33 = min(Zupd(:,33));
72 aupd = rad2deg(atan((Zupd33-Zupd32)/(Xsrt(1,33)-Xsrt(1,32))))
73 % ===== Exporting to a csv file =====
74 m = 1;
75 for k = 1:length(sezioni) % length(sezioni)=43
76     Supd((m:size(X,1)-1,:)) = [Xsrt(:,k), Y(:,k), Zupd(:,k)];
77     m = m + size(X,1);
78 end
79 csvwrite(['40',mat2str(caseID),mat2str(caseIDupd),'.csv'],Supd)
80 end
81 end

```

Listing 6: Part of MATLAB code that modifies the upsweep angle.

4

CFD ANALYSIS RESULTS

Contents

4.1	Variation of the nose length	48
4.2	Variation of the cabin length	55
4.3	Variation of the tail length	59
4.4	Variation of the nose height	63
4.5	Variation of the upsweep angle	66

In this chapter the results of the numerical simulations are reported. For each geometry modification the drag coefficient (C_D), the moment coefficient (C_M) and the moment curve slope (C_{M_α}) are shown.

Moreover, to better understand how the aerodynamic coefficients change, the pressure distribution for each geometry analysed is reported and compared with that of the reference fuselage. The lift coefficient hasn't been reported because it is very close to zero, since the fuselage is not a lifting body. In all charts and tables below, each aerodynamic coefficient is expressed as a ratio between the computed value, which comes from the numerical simulations, and the value of reference fuselage which cannot be specified for industrial reasons. In the case of pressure and friction drag contributions that are reported in the same plot, both are compared with the global reference drag coefficient (that's to say the $C_{D_{ref}}$ is the C_D of the reference fuselage). As regard the moment coefficient and its derivative, the reference center (which corresponds to the center of gravity) is located always with respect the hypothesized wing location: x_{CG}/L_f equal to 0.465 and z equal to 0 (see figure 35). In case of the moment coefficient at α equal to 0° and equal 2° are drawn in the same plot, both are compared with the global reference moment coefficient at α equal to 0° . Finally the flight conditions for all simulations are the following.

- $M = 0.52$
- $Re_{L_f} = 2.02 \times 10^8$

4.1 VARIATION OF THE NOSE LENGTH

The parameters involved in the investigation about the nose geometry are reported in table 10. The nose length, L_n , and the wet surface,

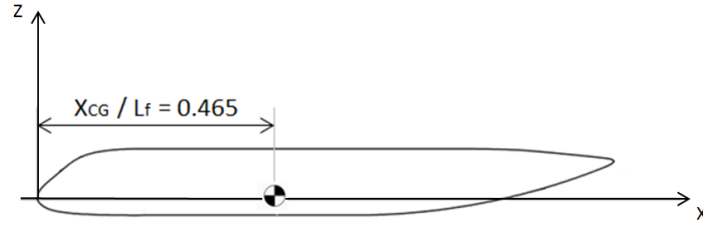


Figure 35: Reference center for the calculation of moment coefficient.

S_{wet} , are reported as a percentage change compared to the reference values which are highlighted in bold. Nose geometries are shown in the figure 36. When the nose geometry is varied the windshield angle is changed too, as represented in figure 37.

ID	FR_n	Windshield (deg)	ΔS_{wet}
101	1.1	49.9	-5%
102	1.2	47.7	-4%
103	1.3	45.0	-3%
104	1.4	43.3	-2%
105	1.5	41.0	-1%
000	1.6	39.7	-
107	1.7	38.0	+1%

Table 10: Parameters of the nose investigation.

The following charts present the results of the numerical analyses as function of the geometry variation. In these charts, the bigger marker represents the reference value. Figure 38 shows that, by altering the nose geometry and holding the same cabin and tail, the pressure distribution is affected only around the nose, as expected. Thus, the variation of the drag coefficient with nose slenderness is only function of the geometry variation and there is no interference effect with the other parts of the fuselage. As the nose is lengthened, the friction contribution to drag increases (due to the bigger wet surface), whereas the pressure contribution decreases (due to the increased slenderness), see figure 39. The sum of the two contributions gives a minimum for FR_n equal to 1.3, although the difference is small with respect to the reference configuration (figure 40).

The effect of nose slenderness on pitching moment coefficient is shown in figure 41. To evaluate the C_{M_α} , all the configurations have been simulated at two angles of attack, 0° and 2° , then the derivative has been estimated as the ratio

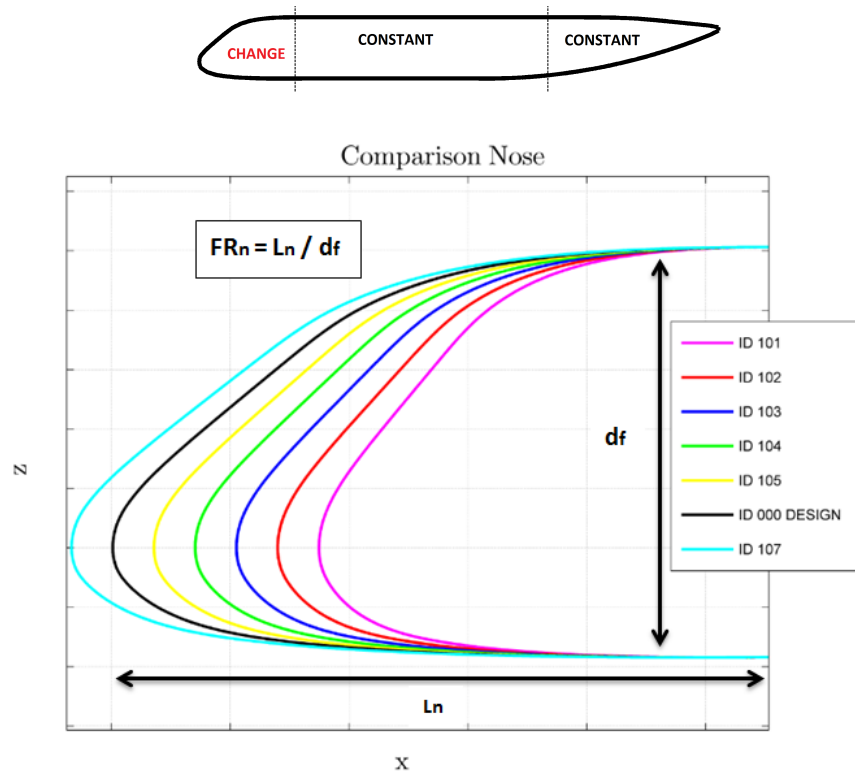


Figure 36: Comparison of different nose.

$$C_{M_\alpha} = \frac{C_M^{\alpha=2^\circ} - C_M^{\alpha=0^\circ}}{2^\circ - 0^\circ} \quad (4.1)$$

The moment coefficient at 0° and 2° are drawn in figure 42. There is a linear variation of C_{M_α} with nose length and the longer is the nose, the bigger is the pitching instability. Figure 43 illustrates the different pressure distributions for two nose configuration: the shorter nose has a shape that increase the flow expansion, giving an increase in pressure drag. Given the results of the analyses for the cruise condition, a nose shorter than the reference configuration, around the slender ratio FR_n equal to 1.2, is advantageous in terms of drag.

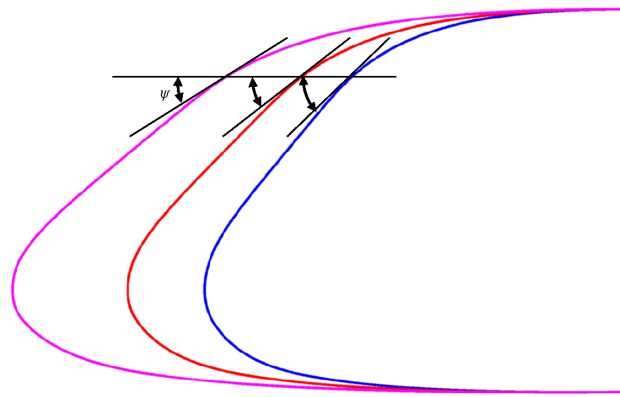


Figure 37: Variation of windshield angle due to the variation of nose length.

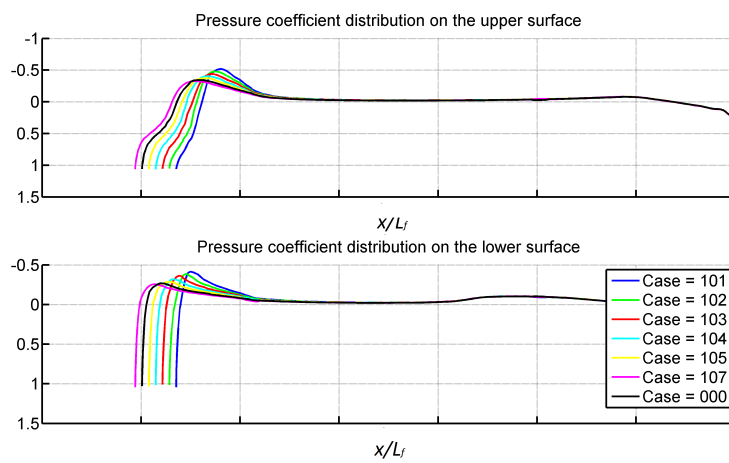


Figure 38: Pressure distribution on the fuselage symmetry plane, due to nose variation, $\alpha = 0$.

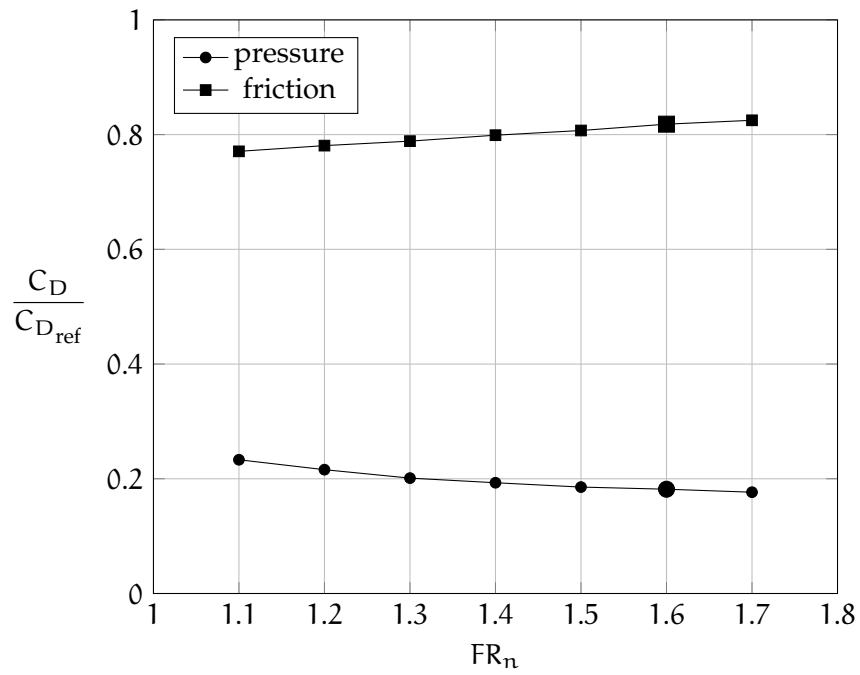


Figure 39: Friction and pressure contributions to drag coefficient due to nose variation, $\alpha = 0^\circ$.

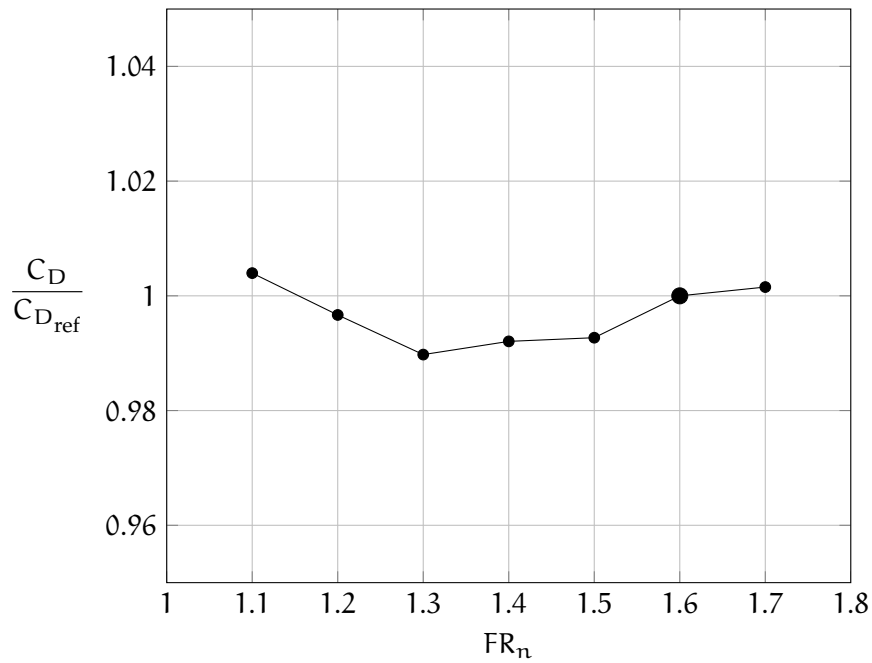


Figure 40: Drag coefficient due to nose variation (sum of pressure and friction contributions), $\alpha = 0^\circ$.

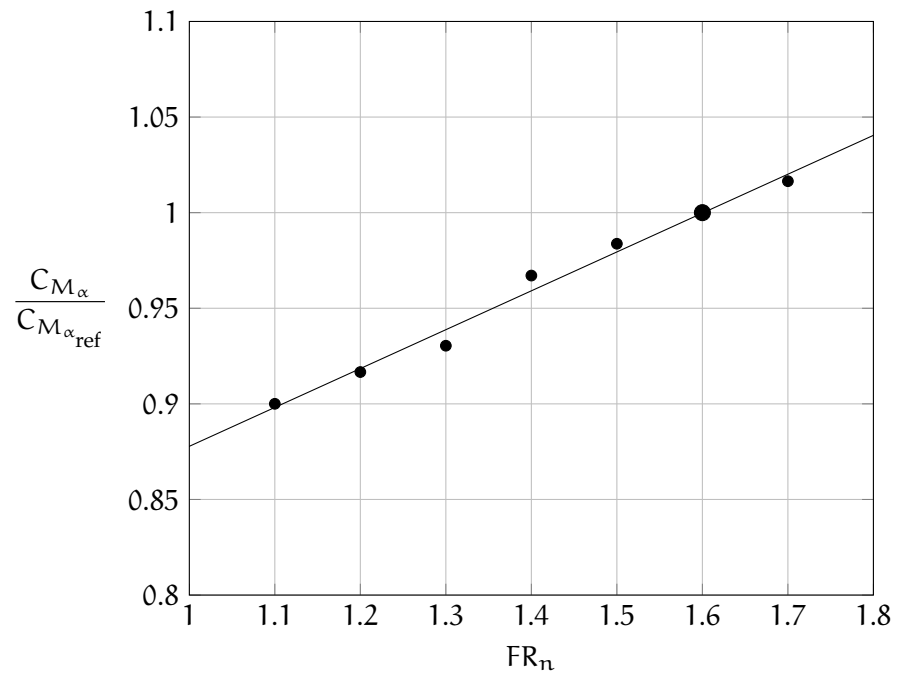


Figure 41: Fuselage pitching instability due to nose variation.

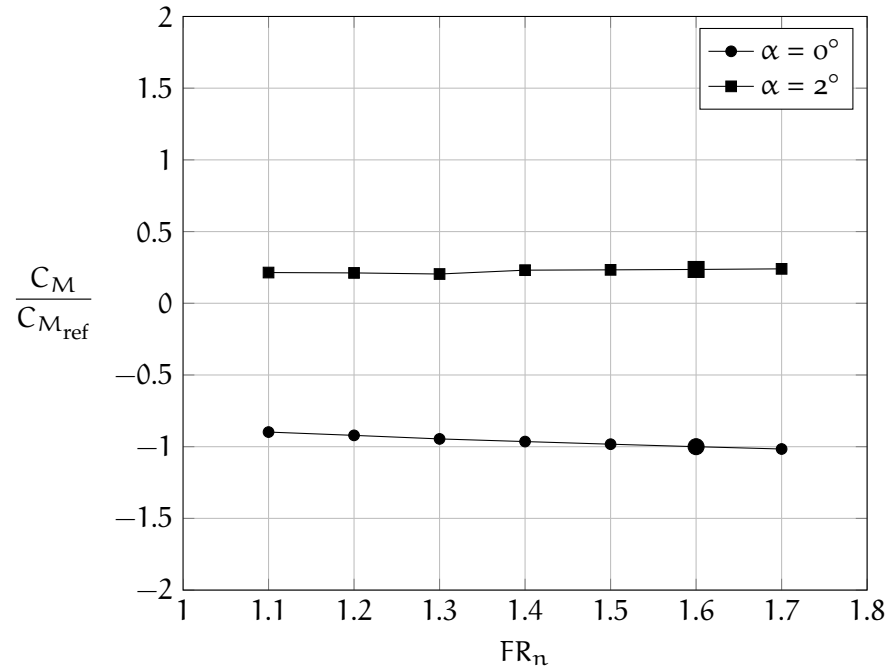


Figure 42: Moment coefficient as function of the nose geometry variation, $\alpha = 0^\circ$ e $\alpha = 2^\circ$

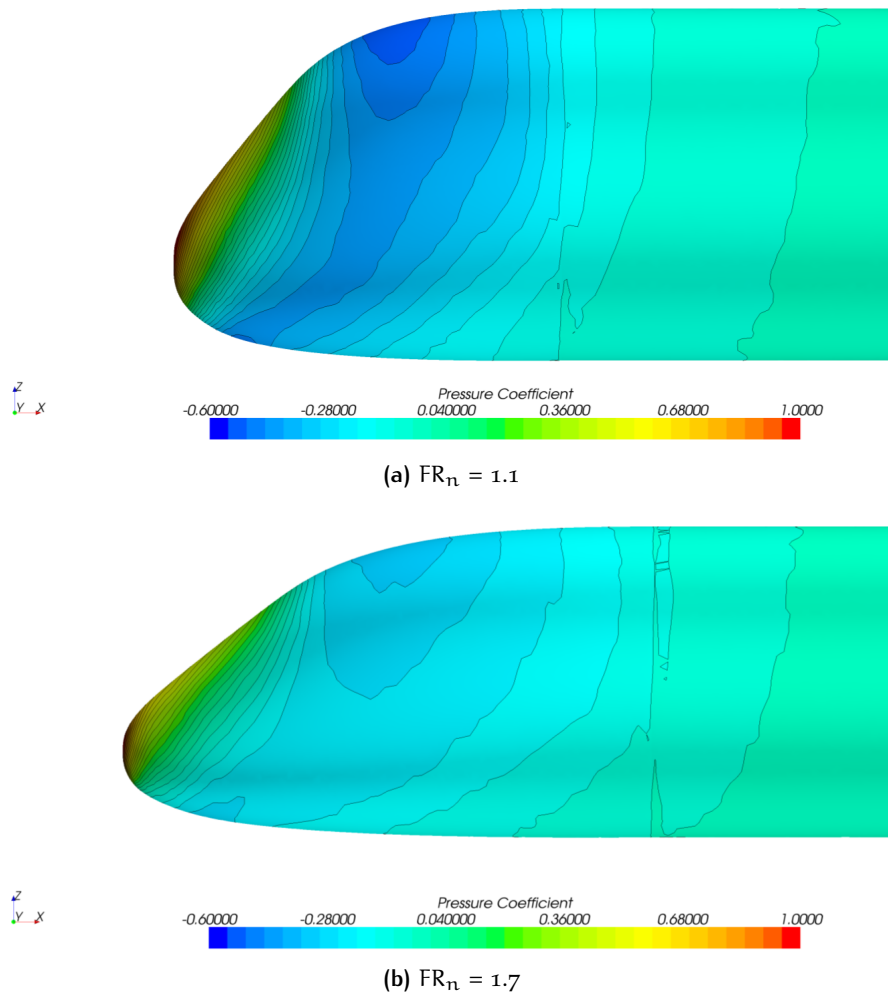


Figure 43: Comparison of the pressure distribution for two nose configurations, $\alpha = 0^\circ$.

4.2 VARIATION OF THE CABIN LENGTH

The parameters involved in the investigation about the cabin are reported in table 11. The reference values are in bold. In this case, the whole slenderness ratio has been considered. Some configurations are shown in figure 44.

ID	FR	ΔS_{wet}
001	7.00	-23%
002	8.00	-9%
000	8.69	-
003	9.50	+11%
004	11.0	+31%
005	12.0	+45%

Table 11: Parameters of the cabin investigation.

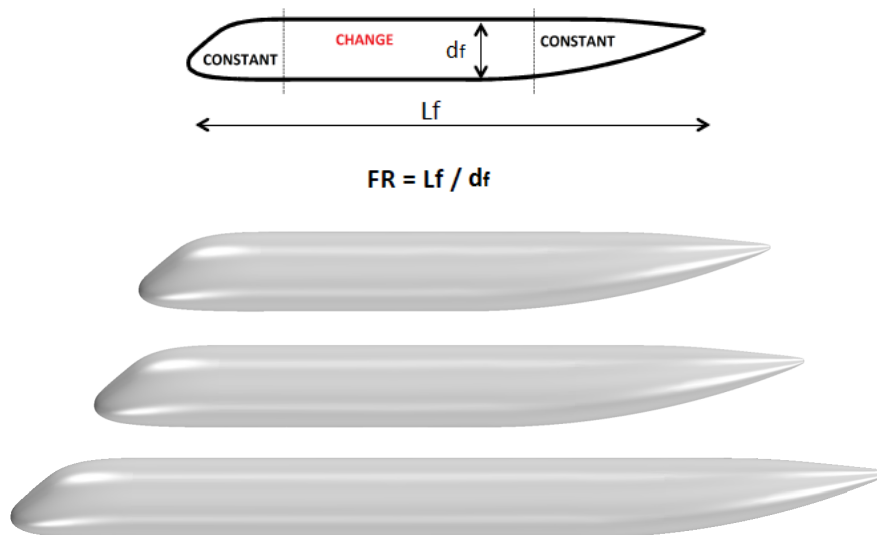


Figure 44: Change of the fuselage slenderness by stretching the cabin.

The following charts present the results of the numerical analyses as function of the geometry variation. In these charts, the bigger marker represents the reference value. In figure 45 the pressure distributions keep the same shape, since only the cabin length is changed, whereas nose and tail are the same. A strong variation in skin friction coefficient with respect to pressure drag is represented in figure 46. This is due to the increase in wet area, whereas the pressure distribution do not change since the cabin is essentially a cylinder. The total drag coefficient is hence a linear function of the slenderness ratio as reported in figure 47, where the two black vertical lines represent length variations by ± 2 m from the reference geometry. The longitu-

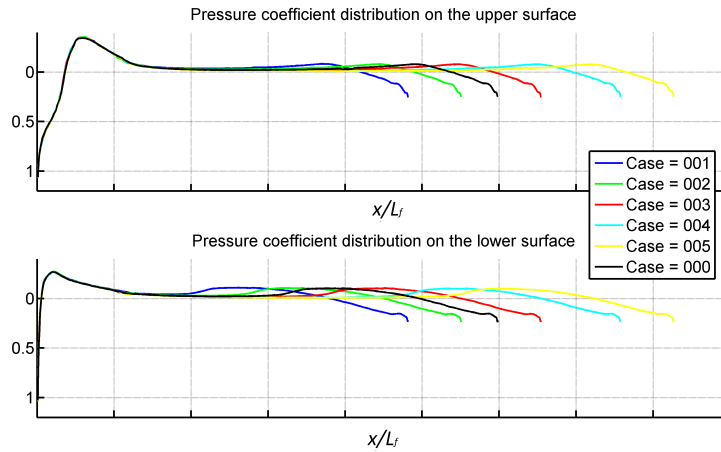


Figure 45: Pressure distribution on the fuselage symmetry plane, due to cabin variation, $\alpha = 0^\circ$.

dinal instability is shown in figure 48. The moment reference center changes its absolute position to keep the same relative position (at x/L_f equal to 0.465 and z equal to 0). As expected, a longer cabin is less stable in pitch.

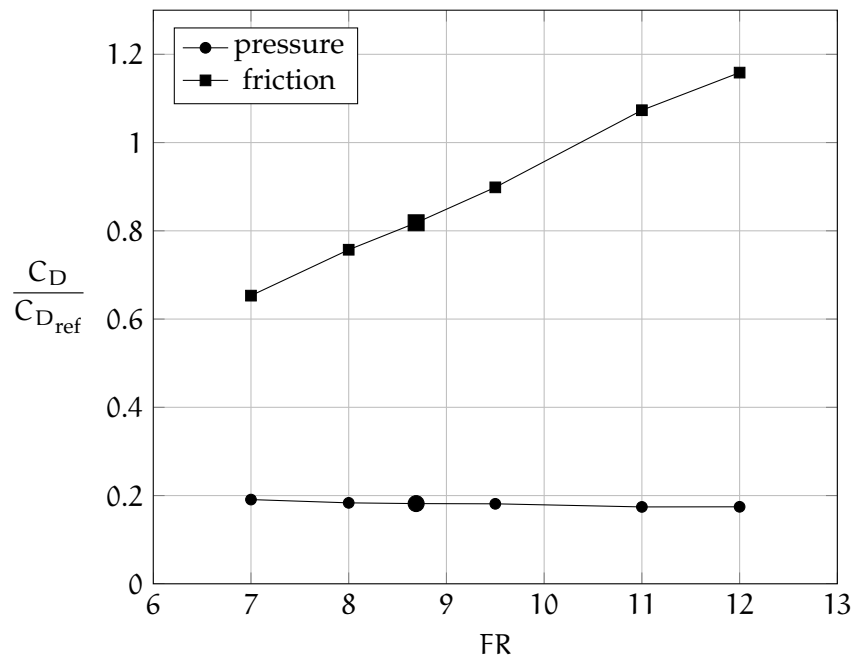


Figure 46: Friction and pressure contributions to drag coefficient due to cabin variation, $\alpha = 0^\circ$.

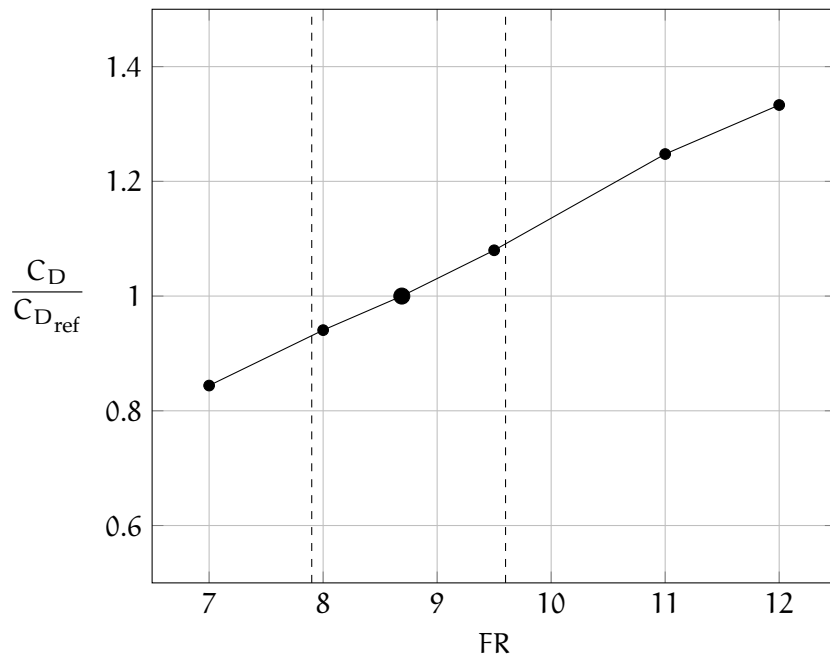


Figure 47: Drag coefficient due to cabin variation (sum of pressure and friction contributions), $\alpha = 0^\circ$.

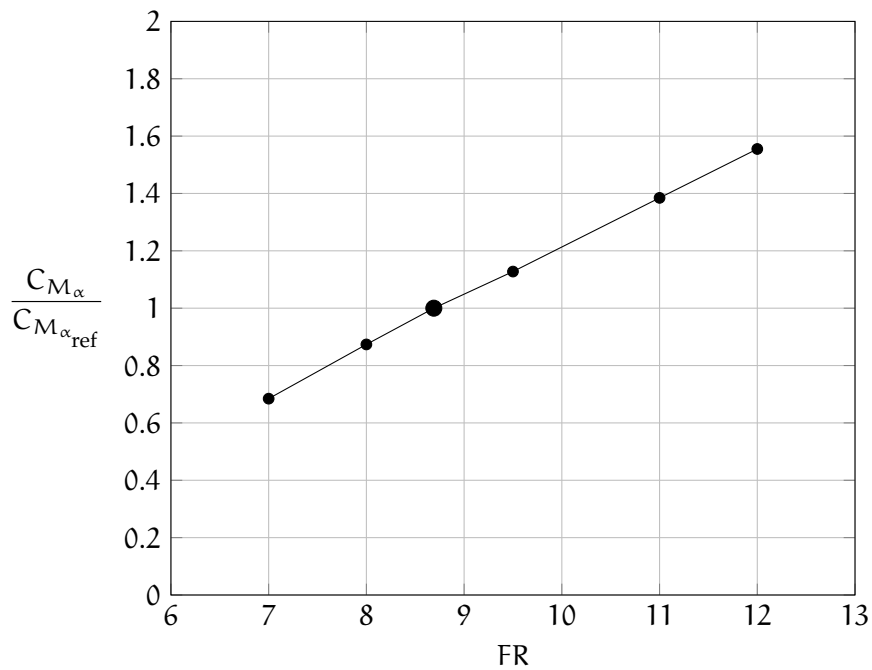


Figure 48: Fuselage pitching instability due to cabin variation.

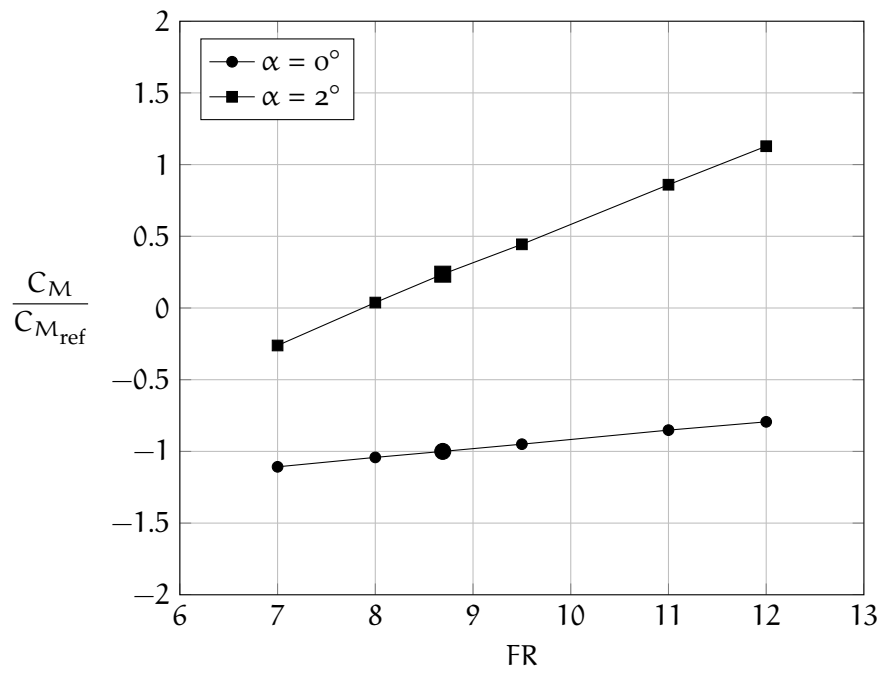


Figure 49: Moment coefficient as function of the cabin geometry, $\alpha = 0^\circ$ e $\alpha = 2^\circ$

4.3 VARIATION OF THE TAIL LENGTH

The parameters involved in the investigation about the tail are reported in table 12. The values of reference configuration are in bold. Configurations are shown in figure 50. When the tail geometry is varied the upsweep angle is changed too, as represented in figure 51.

ID	ΔL_t	Upsweep _(deg)	ΔS_{wet}
208	2.3	16.6	-5%
207	2.4	15.9	-4%
201	2.5	15.3	-3%
202	2.6	14.8	-2%
203	2.7	14.2	-1%
000	2.83	13.6	-
205	2.9	13.3	0%
206	3.0	12.9	+1%

Table 12: Parameters of the tail investigation.

The following charts present the results of the numerical analyses as function of the geometry variation. In these charts, the bigger marker represents the reference value. Having changed only the tail slenderness, the pressure distribution on the fuselage is the same everywhere for the configurations investigated, except for the tail, as shown in figure 52. As expected, as the tail is lengthened, the skin friction increases, whereas the pressure drag decreases, as reported in figure 53. In this case, the pressure and friction variations cancel each other, yielding to a constant drag coefficient with tail slenderness ratio, figure 54.

The effect of fuselage longitudinal instability with tail slenderness ratio is reported in figure 55. The variation of C_{M_α} is, with good approximation, a linear function of the tail length. In figure 56 is reported the moment coefficient as function of the tail geometry variation for both α analysed. Figure 57 shows the different pressure distribution for two tail configurations. As in the case of the nose, a tail shorter than the reference configuration may be advantageous for the cruise conditions.

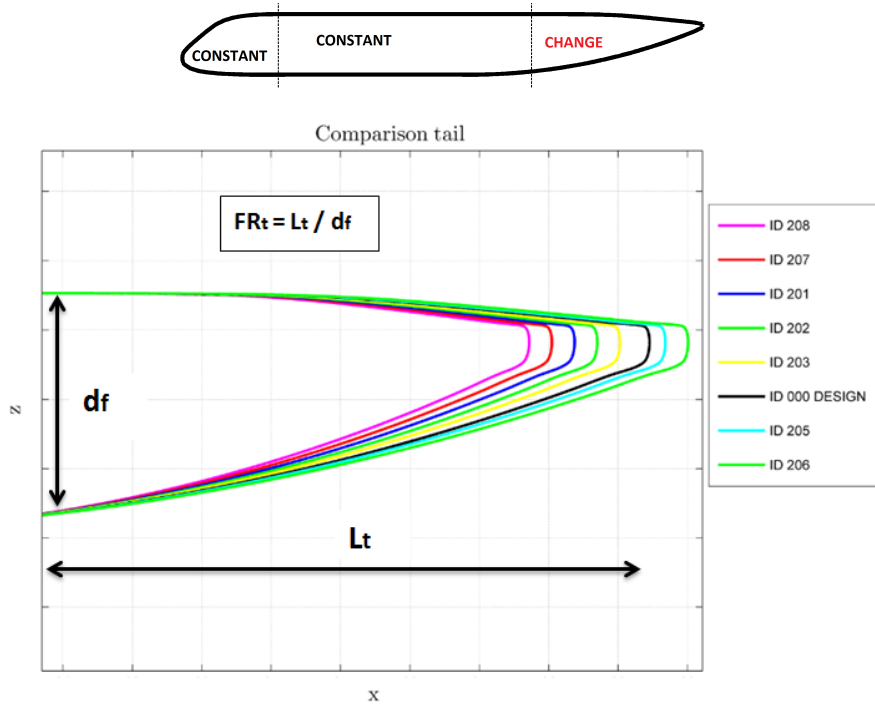


Figure 50: Comparison of different tail.

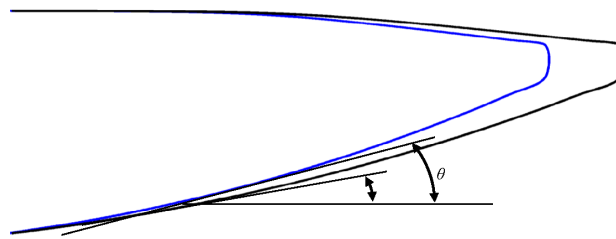


Figure 51: Variation in fuselage tail length and upsweep angle.

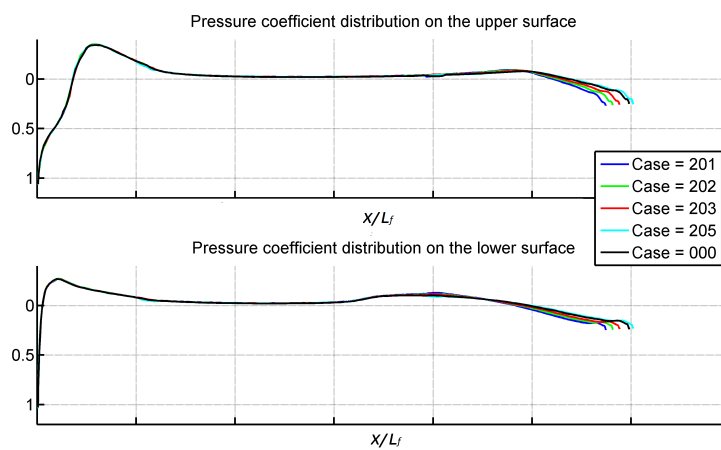


Figure 52: Pressure distribution on the fuselage symmetry plane, due to tail variation, $\alpha = 0^\circ$.

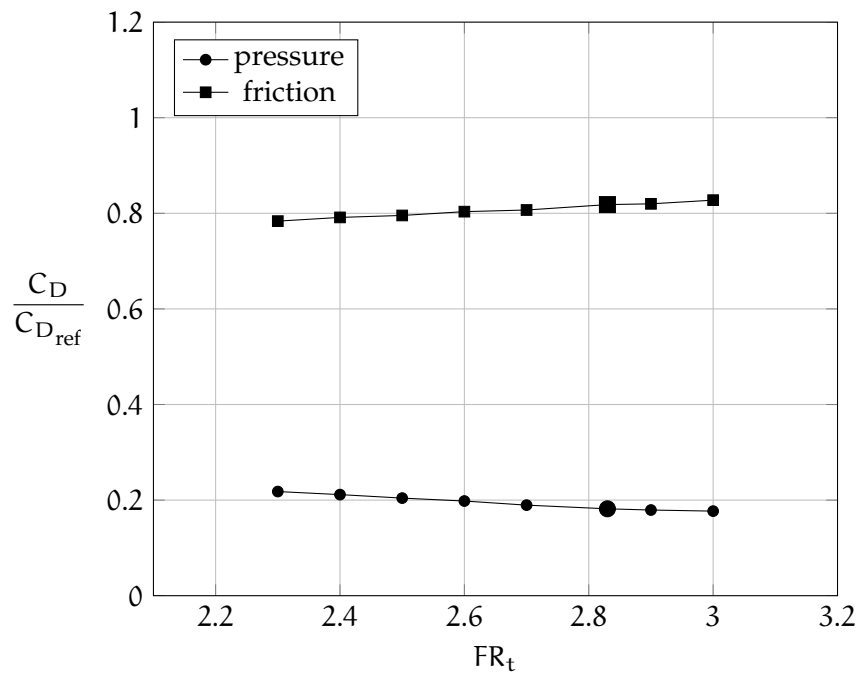


Figure 53: Friction and pressure contributions to drag coefficient due to tail variation, $\alpha = 0^\circ$.

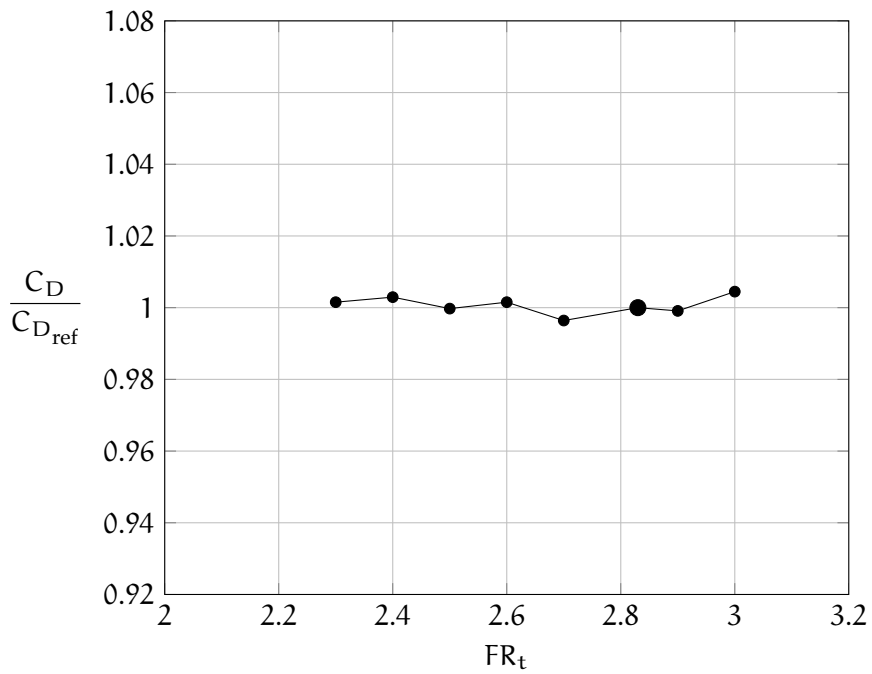


Figure 54: Drag coefficient due to tail variation (sum of pressure and friction contributions), $\alpha = 0^\circ$.

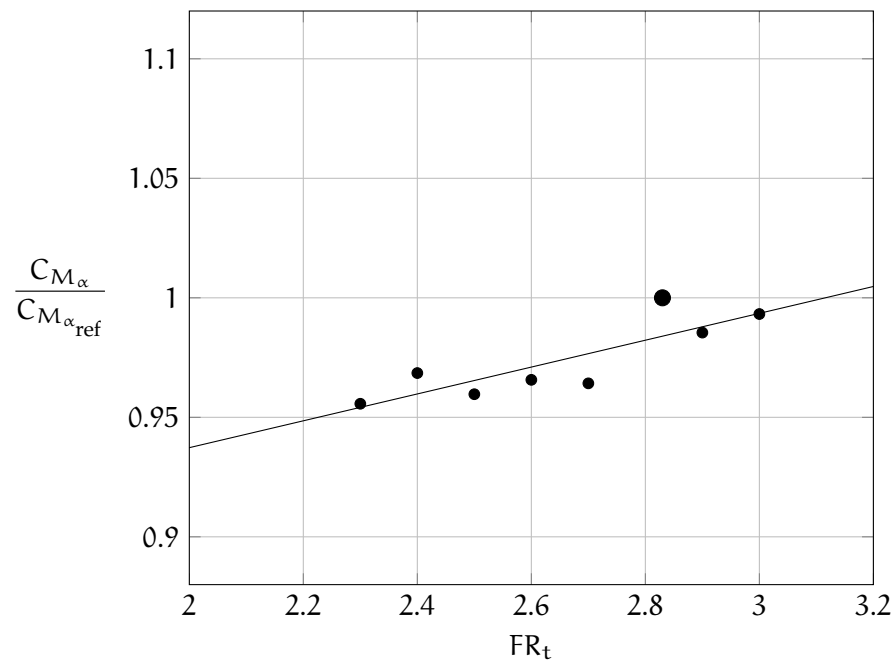


Figure 55: Effect of the upsweep angle on fuselage longitudinal stability.

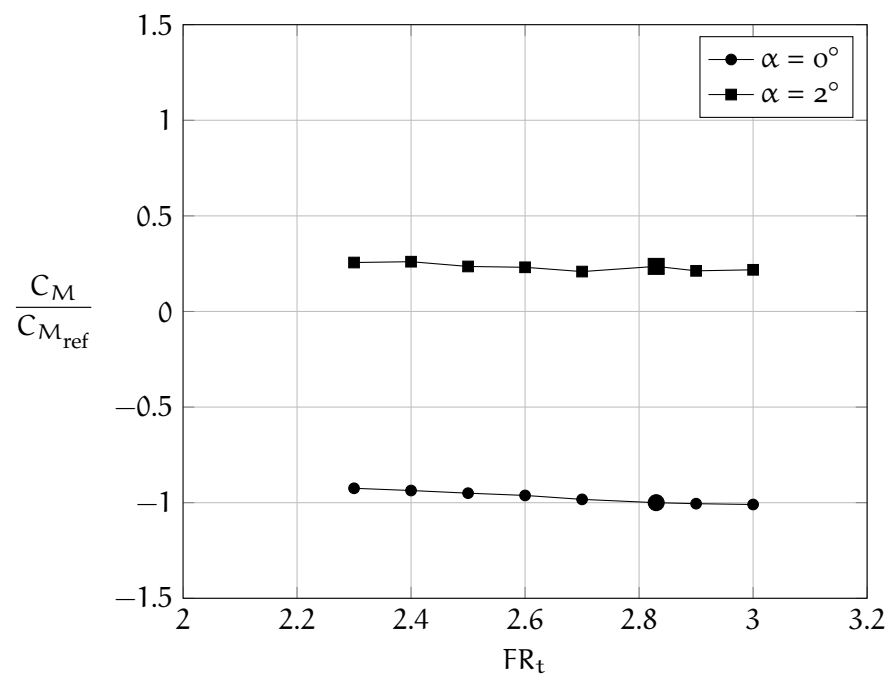


Figure 56: Moment coefficient as function of the tail geometry variation, $\alpha = 0^\circ$ e $\alpha = 2^\circ$

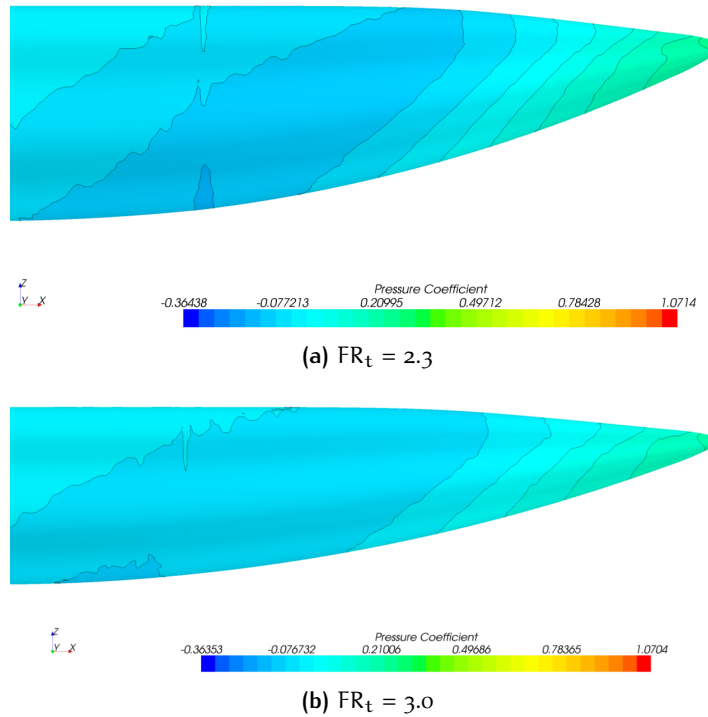


Figure 57: Comparison of the pressure distribution for two nose configurations, $\alpha = 0^\circ$.

4.4 VARIATION OF THE NOSE HEIGHT

The effect of nose height has been investigated with three layout on four slenderness ratio ($FR_n = 1.2, 1.4, 1.6, 1.7$, see also table 8), for a total of 12 combinations (including the reference fuselage). A schematic layout is shown in figure 58, where the black line is the standard layout (the same nose height and windshield angle as reference geometry). As the nose is lowered the windshield angle (considered as the slope of the upper surface on the fuselage symmetry plane) increases.

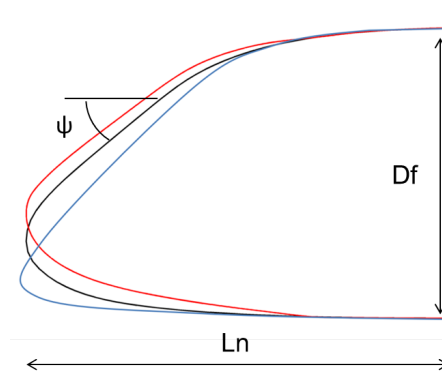


Figure 58: Variation of the windshield angle.

Results are shown in figure 59. In the next charts, the bigger marker represents the reference value. It is clear that, given the smooth refer-

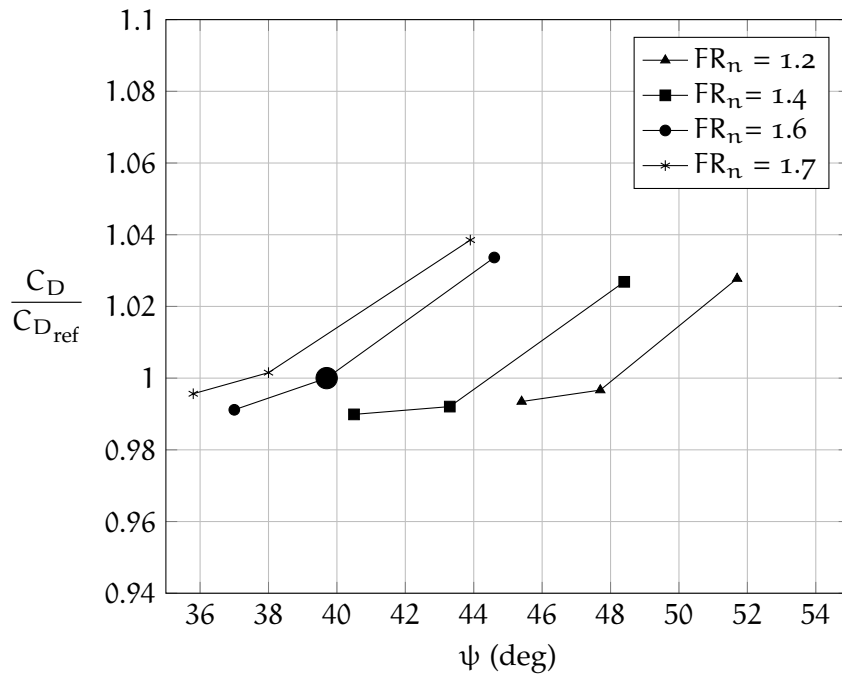


Figure 59: Effect of the nose height (and hence windshield angle) on drag coefficient, $\alpha = 0^\circ$.

ence geometry from which new shapes have been generated, as the slope of the upper surface of the fuselage (and hence the windshield angle) is increased the drag coefficient increases, because of stronger pressure gradients. The longitudinal stability is slightly reduced with the windshield angle, but this effect is negligible, especially if compared with the effect of slenderness ratio (figure 60). The reference layout (central point of each curve) offers good pilot visibility with low drag coefficient (with respect to the configurations analysed).

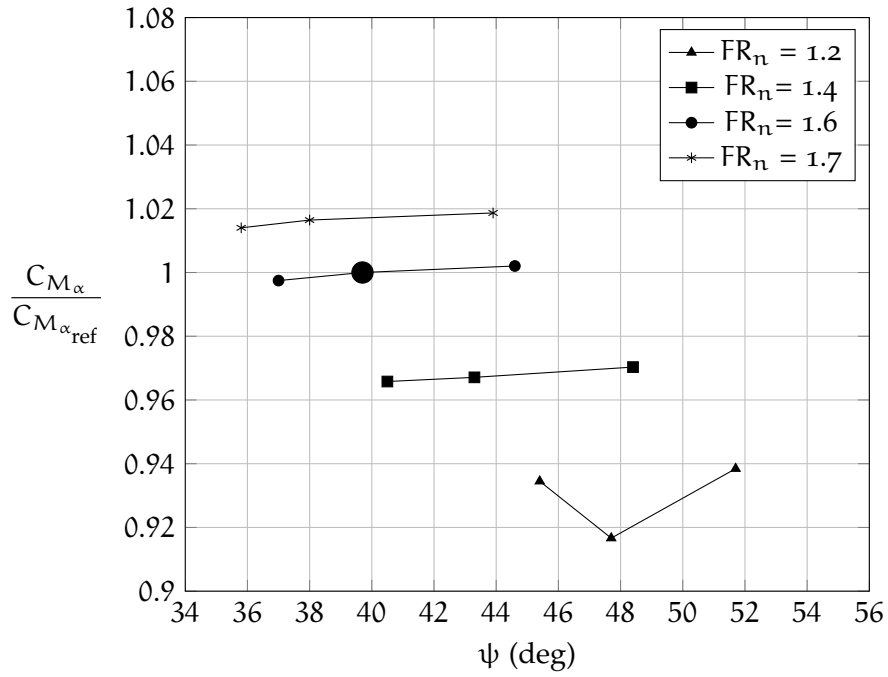


Figure 60: Effect of the nose height (and hence windshield angle) on fuselage longitudinal stability.

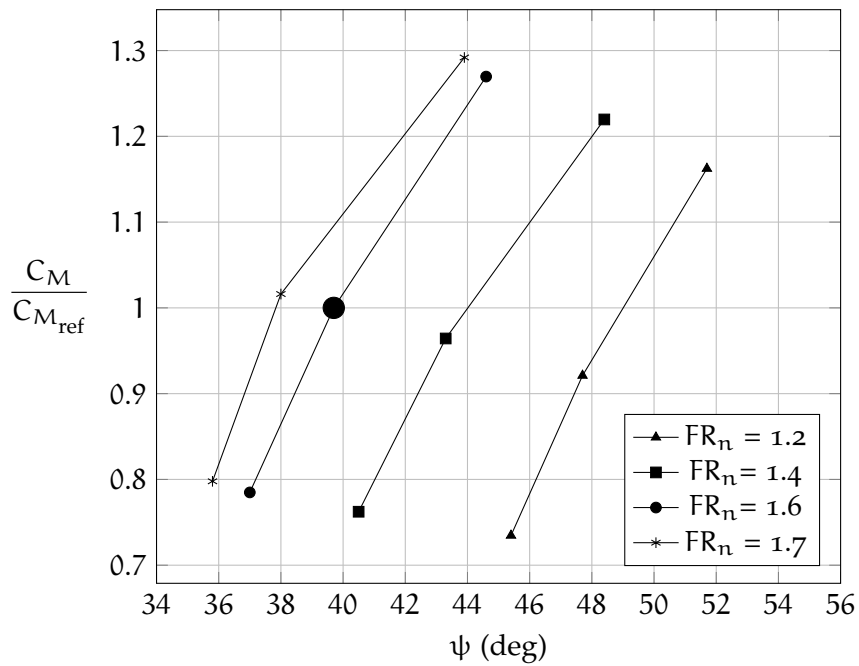


Figure 61: Effect of the nose height (and hence windshield angle) on the moment coefficient, $\alpha = 0^\circ$

4.5 VARIATION OF THE UPSWEEP ANGLE

For three tail configurations ($L_t = 2.50, 2.83, 3.00$, see also table 9) the upswEEP angle, defined in Figure 34, has been varied as depicted in figure 62. The effect of this parameter is to change the pressure drag (and hence the drag coefficient), as shown in figure 63. The reference value is represented by the bigger marker.

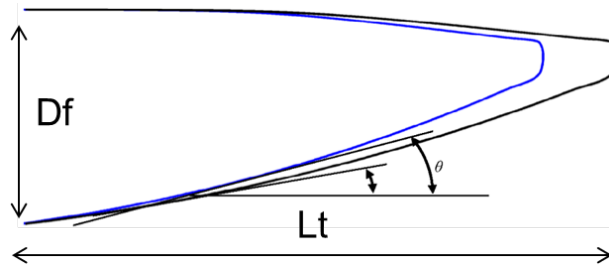


Figure 62: Variation of the upswEEP angle.

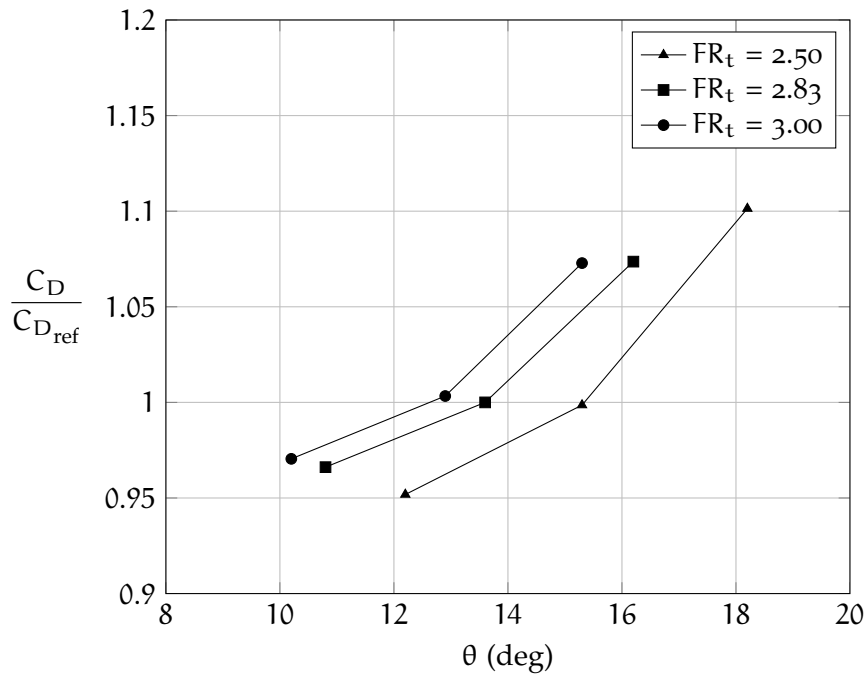


Figure 63: Effect of the upswEEP angle on fuselage longitudinal stability.

For a given upswEEP angle (a vertical line in figure 63), the longer is the tail, the bigger is the drag coefficient. This is due to the increased wet area. Conversely, for a given drag coefficient (a horizontal line in figure 63), the shorter is the tail, the bigger is the upswEEP angle. In this case, what is saved in skin friction (wet area) is lost in pressure drag. The increase in upswEEP angle leads to a slightly reduced longitudinal instability, see figure 64. For a given upswEEP angle, this

instability increases with tail slenderness. However, the variation in C_{M_α} from the reference value (the bigger marker) are very small.

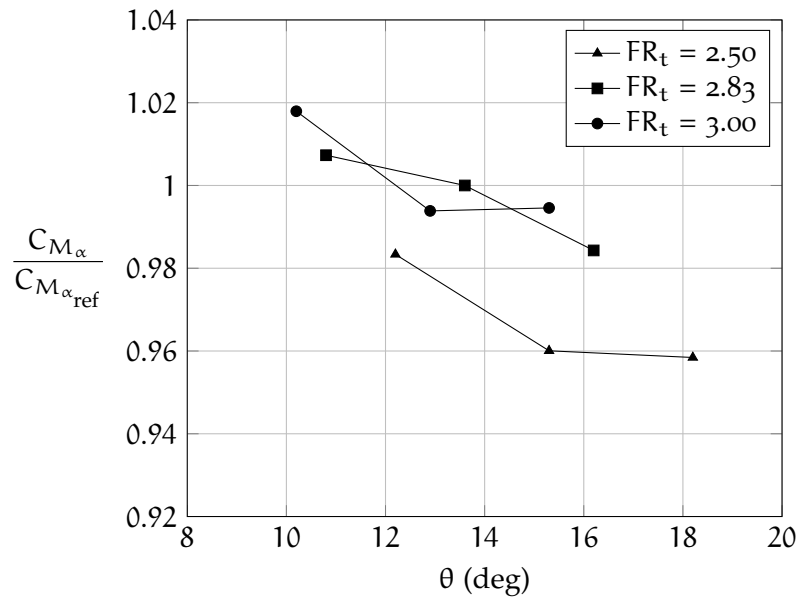


Figure 64: Effect of the upswEEP angle on drag coefficient, $\alpha = 0^\circ$.

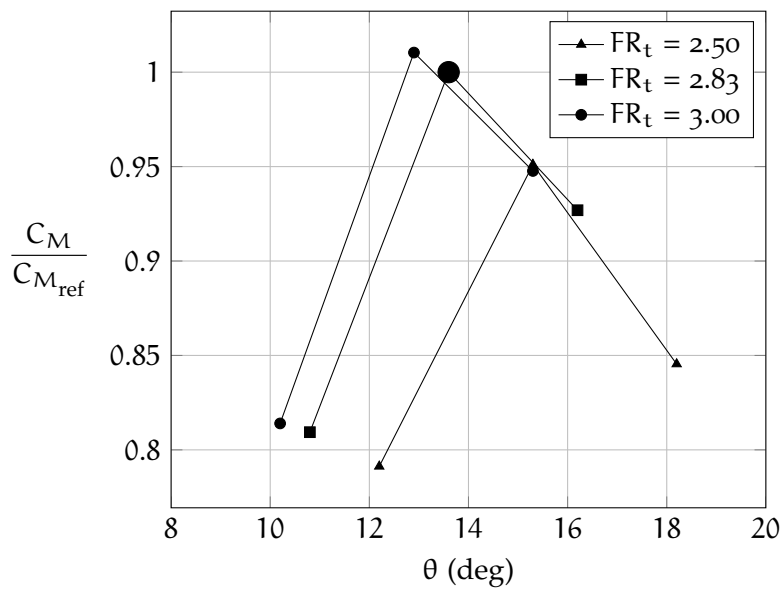


Figure 65: Effect of the upswEEP angle on moment coefficient, $\alpha = 0^\circ$.

5

A NEW METHODOLOGY FOR PREDICTION OF AERODYNAMIC COEFFICIENTS

Contents

5.1	Methodology for drag prediction	68
5.1.1	The shape factor of the nose	69
5.1.2	The shape factor of the cabin	70
5.1.3	The shape factor of the tail	70
5.1.4	Example of application	72
5.2	Pitching moment prediction	79
5.2.1	Example of application	81
5.3	Prediction of the pitching moment derivative	84
5.3.1	Example of application	87

In this chapter it is proposed a methodology to obtain the value of drag and pitching moment coefficient as a function of fuselage geometry and it is suitable for smooth shapes. This approach does not allow to evaluate some sources of drag as leakage, wiper, surface roughness and excrescences.

5.1 METHODOLOGY FOR DRAG PREDICTION

The methodology allows to compute the fuselage drag coefficient as the sum of the contributions of each component (nose, cabin, and tailcone), calculated as follows.

$$S_{\text{front}} C_{D_i} = K_i C_{D_{fp}} S_{\text{wet } i} \quad (5.1)$$

In the previous equation i states the geometry part (nose, cabin or tailcone), S_{front} is the frontal surface (equal to the maximum area of cabin section), $S_{\text{wet } i}$ is the wet surface of the i -th part, the $C_{D_{fp}}$ is the drag coefficient of equivalent flat plate and the K_i is the shape factor which is the core of the method here presented. It wasn't chosen the S_{wing} as the reference surface because the wing could be unknown when the fuselage is designed. The equation 5.1 is quite similar to equation 2.4 proposed by Torenbeek [23] but there is a fundamental conceptual difference: the shape factor just introduced, K_i , takes into account the variation of the pressure drag due to the modifications of the fuselage geometry shape, while the form factor of Torenbeek,

ϕ , it's a number that links the equivalent parasite area of a body of revolution to a flat plate with the same wetted area. The hypothesis of the super-positioning of the effects is verified by the CFD results since the geometry modifications of one part of the fuselage affect only the drag coefficient of that part (see chapter 4). For this reason the formula 5.1 can be expressed in more precise way as follows.

$$S_{\text{front}} C_{D_{\text{fus}}} = \left(K_n \times \frac{S_{\text{wet}_{\text{nose}}}}{S_{\text{wet}}} + K_c \times \frac{S_{\text{wet}_{\text{cabin}}}}{S_{\text{wet}}} + K_t \times \frac{S_{\text{wet}_{\text{tail}}}}{S_{\text{wet}}} \right) C_{D_{\text{fp}}} S_{\text{wet}} \quad (5.2)$$

In the table 13, there are the definitions of the main parameter present in the equation 5.2.

	Definition
$C_{D_{\text{fus}}}$	is the drag coefficient of the fuselage referred to S_{front} .
K_n	is the nose shape factor. It depends on windshield angle, ψ , and on the FR_n .
K_c	is the cabin shape factor. It depends on the FR.
K_t	is the tailcone shape factor. It depends on upsweep angle, θ , and on the FR_t .
$C_{D_{\text{fp}}}$	is the drag coefficient of equivalent flat plate and it coincides with the skin friction coefficient, \bar{C}_f , which can be computed from equation 2.6, reported here for convenience.

$$C_{D_{\text{fp}}} = \frac{0.455}{(\log Re)^{2.58} \cdot (1 + 0.144 \cdot M^2)^{0.58}}$$

Therefore it's known once that M and Re (referred to fuselage length) are fixed.

Table 13: Main parameter of the proposed method.

All the coefficients useful to estimate the shape factors are referred to S_{front} and the $C_{D_{\text{fp}}}$ is evaluated using the Reynolds number based on the fuselage length.

5.1.1 The shape factor of the nose

The nose shape factor, K_n , represents the contribution of the nose to the global drag coefficient and it takes into account the effect of the nose fineness ratio and of the angle of pilot visibility. It is estimated from the CFD value of the coefficient C_{D_n} (see appendix C, table 22), which is referred to S_{front} and the $C_{D_{\text{fp}}}$, referred to $S_{\text{wet}_{\text{nose}}}$.

$$K_n = \frac{C_{D_n} S_{\text{front}}}{C_{D_{\text{fp}}} S_{\text{wet}_{\text{nose}}}} \quad (5.3)$$

In figure 66 the curves of K_n are drawn as a function of FR_n and parametrized in ψ (windshield angle). These curves must be used to calculate the value of the shape factor in order to apply the method. Moreover, from the figure, it's possible to see that the nose shape factor decreases with the fineness ratio for a fixed windshield angle while, for a fixed fineness ratio, the shape factor grows with the windshield angle because there's a stronger pressure gradient and therefore a higher pressure drag. To show in a clearer way what has been just stated, in the figure 67 the curves of K_n are drawn as a function of ψ (upsweep angle) and parametrized in FR_n .

5.1.2 The shape factor of the cabin

The nose shape factor, K_c , represents the contribution of the cabin to the global drag coefficient and it takes into account the effect of the cabin stretching. It is estimated from the CFD value of the coefficient C_{D_c} (see appendix C, table 23), which is referred to S_{front} and the $C_{D_{fp}}$, referred to $S_{wet_{cabin}}$.

$$K_c = \frac{C_{D_c} S_{front}}{C_{D_{fp}} S_{wet_{cabin}}} \quad (5.4)$$

In the figure 68 the curve of K_c is drawn as a function of FR . It is noted a decreasing linear trend. As for the nose shape factor, this curve must be used to extract the value of the shape factor in order to apply the method.

5.1.3 The shape factor of the tail

The tail shape factor, K_t , represents the contribution of the tail to the global drag coefficient and it takes into account the effect of the upsweep angle used as the parameter to consider the rotation angle required to take-off. As usual, it is estimated from the CFD value of the coefficient C_{D_t} (see appendix C, table 24), which is referred to S_{front} and the $C_{D_{fp}}$, referred to $S_{wet_{tail}}$. In the same chart, the curve of θ_{lim} is traced. This curve is the locus of the maximum value of the upsweep angle for fixed fineness ratio, where the meaning of "maximum" is explained with the scheme in figure 70. In fact, aeronautically speaking, it makes no sense to go beyond the maximum value of upsweep angle for a fixed FR_t because it would not be more of a fuselage.

$$K_t = \frac{C_{D_t} S_{front}}{C_{D_{fp}} S_{wet_{tail}}} \quad (5.5)$$

In the figure 69 the curves of K_t are drawn as a function of FR_t and parametrized in θ (upsweep angle). As for the other shape factor,

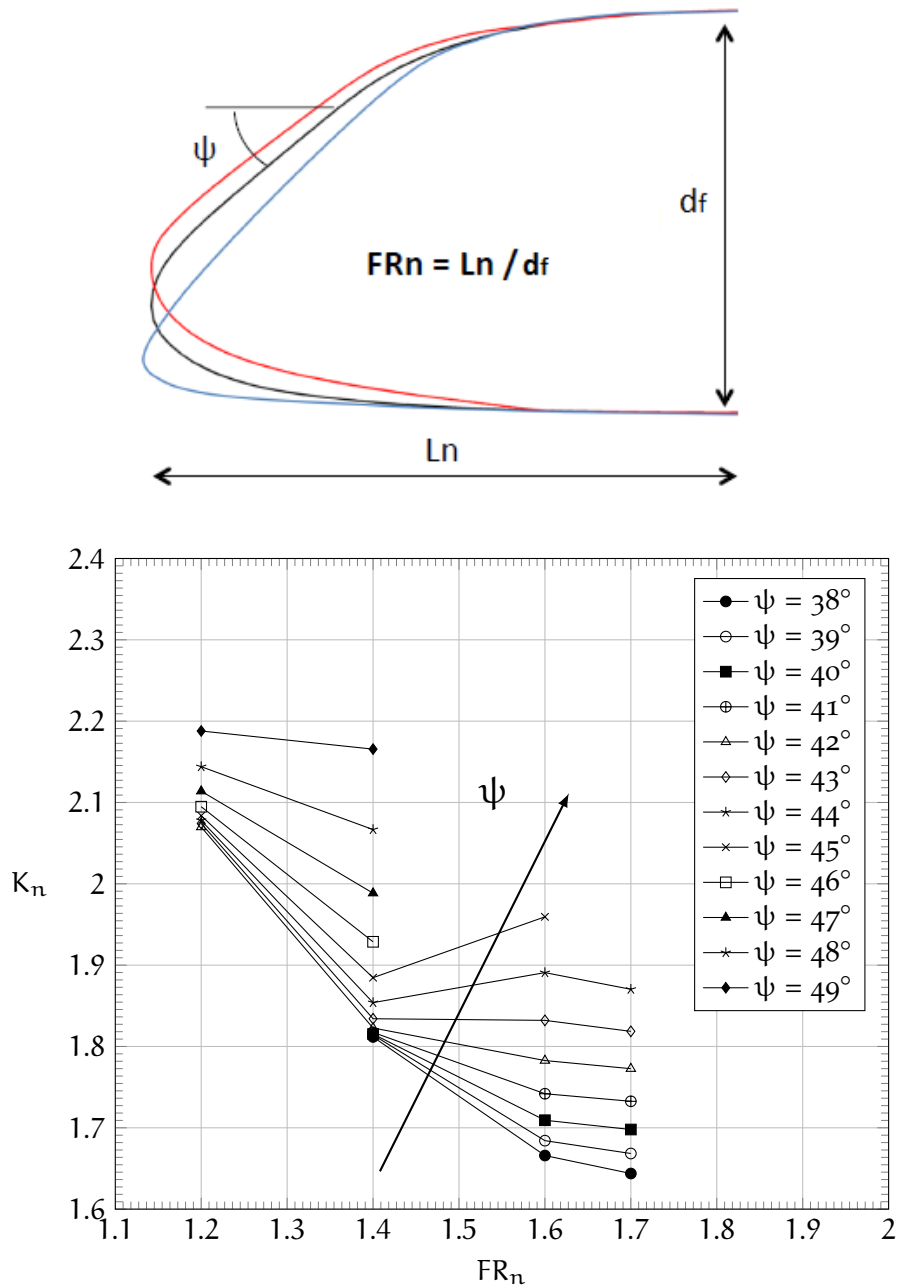


Figure 66: Nose shape factor as a function of FR_n , $\alpha = 0^\circ$.

these curve must be used to extract the value of the shape factor in order to apply the method. The tailcone factor grows with the fineness ratio for a fixed upswep angle, θ , due to the bigger S_{wet} and it grows with the upswep angle for a fixed fineness ratio because there's a stronger pressure gradient. To show in a clearer way what has been just stated, in the figure 71 the curves of K_t are drawn as a function of θ (upswep angle) and parametrized in FR_t .

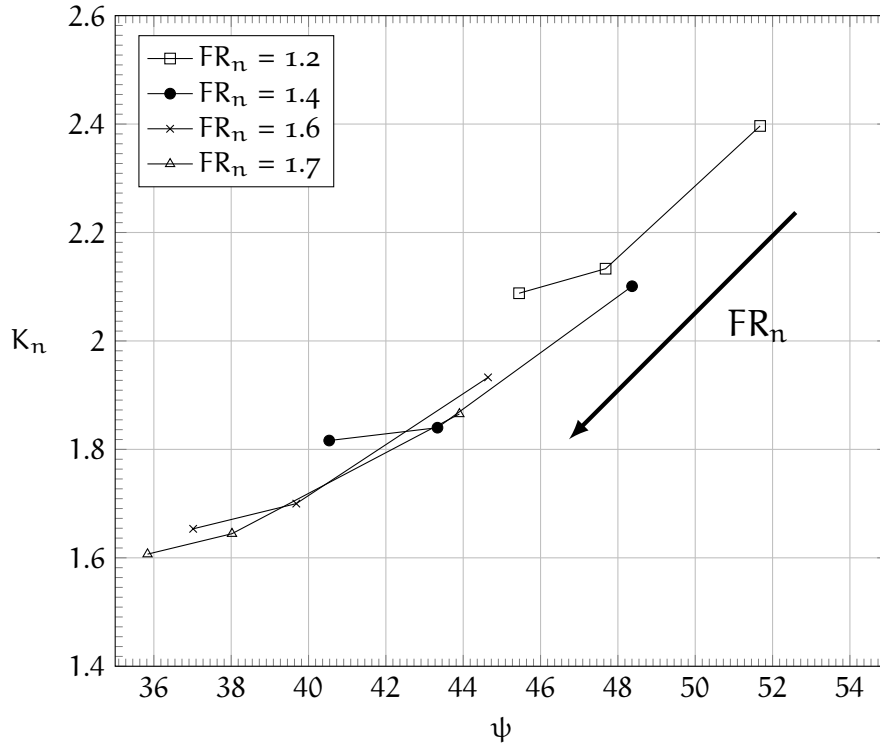


Figure 67: Nose shape factor as a function of windshield angle ψ , $\alpha = 0^\circ$.

5.1.4 Example of application

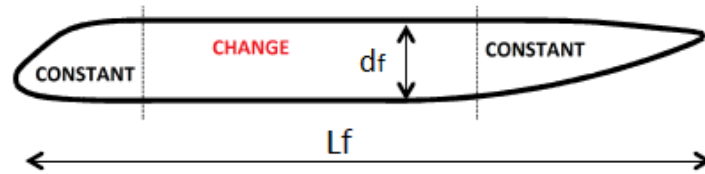
From previous sections, to calculate the global drag coefficient, it must be used the equation 5.2, where K_n , K_c and K_t are the shape factors of different geometry part values of which are extracted from figure 66, 68 and 69 respectively.

$$S_{\text{front}} C_{D_{\text{fus}}} = \left(K_n \times \frac{S_{\text{wet}_{\text{nose}}}}{S_{\text{wet}}} + K_c \times \frac{S_{\text{wet}_{\text{cabin}}}}{S_{\text{wet}}} + K_t \times \frac{S_{\text{wet}_{\text{tail}}}}{S_{\text{wet}}} \right) C_{D_{\text{fp}}} S_{\text{wet}} \quad (5.6)$$

Until now the C_D has been calculated for each configuration of the fuselage which is different from that of reference only for one geometry part. In order to validate the method, some fuselages, which characteristics are reported in table 14, have been simulated.

In order to clarify the different steps of the methodology, the latter is applied to the "103201" fuselage. First of all, the shape factors must be evaluated. These can be obtained from the graphs since the FR , ψ and θ are known. In particular, for the fuselage under consideration, these parameters are the following.

- $FR_n = 1.3$
- $FR = 8.69$



$$FR = L_f / d_f$$

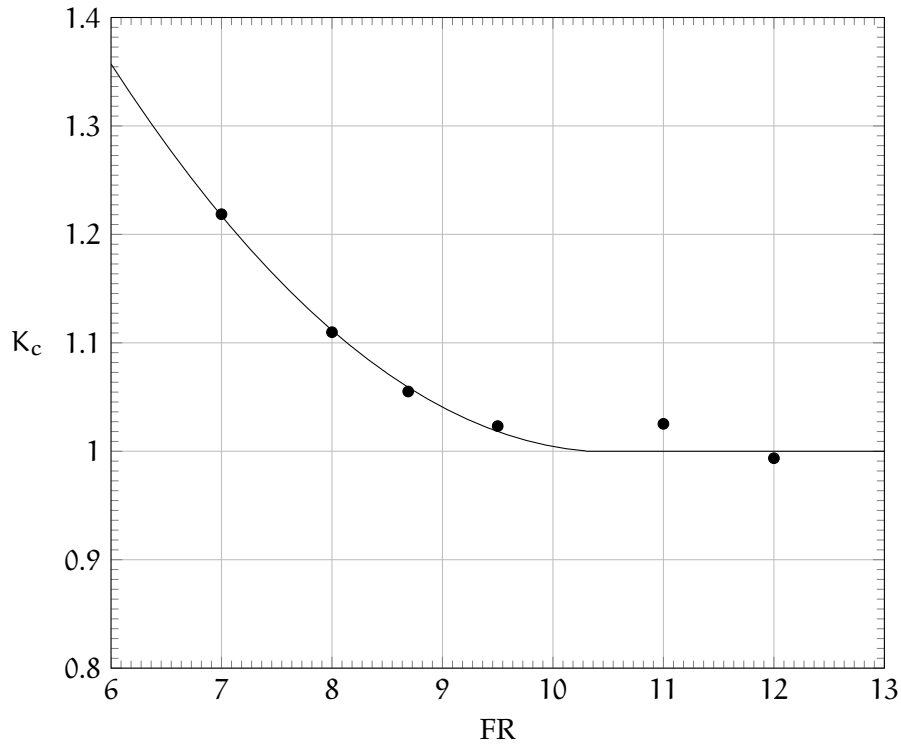


Figure 68: Cabin shape factor as a function of FR , $\alpha = 0^\circ$.

- $FR_t = 2.5$
- $\psi = 45.0^\circ$
- $\theta = 15.3^\circ$

The value of the nose shape factor is extracted from the chart entering with the value of FR_n , as it's possible to see from figure 72.

$$K_n = 1.98$$

Similarly the cabin shape factor is extracted from the relative chart entering with the value of FR (figure 73) and that of the tailcone from the graph in figure 74 entering with the value of FR_t .

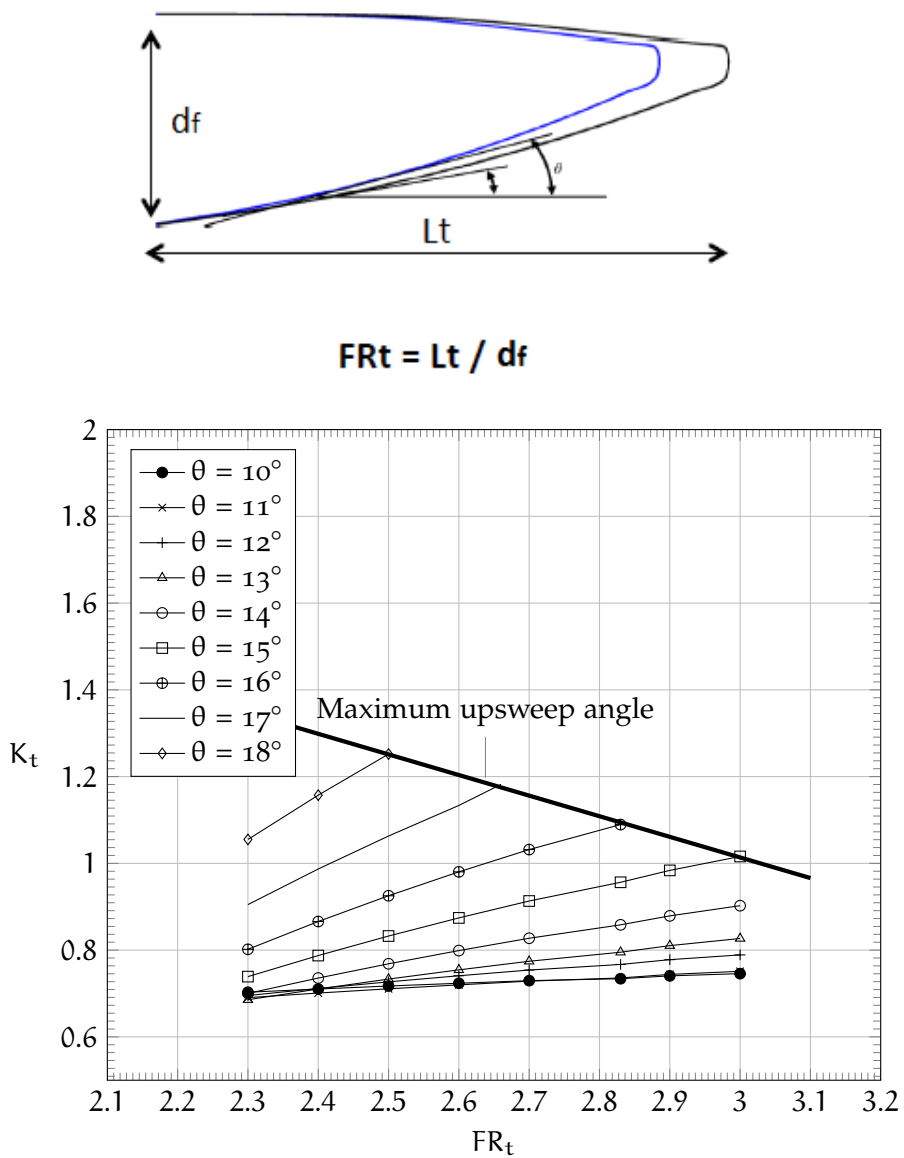


Figure 69: Tail shape factor as a function of FR_t , $\alpha = 0^\circ$.

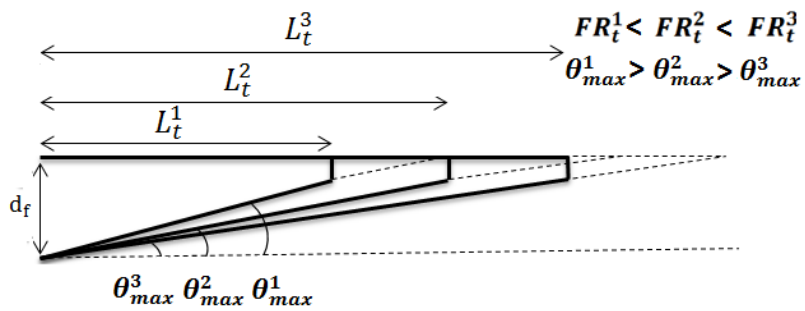


Figure 70: Scheme of the geometric relationship between maximum value of upsweep angle (θ) and the fineness ratio of the tailcone (FR_t).

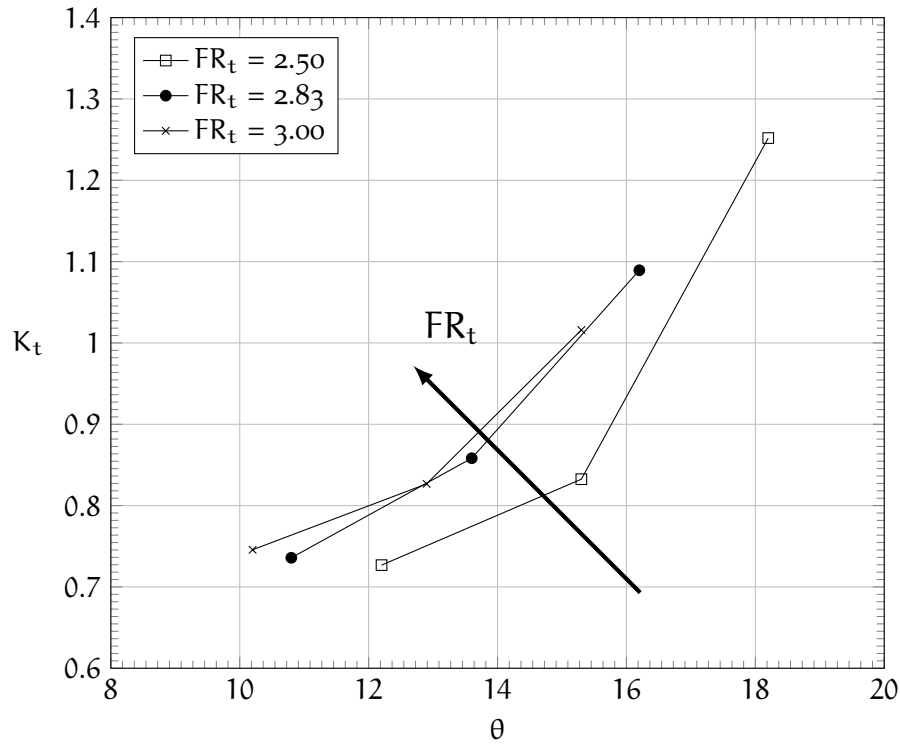


Figure 71: Tail shape factor as a function of upsweep angle θ , $\alpha = 0^\circ$.

$$K_c = 1.06$$

$$K_t = 0.83$$

In order to apply the formula 5.2, the value of $C_{D_{fp}}$ must be computed using the equation 2.6 and, to do it, the Reynolds and the Mach numbers have to be specified. For a flat plate that has the same length of the fuselage in question, the aforementioned values are the following:

- $Re_{L_f} = 187 \times 10^6$,
- $M = 0.52$.

Therefore the value of the drag coefficient of equivalent flat plate is the following.

$$C_{D_{fp}} = \frac{0.455}{(\log Re)^{2.58} \cdot (1 + 0.144 \cdot M^2)^{0.58}} =$$

$$= 0.001952$$

ID	Description
103201	is the fuselage with FR_n equal to 1.3, FR_t equal to 2.5 and the same cabin of the reference configuration (FR equal to 8.69)
101004206	is the fuselage with FR_n equal to 1.1, FR equal to 11 and FR_t equal to 3.0
107002208	is the fuselage with FR_n equal to 1.7, FR equal to 8 and FR_t equal to 2.3

Table 14: Notations about the fuselage configurations used to validate the methodology.

Finally, the value of wet surfaces, that can be estimated with equation 2.8, necessary to apply the methodology, are reported below (table 15).

	$S_{wet_{nose}}/S_{wet}$	$S_{wet_{cabin}}/S_{wet}$	$S_{wet_{tail}}/S_{wet}$	S_{wet}/S_{front}
103201	0.1601	0.6055	0.2343	27.7050

Table 15: The necessary values to apply the methodology for the "103201" fuselage.

From these values and by the equation 5.2, it's possible to estimate, in "modular" way, the drag coefficient of the fuselage.

$$\begin{aligned}
 C_{D_{fus}} &= \left(K_n \times \frac{S_{wet_{nose}}}{S_{wet}} + K_c \times \frac{S_{wet_{cabin}}}{S_{wet}} + K_t \times \frac{S_{wet_{tail}}}{S_{wet}} \right) C_{D_{fp}} \frac{S_{wet}}{S_{front}} = \\
 &= (1.98 \cdot 0.1601 + 1.06 \cdot 0.6055 + 0.83 \cdot 0.2343) \cdot 0.001592 \cdot 27.7050 \\
 &= 0.061844
 \end{aligned}$$

This value is very close to that obtained from the CFD simulation which is equal to 0.062742. The difference between the results is less than 2%.

The methodology has been applied even for the other two fuselage configurations described in the table 14. The useful parameters are in the table 16.

In the table 17 the results of methodology are reported and compared with that obtained by CFD simulations. The maximum difference between the results is less than 2%.

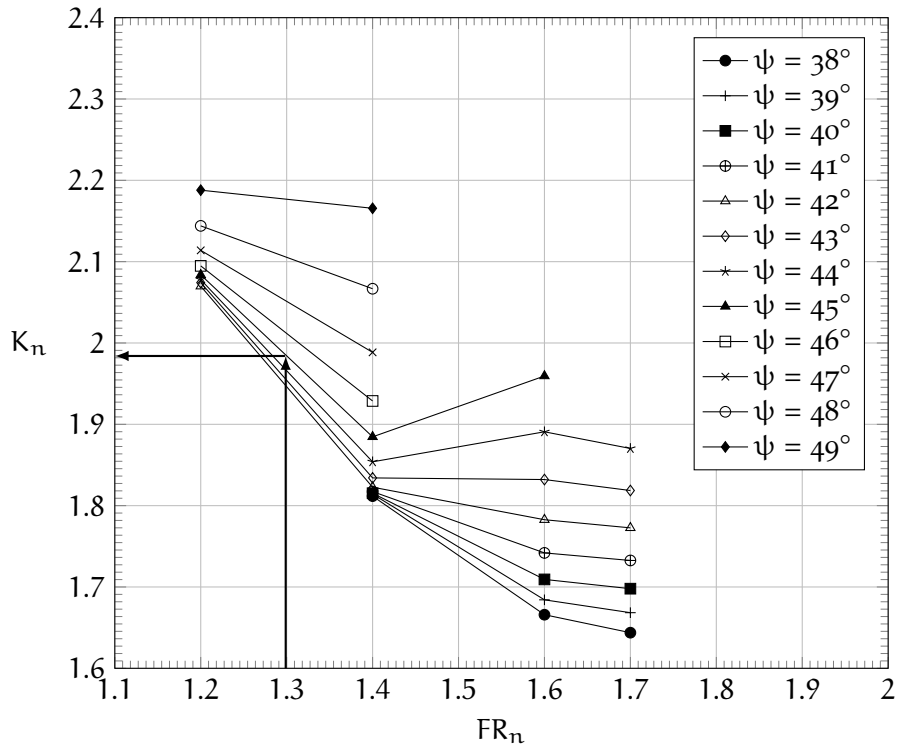


Figure 72: The value of the nose shape factor for the "103201" fuselage, $\alpha = 0^\circ$.

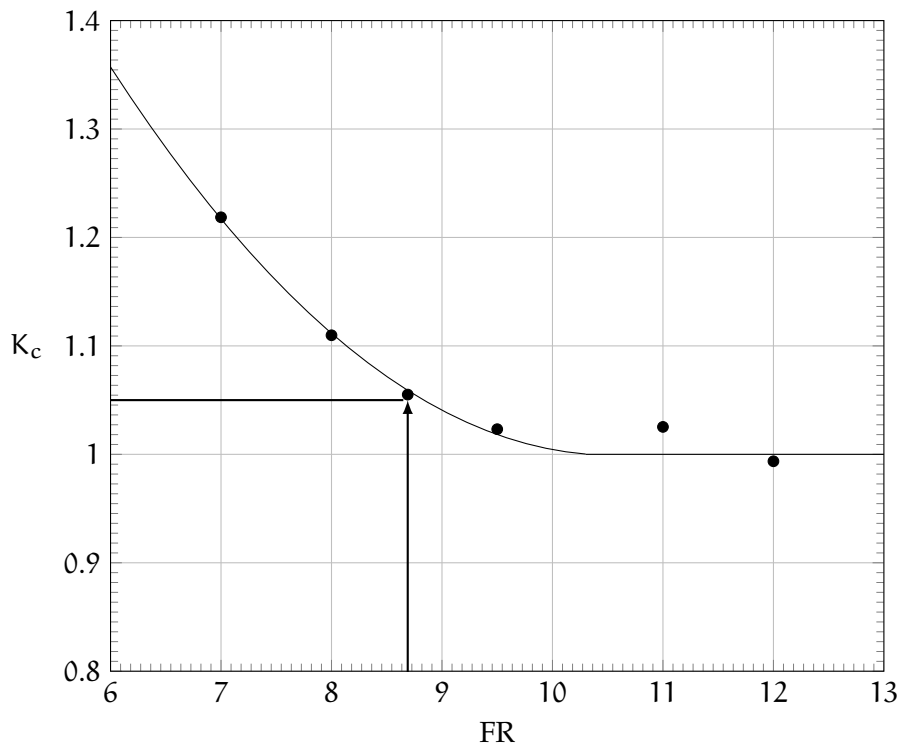


Figure 73: The value of the cabin shape factor for the "103201" fuselage, $\alpha = 0^\circ$.

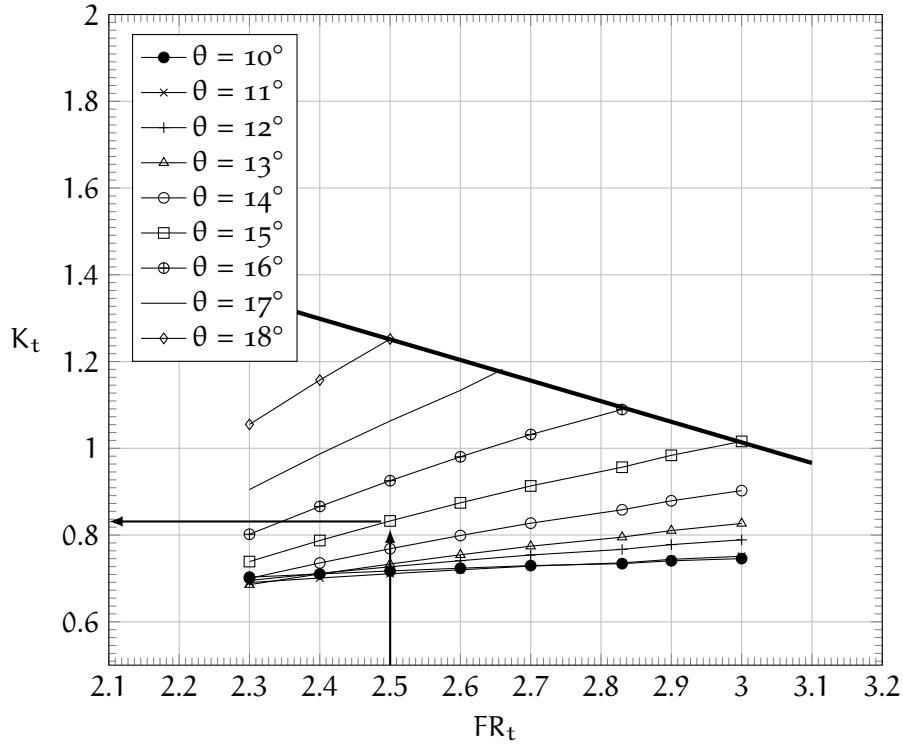


Figure 74: The value of the tailcone shape factor for the "103201" fuselage, $\alpha = 0^\circ$.

	101004206	107002208
K_n	2.33	1.65
K_c	1.03	1.12
K_t	0.82	0.90
$C_{D_{fp}}$	0.001897	0.001945
$S_{wet_{nose}}/S_{wet}$	0.1019	0.2207
$S_{wet_{cabin}}/S_{wet}$	0.6919	0.5462
$S_{wet_{tail}}/S_{wet}$	0.2062	0.2331
S_{wet}/S_{front}	37.5923	25.6906

Table 16: The necessary values to apply the method for drag coefficient.

	103201	101004206	107002208
Method	0.061844	0.079567	0.059249
CFD	0.062388	0.079182	0.060037
Difference	0.57%	-0.49%	1.31%

Table 17: Comparison between the simulation results and that obtained using the proposed methodology for the drag coefficient.

5.2 METHODOLOGY FOR THE PITCHING MOMENT PREDICTION

The proposed methodology allows to compute the pitching moment coefficient at α equal to 0° (α is the angle between the waterline of the fuselage which corresponds to x axis and the flow direction, see figure 75) for a "modular" fuselage as function of the geometry parameters. In the figure 75 also the position of reference center (which corresponds to the center of gravity) is shown. Unlike the drag coefficient, in this case the hypothesis of super-positioning of the effects is not verified and therefore the strategy to evaluate the moment coefficient is quite different from previous one. In fact the moment coefficient (referred to S_{front} and L_f) is estimated as the sum of three contributions (equation 5.7).

$$C_{M_{\alpha=0}} = C_{M_{\text{FR}}} + \Delta C_{M_{\text{nose}}} + \Delta C_{M_{\text{tail}}} \quad (5.7)$$

where $C_{M_{\text{FR}}}$ is the moment coefficient for a given fineness ratio FR, $\Delta C_{M_{\text{nose}}}$ is the correction term due to the nose geometry and $\Delta C_{M_{\text{tail}}}$ is the correction term due to the tailcone geometry. The $C_{M_{\text{FR}}}$ can be expressed as a linear function of fineness ratio (equation 5.8 and figure 76).

$$C_{M_{\text{FR}}} = 0.0021 \cdot \text{FR} - 0.0511 \quad (5.8)$$

The $\Delta C_{M_{\text{nose}}}$ is the difference between the moment coefficient of the fuselage with the nose slenderness ratio FR_n and the moment coefficient of the reference fuselage (which has FR_n equal to 1.6). It is drawn in the figure 77 as a function of windshield angle.

The $\Delta C_{M_{\text{tail}}}$ is the difference between the moment coefficient of the fuselage with the tailcone slenderness ratio FR_t and the moment coefficient of the reference fuselage (which has FR_t equal to 2.83). It is drawn in the figure 78 as a function of upsweep angle.

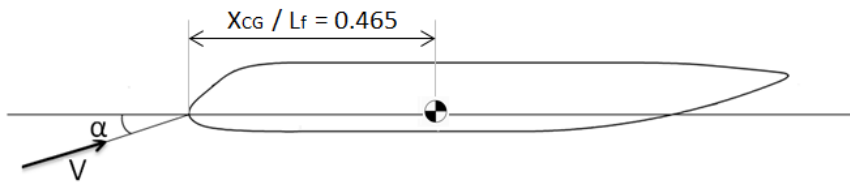


Figure 75: Definition of the position of reference center and of the angle of attack α .

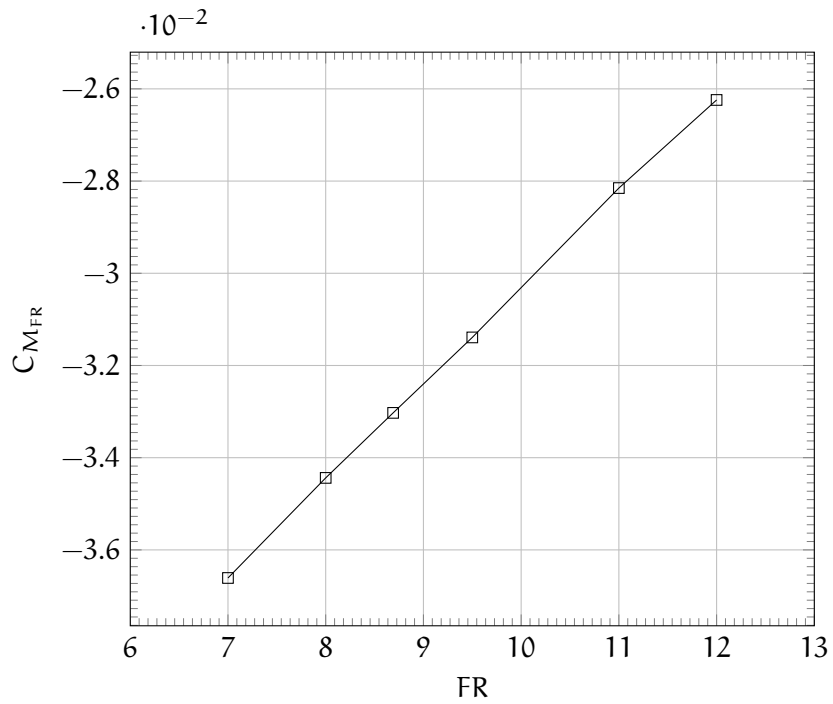


Figure 76: Moment coefficient (referred to S_{front} and L_f) as a function of fineness ratio FR, $\alpha = 0^\circ$.

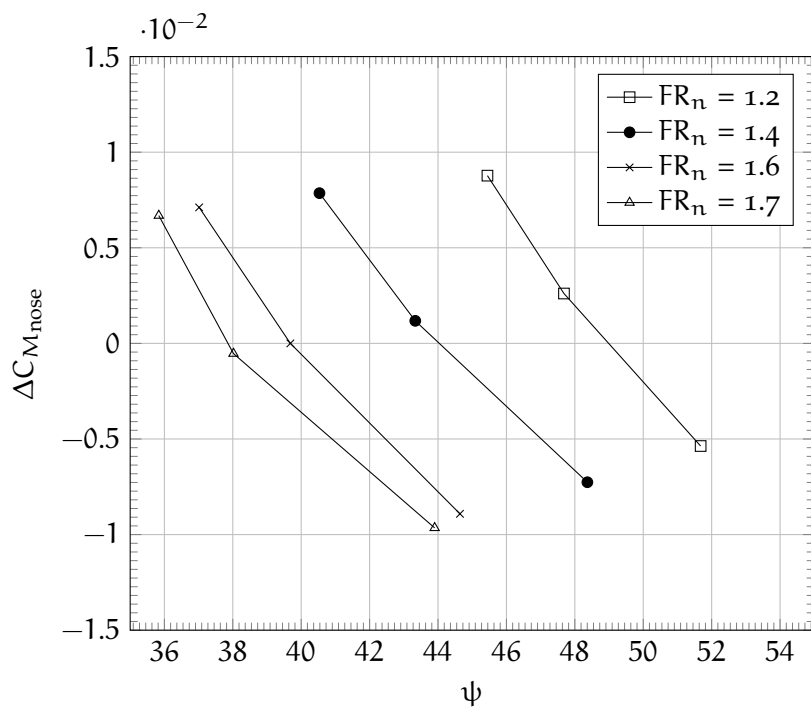


Figure 77: The nose correction term for the moment coefficient as a function of windshield angle ψ , $\alpha = 0^\circ$.

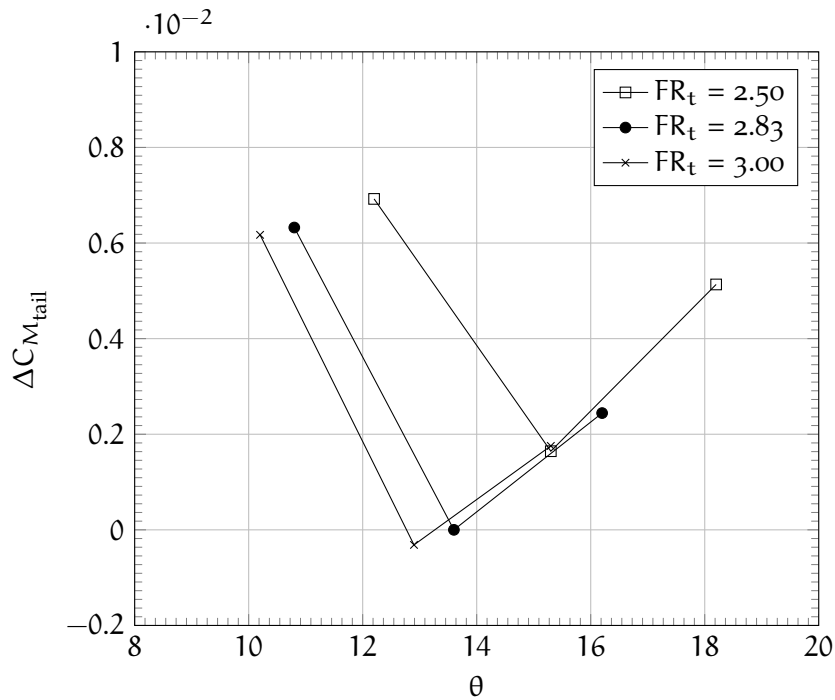


Figure 78: The tail correction term for the moment coefficient as a function of upsweep angle θ , $\alpha = 0^\circ$.

5.2.1 Example of application

The method is here applied to the same geometries previously defined in table 14. For convenience the main geometrical parameters of "103201" fuselage are reported below.

- $FR_n = 1.3$
- $FR = 8.69$
- $FR_t = 2.5$
- $\psi = 45.0^\circ$
- $\theta = 15.3^\circ$

First of all, the moment coefficient must be evaluated. These can be obtained from the equation 5.7 or graphically (figure 79).

$$C_{M_{FR}} = 0.0021 \cdot FR - 0.0511 = -0.033028$$

The value of $\Delta C_{M_{nose}}$ is extracted from the chart entering with the value of FR_n and of the windshield angle, as it's possible to see from figure 80.

$$\Delta C_{M_{nose}} = 0.001791$$

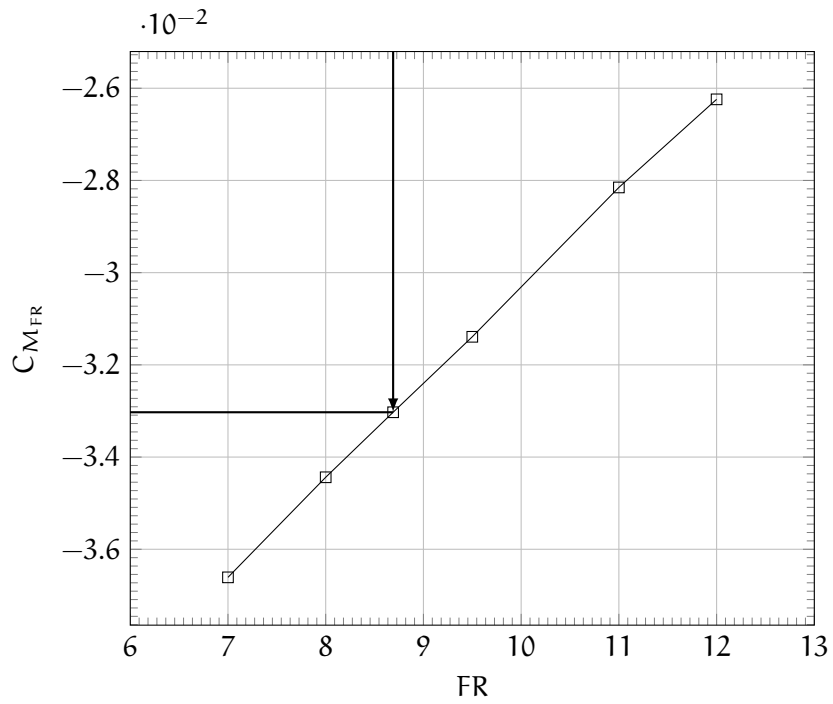


Figure 79: Moment coefficient as a function of fineness ratio FR, $\alpha = 0^\circ$.

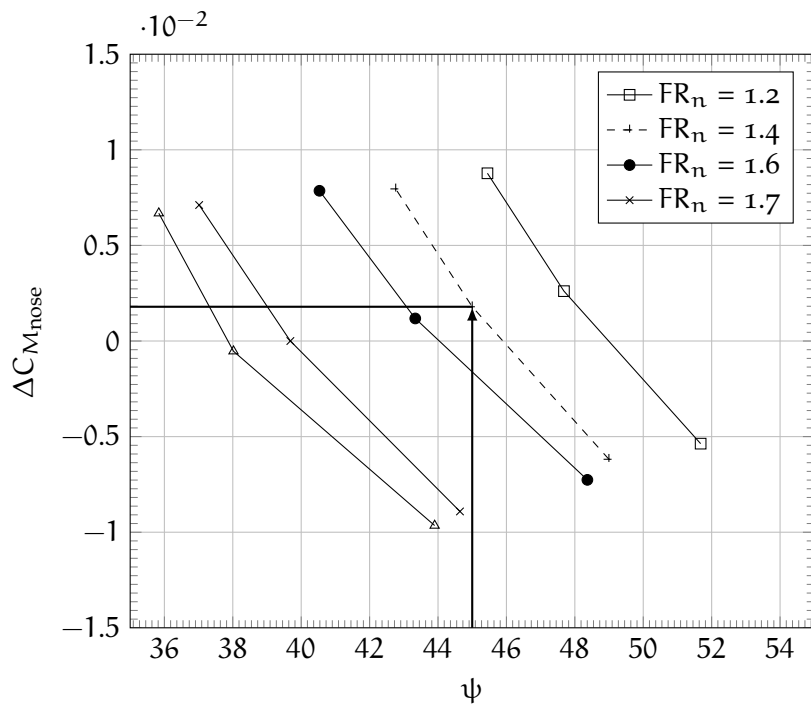


Figure 80: The nose correction term for the moment coefficient as a function of windshield angle ψ , $\alpha = 0^\circ$.

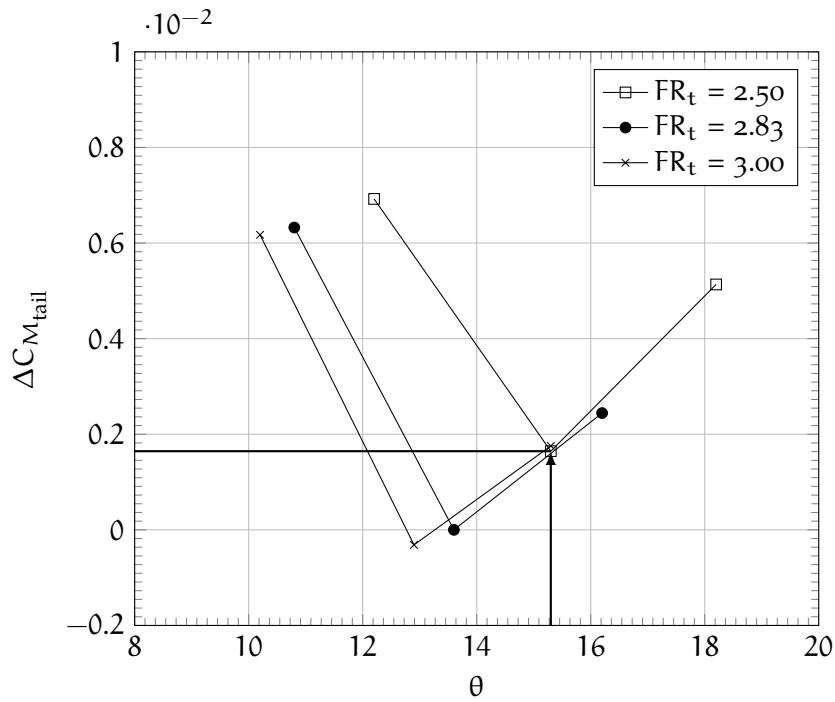


Figure 81: The tail correction term for the moment coefficient as a function of upsweep angle θ , $\alpha = 0^\circ$.

Similarly the value of $\Delta C_{M_{tail}}$ is extracted from the chart entering with the value of FR_t and of the upsweep angle, as it's possible to see from figure 81.

$$\Delta C_{M_{tail}} = 0.001645$$

From these values and by the equation 5.7, it's possible to estimate, in "modular" way, the moment coefficient of the fuselage.

$$\begin{aligned} C_M &= C_{M_{FR}} + \Delta C_{M_{nose}} + \Delta C_{M_{tail}} = -0.033028 + 0.001791 + 0.001645 = \\ &= -0.029591 \end{aligned}$$

This value is very close to that obtained from the numerical simulation which is equal to -0.029571. The difference between the results is about 0.1%.

The methodology has been applied even for the other two fuselage configurations described in the table 14. The useful parameters are in the table 18.

In the table 17 the results of methodology are reported and compared with that obtained by CFD simulations. The maximum difference among the results is about 1%. This approach is valid for a fuselage not too different from the models analysed. The effects of Mach and Reynolds number are supposed to be small.

	101004206	107002208
$C_{M_{FR}}$	-028152	-034438
$\Delta C_{M_{nose}}$	0.003370	-0.000534
$\Delta C_{M_{tail}}$	-0.000315	0.002082

Table 18: The necessary values to apply the method for the moment coefficient.

	103201	101004206	107002208
Method	-0.029591	-0.025096	-0.032890
CFD	-0.029571	-0.025402	-0.032737
Difference	-0.10%	1.2%	-0.5%

Table 19: Comparison between the simulation results and that obtained using the proposed methodology for moment coefficient.

5.3 METHODOLOGY FOR THE PREDICTION OF THE PITCHING MOMENT DERIVATIVE

In order to compute the curve slope of the pitching moment coefficient C_{M_α} , the same methodology for the prediction of moment coefficient is applied.

$$C_{M_\alpha} = C_{M_{\alpha_{FR}}} + \Delta C_{M_{\alpha_{nose}}} + \Delta C_{M_{\alpha_{tail}}} \quad (5.9)$$

where $C_{M_{\alpha_{FR}}}$ is the value of the curve slope of moment coefficient for a given fineness ratio FR, $\Delta C_{M_{\alpha_{nose}}}$ is the correction term due to the nose geometry and $\Delta C_{M_{\alpha_{tail}}}$ is the correction term due to the tailcone geometry. The $C_{M_{\alpha_{FR}}}$ can be expressed as a linear function of fineness ratio (equation 5.10 and figure 82).

$$C_{M_{\alpha_{FR}}} = 0.0035 \cdot FR - 0.0106 \quad (5.10)$$

The $\Delta C_{M_{\alpha_{nose}}}$ is the difference between C_{M_α} of the fuselage with the nose slenderness ratio FR_n and C_{M_α} of the reference fuselage (which has FR_n equal to 1.6). It is drawn in the figure 83 as a function of windshield angle.

The $\Delta C_{M_{\alpha_{tail}}}$ is the difference between $C_{M_{\alpha_{tail}}}$ of the fuselage with the tailcone slenderness ratio FR_t and $C_{M_{\alpha_{tail}}}$ of the reference fuselage (which has FR_t equal to 2.83). It is drawn in the figure 84 as a function of upsweep angle.

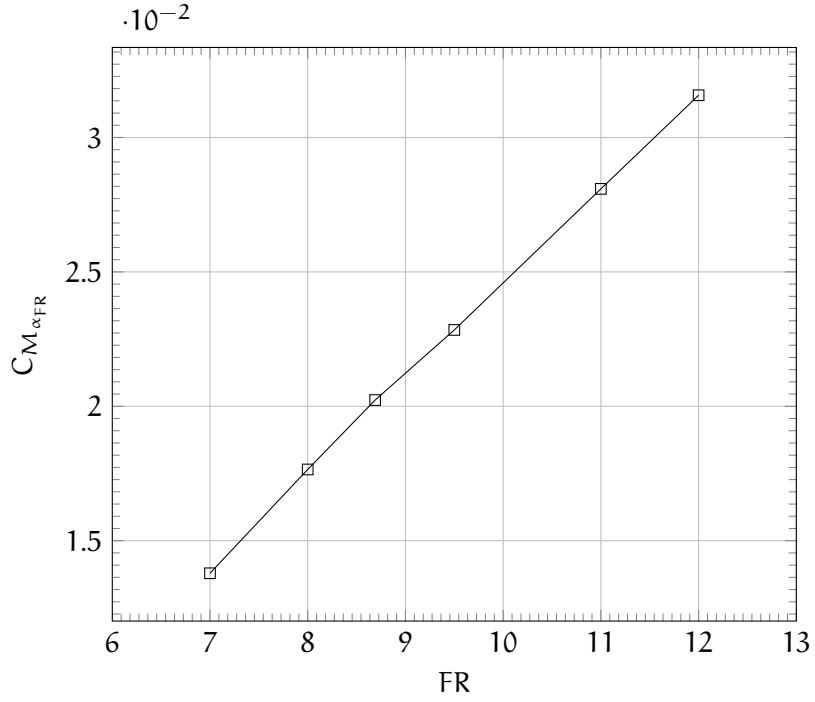


Figure 82: The curve slope of moment coefficient (referred to S_{front}) as a function of fineness ratio FR.

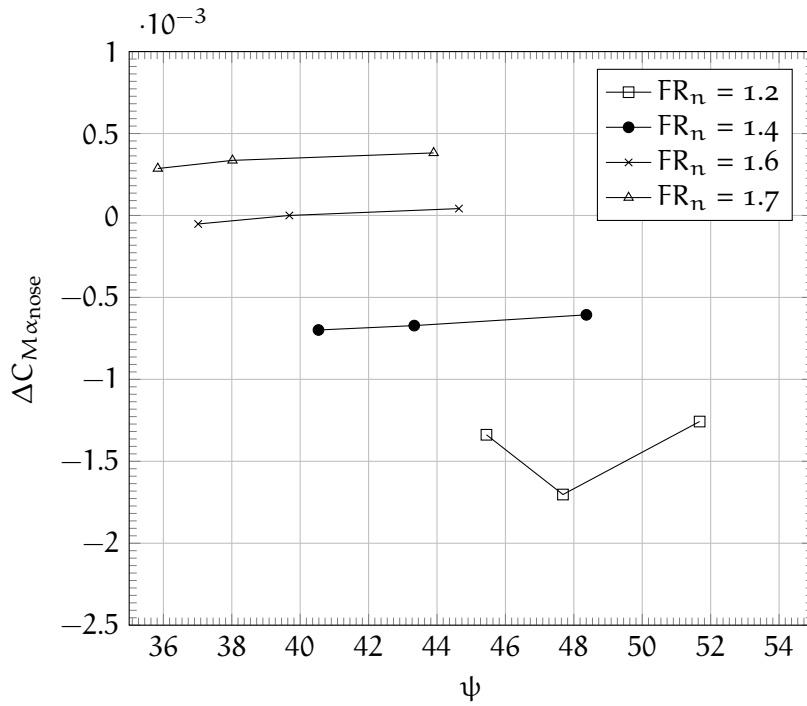


Figure 83: The nose correction term for the curve slope of the moment coefficient as a function of windshield angle ψ .

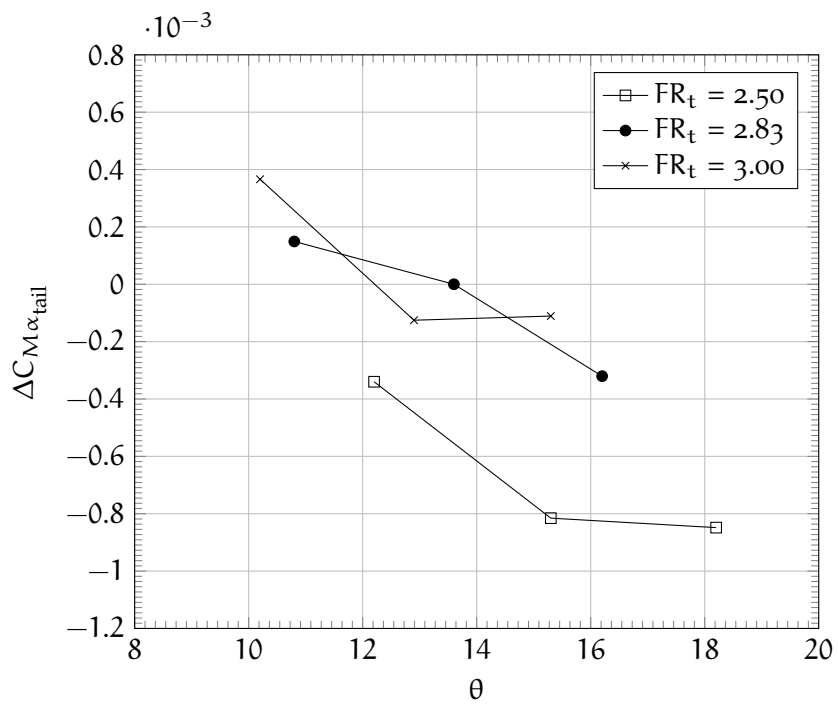


Figure 84: The tail correction term for the moment coefficient as a function of up sweep angle θ .

5.3.1 Example of application

The method is here applied to the same geometries previously defined in table 14. Below it has been reported the example of "103201" fuselage. The $C_{M_{\alpha_{FR}}}$ can be evaluated from equation 5.10 and figure 85.

$$C_{M_{\alpha_{FR}}} = 0.0035 \cdot FR - 0.0106 = 0.020232$$

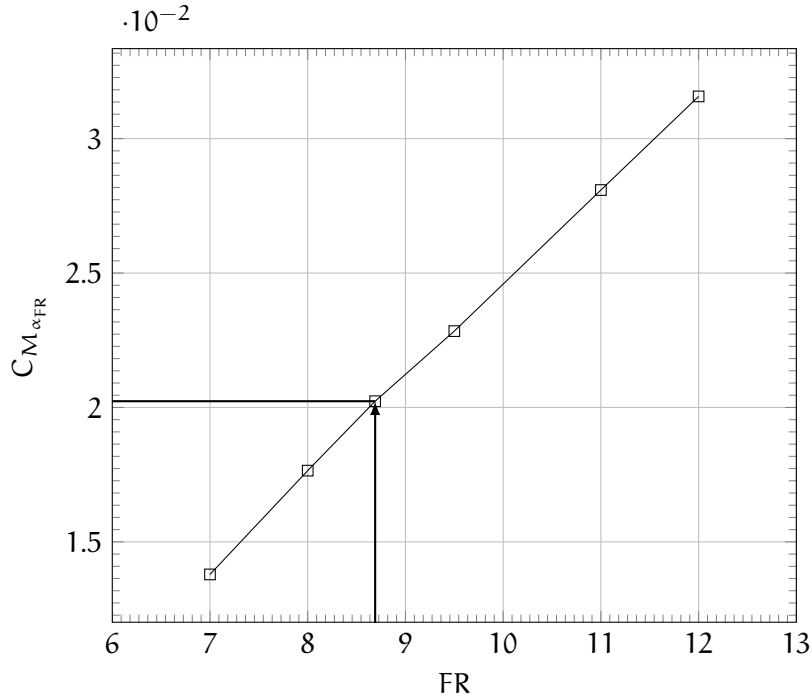


Figure 85: The curve slope of moment coefficient (referred to S_{front}) as a function of fineness ratio FR.

The value of $\Delta C_{M_{\alpha_{\text{nose}}}}$ is extracted from the chart entering with the value of FR_n and of the windshield angle, as it's possible to see from figure 86.

$$\Delta C_{M_{\alpha_{\text{nose}}}} = -0.001616$$

The value of $\Delta C_{M_{\alpha_{\text{tail}}}}$ is extracted from the chart entering with the value of FR_t and of the upsweep angle, as it's possible to see from figure 81.

$$\Delta C_{M_{\alpha_{\text{tail}}}} = -0.000815$$

From these values and by the equation 5.9, it's possible to estimate, in "modular" way, the moment coefficient of the fuselage.

$$C_{M_{\alpha}} = C_{M_{\alpha_{FR}}} + \Delta C_{M_{\alpha_{\text{nose}}}} + \Delta C_{M_{\alpha_{\text{tail}}}} = 0.017801$$

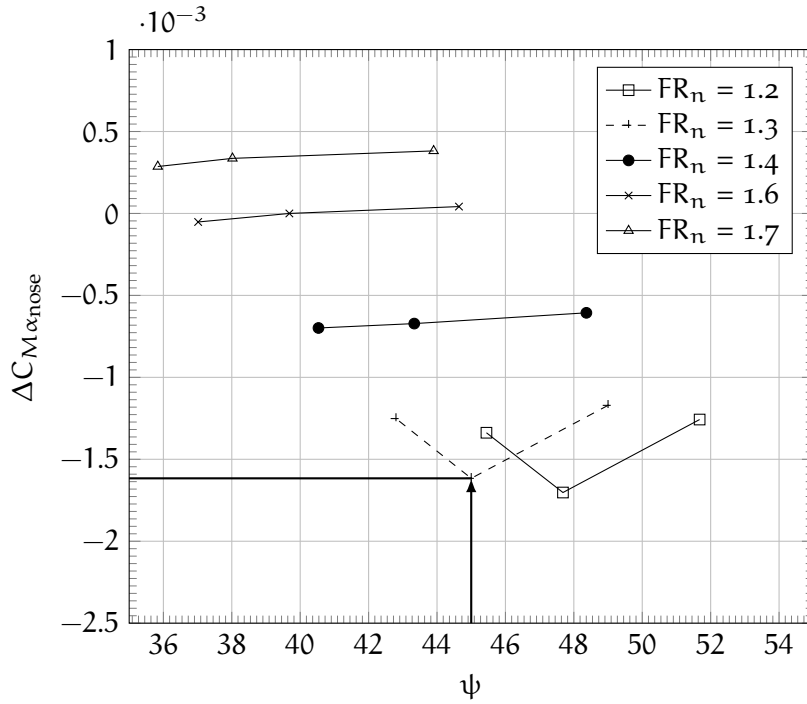


Figure 86: The nose correction term for the moment curve slope coefficient as a function of windshield angle ψ .

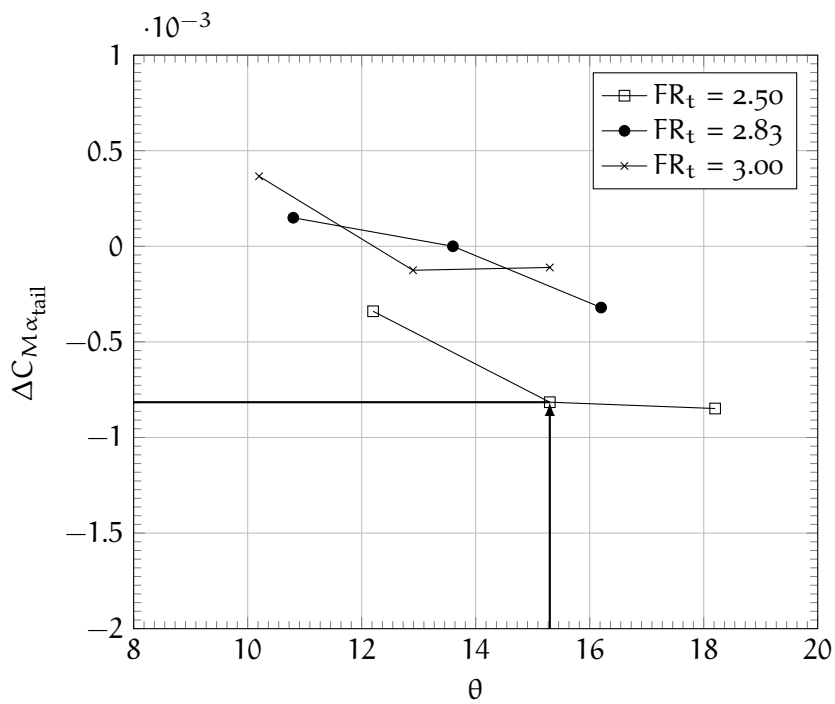


Figure 87: The tail correction term for the derivative of moment coefficient as a function of upsweep angle θ .

This value is very close to that obtained from the numerical simulation which is equal to 0.018869. The difference between the results is about 5%.

As before, the methodology has been applied even for the other two fuselage configurations described in the table 14. The useful parameters are in the table 20.

	101004206	107002208
$C_{M_{\alpha_{FR}}}$	0.028089	0.017650
$\Delta C_{M_{\alpha_{nose}}}$	-0.002237	0.000336
$\Delta C_{M_{\alpha_{tail}}}$	-0.000125	-0.000759

Table 20: The necessary values to apply the method for the curve slope moment coefficient

In the table 21 the results of methodology are reported and compared with that obtained by CFD simulations. The maximum difference among the results is about of 5%. This approach is valid for a fuselage not too different from the models analysed. The effects of Mach and Reynolds number are supposed to be small.

	103201	101004206	107002208
Method	0.017801	0.025726	0.017228
CFD	0.018869	0.026742	0.016530
Difference	5.7%	3.8%	-4.2%

Table 21: Comparison between the simulation results and that obtained using the proposed methodology for curve slope moment coefficient.

6 | CONCLUSIONS

The goal of this work was to develop a new approach for the evaluation of aerodynamic characteristics of the fuselage of a generic turbo-prop transport aircraft. For this purpose the fuselage geometry has been conceptually divided into three main components: nose, cabin and tailcone. It has been investigated the relationship between aerodynamic coefficients and the main geometrical parameters.

Usually, in the preliminary design, the aerodynamic studies are conducted with semi-empirical methods, such as USAF DATCOM. To predict the drag coefficient, these methods consider the sum of different contributions due to skin friction, upsweep angle, windshield (or canopy) and base drag. These contributions are estimated with results based on wind-tunnel tests. Unfortunately, the latter are based on geometries very different from a turboprop.

In order to overcome this issue, the aerodynamic studies have been performed with a numerical approach. The reference fuselage has been drawn by a MATLAB script that allows to modify the fineness ratio of each part of the fuselage (nose, cabin and tailcone), the windshield and/or the upsweep angle. For all modifications, the fuselage diameter is always constant. Therefore, to change the fineness ratio of the fuselage components, these are simply stretched (or shortened). This has been done by translating rigidly the sections along x axis. Instead, in the case of windshield and upsweep angle modifications, the sections are translated along z axis in opportune way. Each parameter is changed keeping the other constant. For instance, a change in fuselage slenderness ratio requires a stretch of the cabin, without changing the shape of nose and tail. Conversely, a change in nose or tail shape does not alter the geometry of the other components. The viscous (to allow for drag prediction), compressible (to include a high speed cruise at altitude) simulations have been carried out using the commercial software *Star-CCM+* on the SCoPE grid infrastructure of the University of Naples Federico II.

The results of the numerical approach are presumably more suitable for a preliminary design than those achieved with semi-empirical methods because they are based on an actual fuselage shape.

From numerical results a new methodology has been developed to predict the drag and pitching moment coefficient. As regard the drag, the methodology allows to compute the coefficient as the sum of the contributions of each component (nose, cabin, and tailcone) since the hypothesis of the super-positioning of the effects has been verified. The effect of the geometry of each part on the drag coefficient is eval-

uated with a shape factor which is function of fineness ratio of the part and of windshield angle for the nose or of the upsweep angle for the tailcone. The results are significant because there is a small difference between the results of numerical tests performed on different geometries and those obtained with the proposed methodology (about of 1%). As regard the moment, the methodology allows to estimate the value of the coefficient at angle of attack equal to 0° and the moment curve slope coefficient. In this case the hypothesis of the super-positioning of the effects is not verified. The moment coefficient is estimated as the sum of three contributions, one of which is the moment coefficient for a given fineness ratio and the others two are corrective terms due to the nose and the tailcone geometry. As just stated it's valid both for the pitching moment coefficient and its derivative. Also in this case the results are significant because there is a difference between the results of numerical tests performed on different geometries and those obtained with the methodology about of 1% for the moment coefficient and less than 6% for the moment curve slope coefficient.

Thus, it is the author's opinion that this work gives a new, simple, and reliable approach in the evaluation of the aerodynamic characteristics (drag, pitching moment and static longitudinal stability) of the fuselage of a generic regional turboprop transport airplane. Future investigations may consider sideslip conditions and non-linearities in both the longitudinal and directional stability curves.

A

FAR RELATED TO WINDSHIELDS AND WINDOWS

The Federal Aviation Regulations, or FARs, are rules prescribed by the Federal Aviation Administration (FAA) governing all aviation activities in the United States.

A wide variety of activities are regulated, such as aircraft design and maintenance, typical airline flights, pilot training activities, hot-air ballooning, lighter-than-air aircraft, man-made structure heights, obstruction lighting and marking, and even model rocket launches and model aircraft operation.

The rules are designed to promote safe aviation, protecting pilots, flight attendants, passengers and the general public from unnecessary risk. Since 1958, these rules have typically been referred to as *FARs* short for Federal Aviation Regulations.

The FARs are organized into sections, called parts due to their organization within the Code of Federal Regulations (CFR). Each part deals with a specific type of activity.

The part relating to windshield is 25.775 and it is reported below.

FAR 25.775 Windshields and windows.

- A. Internal panes must be made of nonsplintering material.
- B. Windshield panes directly in front of the pilots in the normal conduct of their duties, and the supporting structures for these panes, must withstand, without penetration, the impact of a four-pound bird when the velocity of the airplane (relative to the bird along the airplane's flight path) is equal to the value of VC, at sea level, selected under § 25.335(a).
- C. Unless it can be shown by analysis or tests that the probability of occurrence of a critical windshield fragmentation condition is of a low order, the airplane must have a means to minimize the danger to the pilots from flying windshield fragments due to bird impact. This must be shown for each transparent pane in the cockpit that —
 - a) Appears in the front view of the airplane;
 - b) Is inclined 15 degrees or more to the longitudinal axis of the airplane; and
 - c) Has any part of the pane located where its fragmentation will constitute a hazard to the pilots.

- D. The design of windshields and windows in pressurized airplanes must be based on factors peculiar to high altitude operation, including the effects of continuous and cyclic pressurization loadings, the inherent characteristics of the material used, and the effects of temperatures and temperature differentials. The windshield and window panels must be capable of withstanding the maximum cabin pressure differential loads combined with critical aerodynamic pressure and temperature effects after any single failure in the installation or associated systems. It may be assumed that, after a single failure that is obvious to the flight crew (established under §25.1523), the cabin pressure differential is reduced from the maximum, in accordance with appropriate operating limitations, to allow continued safe flight of the airplane with a cabin pressure altitude of not more than 15,000 feet.
- E. The windshield panels in front of the pilots must be arranged so that, assuming the loss of vision through any one panel, one or more panels remain available for use by a pilot seated at a pilot station to permit continued safe flight and landing.

B | STAR-CCM+ ON SCOPE USER GUIDE

In this appendix it is described how to run the software Star-CCM+ on the Sistema Cooperativo Per Elaborazioni Scientifiche Multidisciplinari (SCoPE) grid infrastructure:

1. writing the files necessary to the job;
2. transferring these files on SCoPE;
3. access to the Local File Catalogue (LFC);
4. running, monitoring and retrieving the job.

It is necessary to have an internet connection, a software to transfer files by Secure File Transfer Protocol (SFTP) (e.g. [WinSCP](#) or [Filezilla](#)) and a Secure Shell (SSH) client (e.g. [Putty](#) or simply a unix terminal). The user guide is an excerpt of the manual written by Eng. Elia Daniele of the DIAS (now DII).

B.1 FILES NECESSARY TO THE JOB

In order to use the Star-CCM+ library on SCoPE, four files are necessary:

- an input file, `filename.sim`, the same that runs locally;
- a Java macro, `macro_filename.java`, containing the instructions for Star-CCM+ and at least an autosave statement at the end of the iterations;
- an executable unix file, `filename.sh`, containing the instructions for SCoPE;
- a job file, `filename.jdl`, calling the input `.sim`, naming the output, assigning the CPUs number, calling the executable `.sh` file and, if any, some utilities.

B.1.1 Java macro example

```
// STAR-CCM+ macro: macro_102_a0.java
package macro;

import java.util.*;
```

```

import star.common.*;
import star.base.neo.*;
import star.vis.*;
import star.base.report.*;
import star.flow.*;
import star.meshing.*;

public class macro_102_a0 extends StarMacro {

    public void execute() {
        execute0();
    }

    private void execute0() {

        Simulation simulation_0 =
            getActiveSimulation();

        MeshPipelineController meshPipelineController_0 =
            simulation_0.get(MeshPipelineController.class);

        meshPipelineController_0.generateVolumeMesh();

        simulation_0.getSimulationIterator().run();

        simulation_0.saveState(resolvePath("102_ao_out.sim"));

    }
}

```

B.1.2 Executable file example

```

#!/bin/sh
#
# this parameter is the number of CPU's to be reserved for
# parallel
# execution
CPU_NEEDED=$1
SIMFILE=$2
SIMFILEOUT=$3
MACROJAVA=$4

echo "Copy SIMFILE on Local File Catalogue for size in excess of
100MB -> lcg-cp lfn:/grid/unina.it/dcilibertiDIR/Cusati/
$SIMFILE file:$PWD/$SIMFILE"
lcg-cp lfn:/grid/unina.it/dcilibertiDIR/Cusati/$SIMFILE file:$PWD
/$SIMFILE

HOST_NODEFILE=$PBS_NODEFILE

```

```

# copy files on the nodes different from the first one
NPROCTOCOPY='expr $CPU_NEEDED - 1'
FIRSTPROC='head -1 $HOST_NODEFILE'
j=0
for i in `tail -n $NPROCTOCOPY $HOST_NODEFILE | sort -u` ; do
# creates the working directories on all the nodes allocated for
# parallel execution
    if [ "$i" != "$FIRSTPROC" ]
    then
        WORKING_DIR='pwd'
        DIR_EXISTS[$j]='ssh $i "if [ -f $WORKING_DIR/
            starccm.sh ]; then echo SI; else echo NO; fi"'
        if [ ${DIR_EXISTS[$j]} = 'NO' ]
        then
            echo "Working directory on node $i doesn'
                t exist ... Creating"
# copies the needed files on all the nodes allocated for #
# parallel execution
                /usr/bin/scp -rp $WORKING_DIR/$SIMFILE $i
                :$WORKING_DIR
            else
                echo "Working directory exists on node $i
                    "
            fi
        fi
        j='expr $j + 1'
done

# this is the demo molecule
export STARCCMEXE=/opt/exp_soft/unina.it/STAR-CCM+/STAR-CCM
    +8.04.010/star/bin/starccm+

if [ -f /home/$LOGNAME/.flexlmrc ]
then
    cp /home/$LOGNAME/.flexlmrc $HOME
fi

echo "starting parallel starccm on nodes ..."
cat $HOST_NODEFILE

echo "Indication of date for calculation start..."
date
echo "Executing $STARCCMEXE --machinefile $HOST_NODEFILE --rsh ssh
    --np $CPU_NEEDED --batch $MACROJAVA $PWD/$SIMFILE"
$STARCCMEXE -machinefile $HOST_NODEFILE -rsh ssh -np $CPU_NEEDED
    -batch $MACROJAVA $PWD/$SIMFILE

#echo "move the file to sim file Out-->"
#cp $SIMFILE $SIMFILEOUT
#ls > ls.log

```

```

echo "Indication of date for calculation end..."
date

j=0
for i in `tail -n $NPROCTOCOPY $HOST_NODEFILE | sort -u` ; do
# remove created directory on all the nodes allocated for
parallel execution
    if [ "$i" != "$FIRSTPROC" ]
    then
        if [ ${DIR_EXISTS[$j]} = 'NO' ]
        then
            echo "Deleting working directory on node
                $i"
            /usr/bin/ssh $i rm -rf $WORKING_DIR
        else
            echo "Not needed to delete working
                directory on node $i"
        fi
    fi
    j=`expr $j + 1`
done

# Instruction added on 20121108 to copy output on lfc for big
file (see https://www.opensciencegrid.org/bin/view/Documentation/SrmBasics)
echo "Copy SIMFILEOUT on Local File Catalogue for size in excess
of 100MB → lcg-cr file:$PWD/$SIMFILEOUT lfn:/grid/unina.it/
dcilibertiDIR/Cusati/$SIMFILEOUT"
lcg-cr -v --vo unina.it -l lfn:/grid/unina.it/dcilibertiDIR/
Cusati/$SIMFILEOUT file:$PWD/$SIMFILEOUT

```

B.1.3 Job file example

```

Executable = "script.sh";
Arguments = "8 102_ao.sim 102_ao_out.sim macro_102_ao.java";
CpuNumber = 8;

StdOutput = "starccm.log";
StdError = "starccm.err";

Requirements = RegExp("ceo[1-2].scope.unina.it:8443/cream-pbs-
unina_hpc", other.GlueCEUniqueID);
InputSandbox = {"script.sh", "macro_102_ao.java"};
OutputSandbox = {"starccm.log", "starccm.err"};

PerusalFileEnable = true;
PerusalTimeInterval = 1000;

RetryCount = 0;

```


B.2 TRANSFERRING FILES ON SCOPE

The previously mentioned files must be copied on the user's personal directory on SCoPE. To do this, it is necessary a SFTP software as [WinSCP](#), [Filezilla](#) or others, connecting to the address

```
ui01.scope.unina.it
```

with the credentials provided after the registration. More info are available on www.scope.unina.it.

B.3 COPYING THE SIMULATION FILE ON THE LFC

First of all, a SSH tunnel must be opened on `ui01.scope.unina.it`. This can be done with a unix terminal with the command

```
ssh -l username ui01.scope.unina.it
```

or by means of an emulator like [Putty](#). Then it is mandatory to create a proxy before giving any command to the jobs, if more than 12 hours have passed, typing

```
voms-proxy-init --voms unina.it
```

The Local File Catalogue is a space dedicated to simulation files bigger than 100 MB. Every user has his own personal directory on the LFC (to not be confused with the *local* personal directory). If not existent, it must be created with the command

```
lfc-mkdir /grid/unina.it/usernameDIR/folder
```

and then the `filename.sim` file can be copied on LFC with the statement

```
lcg-cr -v --vo unina.it file:/home/username/folders/filename.sim
-l lfn:/grid/unina.it/usernameDIR/folders/filename.sim
```

B.4 RUNNING, MONITORING AND RETRIEVING THE JOB

From the user's *local* folder where there are the previously discussed files, a job can be launched from the shell with the command

```
glite-wms-job-submit -a -o job_ID_filename.txt filename.jdl
```

that includes the registration of the job. Now any further command for that job will refer to its job identifier. For example, the job monitoring is obtained giving

```
watch "glite-wms-job-status -i job_ID_filename.txt"
```

and the job status is updated every two seconds. However this tells the user only if the run is scheduled, running, completed, aborted or cleared. To get a log file, the same that will be obtained when the job ends, but incomplete for obvious reasons, the *perusal* option can be enable in the filename.jdl and giving the following commands

```
glite-wms-job-perusal --set -f starccm.log https://scopedma-ce.  
scope.unina.it:9000/U51oobm0GTvXzMKP_pWGZw
```

to *set* the perusal and

```
glite-wms-job-perusal --get -f starccm.log https://scopedma-ce.  
scope.unina.it:9000/U51oobm0GTvXzMKP_pWGZw
```

to *get* the partial log file. The last string of the command is an internal identifier displayed on the shell once launched the job.

Once the job is completed, it can be get by typing

```
glite-wms-job-output -i job_ID_filename.txt
```

and retrieved from the temporary folder

```
/root/tmp/jobOutput
```

with the SFTP client.

C | NUMERICAL SIMULATION RESULTS

In all tables below, each aerodynamic coefficient is expressed as a ratio between the computed value, which comes from the numerical simulations, and the baseline value which cannot be specified for industrial reasons. In the case of pressure and friction drag contributions (C_{D_p} and C_{D_f}), both are compared with the global baseline drag coefficient (C_D). As regard the moment coefficient at α equal to 0° and equal 2° , these are compared with the global baseline moment coefficient at α equal to 0° .

FR _n	1.1	1.2	1.3	1.4	1.5	1.6	1.7
$\alpha = 0^\circ$							
C_{D_n}	0.27537	0.27166	0.26603	0.26807	0.27230	0.27889	0.28496
C_{D_c}	0.54651	0.54536	0.54306	0.54293	0.54037	0.54102	0.53819
C_{D_t}	0.18208	0.17965	0.18068	0.18106	0.18004	0.18009	0.17837
C_{D_p}	0.23314	0.21587	0.20115	0.19309	0.18554	0.18180	0.17658
C_{D_f}	0.77082	0.78080	0.78861	0.79897	0.80716	0.81820	0.82495
C_D	1.00396	0.99667	0.98976	0.99206	0.99270	1.00000	1.00153
C_L	-0.98888	-0.98267	-0.99217	-0.99437	-1.00058	-1.00000	-1.00003
C_M	-0.89805	-0.92110	-0.94581	-0.96432	-0.98266	-1.00000	-1.01615
C_{M_α}	0.90003	0.91664	0.93041	0.96710	0.98375	1.00000	1.01646
C_{L_α}	1.05667	1.06017	1.07913	0.99134	0.99542	1.00000	1.00038
$\alpha = 2^\circ$							
C_{D_n}	0.26603	0.26487	0.26065	0.26359	0.26935	0.28074	0.28394
C_{D_c}	0.52591	0.52309	0.52105	0.51862	0.51542	0.51260	0.51145
C_{D_t}	0.18055	0.18042	0.18017	0.18068	0.18042	0.17581	0.17927
C_{D_p}	0.20358	0.18951	0.17262	0.16391	0.15713	0.15201	0.14856
C_{D_f}	0.76890	0.77888	0.78925	0.79897	0.80806	0.81714	0.82610
C_D	0.97248	0.96839	0.96186	0.96289	0.96519	0.96916	0.97466
C_L	-0.32664	-0.31823	-0.31586	-0.37307	-0.37673	-0.37327	-0.37307
C_M	0.21431	0.21178	0.20408	0.23092	0.23315	0.23590	0.24009

Table 22: Results of numerical simulation for the configuration with nose geometry modifications, $M = 0.52$, $Re_{L_f} = 2.02 \times 10^8$.

FR	7	8	8.69	9.5	11	12
$\alpha = 0^\circ$						
C_{D_n}	0.24722	0.26756	0.27889	0.28867	0.29034	0.29840
C_{D_c}	0.38567	0.48215	0.54102	0.61970	0.79104	0.87396
C_{D_t}	0.21113	0.19091	0.18009	0.17146	0.16622	0.16072
C_{D_p}	0.19091	0.18349	0.18180	0.18132	0.17428	0.17454
C_{D_f}	0.65310	0.75713	0.81820	0.89852	1.07331	1.15853
C_D	0.84401	0.94062	1.00000	1.07984	1.24759	1.33307
C_L	-1.05249	-1.01795	-1.00000	-0.98029	-0.95946	-0.93825
C_M	-1.10748	-1.04182	-1.00000	-0.94964	-0.85164	-0.79383
C_{M_α}	0.68456	0.87360	1.00000	1.12769	1.38460	1.55510
C_{L_α}	0.91755	0.94759	1.00000	1.09109	1.12813	1.15817
$\alpha = 2^\circ$						
C_{D_n}	0.24171	0.26590	0.27793	0.28650	0.29571	0.29917
C_{D_c}	0.35508	0.45400	0.51350	0.59501	0.76199	0.85041
C_{D_t}	0.20755	0.18963	0.17901	0.17466	0.16596	0.16430
C_{D_p}	0.15355	0.15265	0.15227	0.15624	0.15265	0.15496
C_{D_f}	0.65080	0.75687	0.81817	0.89993	1.07101	1.15892
C_D	0.80435	0.90953	0.97044	1.05617	1.22367	1.31388
C_L	-0.47744	-0.42407	-0.37327	-0.29648	-0.25243	-0.21240
C_M	-0.26144	0.03786	0.23590	0.44407	0.85960	1.12813

Table 23: Results of numerical simulation for the configuration with cabin geometry modifications, $M = 0.52$, $Re_{L_f} = 2.02 \times 10^8$.

FR	2.3	2.4	2.5	2.6	2.7	2.83	2.9	3
$\alpha = 0^\circ$								
C_{D_n}	0.27613	0.27741	0.27716	0.27844	0.27844	0.27889	0.27933	0.28010
C_{D_c}	0.56570	0.56059	0.55508	0.55176	0.54446	0.54102	0.53717	0.53499
C_{D_t}	0.15969	0.16494	0.16750	0.17134	0.17351	0.18009	0.18260	0.18938
C_{D_p}	0.21791	0.21152	0.20422	0.19808	0.18951	0.18180	0.17927	0.17697
C_{D_f}	0.78362	0.79142	0.79552	0.80345	0.80691	0.81820	0.81983	0.82751
C_D	1.00153	1.00294	0.99974	1.00153	0.99641	1.00000	0.99910	1.00447
C_L	-1.20000	-1.16290	-1.12634	-1.09271	-1.04591	-1.00000	-0.98486	-0.97079
C_M	-0.92472	-0.93637	-0.95023	-0.96209	-0.98268	-1.00000	-1.00519	-1.00952
C_{M_α}	0.95567	0.96852	0.95967	0.96568	0.96421	1.00000	0.98544	0.99322
C_{L_α}	1.08263	0.96480	1.07534	1.07242	1.12346	1.00000	1.07184	1.06600
$\alpha = 2^\circ$								
C_{D_n}	0.27485	0.27447	0.27498	0.27447	0.27959	0.28074	0.27332	0.27882
C_{D_c}	0.52821	0.53384	0.52540	0.52156	0.51631	0.51260	0.51196	0.50851
C_{D_t}	0.16110	0.15624	0.16647	0.16775	0.17428	0.17581	0.18157	0.18938
C_{D_p}	0.17415	0.17978	0.17108	0.16174	0.16289	0.15201	0.14613	0.15112
C_{D_f}	0.79001	0.78477	0.79577	0.80204	0.80729	0.81714	0.82072	0.82559
C_D	0.96417	0.96455	0.96685	0.96378	0.97018	0.96916	0.96685	0.97671
C_L	-0.52149	-0.55824	-0.45240	-0.42060	-0.34181	-0.37327	-0.31312	-0.30270
C_M	0.25603	0.26036	0.23549	0.23111	0.20869	0.23590	0.21260	0.21794

Table 24: Results of numerical simulation for the configuration with tail-cone geometry modifications, $M = 0.52$, $Re_{L_f} = 2.02 \times 10^8$.

FR _n	1.2	1.2	1.2	1.4	1.4	1.4	1.4	1.4	1.6	1.6	1.6	1.6	1.7	1.7	1.7
ψ	51.7°	47.7°	45.4°	48.4°	43.3°	40.5°	44.6°	39.7°	37.0°	43.9°	38.0°	35.8°			
$\alpha = 0^\circ$															
C _{D_n}	0.30518	0.27166	0.26590	0.30608	0.26807	0.26462	0.31708	0.27889	0.27127	0.32322	0.28496	0.27844			
C _{D_c}	0.54190	0.54536	0.54574	0.54062	0.54293	0.54369	0.53806	0.54102	0.53986	0.53653	0.53819	0.53781			
C _{D_t}	0.18068	0.17965	0.18183	0.18017	0.18106	0.18157	0.17850	0.18009	0.18004	0.17876	0.17837	0.17940			
C _{D_p}	0.25477	0.21587	0.21305	0.23340	0.19309	0.18976	0.22265	0.18180	0.17454	0.21830	0.17658	0.17070			
C _{D_f}	0.77300	0.78080	0.78042	0.79347	0.79897	0.80012	0.81100	0.81820	0.81663	0.82021	0.82495	0.82495			
C _D	1.02776	0.99667	0.99347	1.02687	0.99206	0.98989	1.03365	1.00000	0.99117	1.03851	1.00153	0.99564			
C _L	-1.07717	-0.98267	-0.93606	-1.07790	-0.99437	-0.94355	-1.09234	-1.00000	-0.95251	-1.09490	-1.00003	-0.95141			
C _M	-1.16239	-0.92110	-0.73462	-1.21968	-0.96432	-0.76232	-1.26966	-1.00000	-0.78485	-1.29193	-1.01615	-0.79780			
C _{Mα}	0.93844	0.91664	0.93449	0.97032	0.96710	0.96579	1.00204	1.00000	0.99746	1.01868	1.01646	1.01402			
C _{Lα}	0.98959	1.06017	0.98376	0.99921	0.99134	0.99396	1.01117	1.00000	1.00621	1.01350	1.00038	1.00825			
$\alpha = 2^\circ$															
C _{D_n}	0.28778	0.26487	0.26449	0.29290	0.26359	0.26551	0.30697	0.28074	0.27421	0.31414	0.28394	0.28202			
C _{D_c}	0.52399	0.52309	0.52002	0.51900	0.51862	0.51554	0.51324	0.51260	0.50953	0.51030	0.51145	0.50697			
C _{D_t}	0.18029	0.18042	0.18144	0.17965	0.18068	0.18119	0.17812	0.17581	0.17965	0.17850	0.17927	0.17927			
C _{D_p}	0.21855	0.18951	0.18631	0.19782	0.16391	0.16276	0.18708	0.15201	0.14754	0.18247	0.14856	0.14395			
C _{D_f}	0.77351	0.77888	0.77965	0.79373	0.79897	0.79948	0.81126	0.81714	0.81586	0.82047	0.82610	0.82431			
C _D	0.99206	0.96839	0.96596	0.99155	0.96289	0.96225	0.99833	0.96916	0.96340	1.00294	0.97466	0.96826			
C _L	-1.22422	-0.85255	-0.85597	-1.21002	-0.99945	-0.85891	-1.22863	-1.00000	-0.86234	-1.23157	-0.99945	-0.85597			
C _M	-0.01088	0.89776	1.78178	-0.08675	0.97889	1.82833	-0.13240	1.00000	1.89876	-0.13963	1.01777	1.93059			

Table 25: Results of numerical simulation for the configuration with windshield geometry modifications, $M = 0.52$, $Re_{L_f} = 2.02 \times 10^8$.

FR _t	2.5	2.5	2.5	2.83	2.83	2.83	2.83	3	3	3
θ	12.2°	15.3°	18.2°	10.8°	13.6°	16.2°	10.2°	12.9°	15.3°	15.3°
$\alpha = 0^\circ$										
C _{Dn}	0.27595	0.27684	0.27761	0.27876	0.27837	0.27876	0.27837	0.27978	0.28016	0.28016
C _{Dc}	0.52901	0.55445	0.55726	0.51828	0.54128	0.54090	0.51214	0.53438	0.53515	0.53515
C _{Dt}	0.14686	0.16731	0.26649	0.16910	0.18034	0.25396	0.17996	0.18916	0.25754	0.25754
C _{Dp}	0.16130	0.20399	0.29921	0.15325	0.18162	0.25396	0.14788	0.17676	0.24093	0.24093
C _{Df}	0.79052	0.79461	0.80215	0.81288	0.81838	0.81966	0.82260	0.82656	0.83193	0.83193
C _D	0.95181	0.99859	1.10135	0.96613	1.00000	1.07362	0.97048	1.00332	1.07285	1.07285
C _L	-0.61263	-1.12486	-1.68036	-0.56207	-1.00000	-1.47773	-0.54454	-0.96951	-1.41548	-1.41548
C _M	-0.79124	-0.95104	-0.84542	-0.80936	-1.00000	-0.92689	-0.81399	-1.01038	-0.94769	-0.94769
C _{Mα}	0.98335	0.96005	0.95843	1.00731	1.00000	0.98430	1.01794	0.99386	0.99457	0.99457
C _{Lα}	0.98403	1.07309	1.06843	0.97297	1.00000	1.04573	0.97646	1.06377	1.04631	1.04631
$\alpha = 2^\circ$										
C _{Dn}	0.27441	0.27467	0.27505	0.27646	0.28042	0.27671	0.27646	0.27850	0.27748	0.27748
C _{Dc}	0.52377	0.52480	0.52390	0.51253	0.51201	0.51329	0.50690	0.50792	0.50741	0.50741
C _{Dt}	0.14558	0.16628	0.23581	0.16782	0.17561	0.22981	0.17919	0.18916	0.23364	0.23364
C _{Dp}	0.14954	0.17088	0.23543	0.14238	0.15184	0.20066	0.13829	0.15095	0.18942	0.18942
C _{Df}	0.79422	0.79486	0.79934	0.81442	0.81621	0.81915	0.82426	0.82464	0.82912	0.82912
C _D	0.94376	0.96575	1.03476	0.95680	0.96805	1.01981	0.96255	0.97559	1.01853	1.01853
C _L	0.00456	-0.45181	-1.01022	0.04819	-0.37278	-0.82183	0.06791	-0.30230	-0.75922	-0.75922
C _M	0.42428	0.23569	0.33930	0.43577	0.23610	0.28981	0.44428	0.21813	0.28170	0.28170

Table 26: Results of numerical simulation for the configuration with upsweep geometry modifications, $M = 0.52$, $Re_{L_f} = 2.02 \times 10^8$.

BIBLIOGRAPHY

- [1] I.H. Abbott, *Fuselage drag tests in the variable density wind tunnel: streamline bodies of revolution, fineness ratio of 5*, NACA tn 614, Washington, 1939.
- [2] ATR, The ATR web site, 2014, URL <http://www.atraircraft.com>.
- [3] CFR, U.S. Government, 2014, URL <http://ecfr.gov>.
- [4] D. Ciliberti, *A new vertical tailplane design procedure through CFD*, Master thesis in Aerospace Engineering, Department of Aerospace Engineering, University of Naples Federico II, 2012
- [5] P. Della Vecchia, *Development of Methodologies for the Aerodynamic Design and Optimization of New Regional Turboprop Aircraft*, PhD thesis in Aerospace Engineering, Department of Aerospace Engineering, University of Naples Federico II, 2013
- [6] E.C. Draley, *High speed drag test of several fuselage shapes in combination with a wing*, NACA wr-l-542, Washington, 1947.
- [7] R.R. Gilruth and M.D. White, *Analysis and Prediction of Longitudinal Stability of Airplanes*, NACA TR 711, 1941.
- [8] P. Iaia, *Verso horizon 2020: il ruolo di nuovi materiali e delle tecnologie di manifattura per l'aerospazio: I Materiali e i Processi Manifatturieri per il Nuovo Velivolo da Trasporto Regionale*, associazione ARMA aeronautica, CESMA, 2012.
- [9] *Jane's. All The World Aircrafts*, 2004-2005, Edited by Paul Jackson, MRAeS.
- [10] I. Kroo et al., *Aircraft Design: Synthesis and Analysis*, Stanford University, January 2001. URL <http://adg.stanford.edu/aa241/AircraftDesign.html>
- [11] D.W. Levy, *The CFD Drag Prediction Workshop Series: Summary and Retrospective*, Jameson, Roe, van Leer Symposium AIAA, San Diego (CA), 22-23 June 2013
- [12] MATLAB, *Matlab R2010b User Guide*, Mathworks, 2010
- [13] L. Merola, *The S.Co.P.E. Project*, Università degli Studi di Napoli Federico II.
- [14] H. Multhopp, *Aerodynamics of the fuselage*, NACA TM 1036, Washington, 1942.

- [15] M. Munk, *The Aerodynamic forces on airship hulls*, NACA TR 184, 1924.
- [16] F. Nicolosi and P. Della Vecchia, *Aerodynamic guidelines in the design and optimization of new regional turboprop aircraft*, III CEAS Air&Space Conference, XXI AIDAA Congress, Naples, 2011.
- [17] C. D. Perkins and R. E. Hage, *Airplane performance stability and control.*, Wiley, New York, 1949.
- [18] D. Raymer, *Aircraft Design - A Conceptual Approach* 2nd ed., 1992.
- [19] J. Roskam, *Airplane Design*, University of Kansas, 1985.
- [20] J. Roskam, *Methods for estimating drag polars of subsonic airplanes*, University of Kansas, 1971.
- [21] Star-CCM, *Star-CCM+ Version 8.04.007 User Guide*, CD-adapco, 2013
- [22] SCoPE, Università degli Studi di Napoli Federico II, 2014, URL <http://scope.unina.it>.
- [23] E. Torenbeek, *Synthesis of subsonic airplane design*, Delft University Press, 1976.

COLOPHON

This work was realized with \LaTeX using *arsclassica*, a re-style of the typographical look-and-feel *classicthesis* developed by André Miede. The style was inspired by Robert Bringhurst's seminal book on typography "*The Elements of Typographic Style*".

Charts were generated with `pgfplots` and graphics were realized with `TikZ`.

